SYNTHESIS, CHARACTERIZATION AND CATALYTIC PROPERTIES OF SOME VANADOSILICATE MOLECULAR SIEVES

A THESIS

SUBMITTED TO

THE UNIVERSITY OF POONA

FOR THE DEGREE OF

DOCTOR OF PHILOSOPHY

(IN CHEMISTRY)

BY

TAPAS SEN

CATALYSIS DIVISION

NATIONAL CHEMICAL LABORATORY

PUNE - 411 008, INDIA

JUNE 1997

DEDICATED TO

MY BELOVED PARENTS

ACKNOWLEDGMENTS

I wish to expressed my deep sense of gratitude to my suprervisor, Dr. S. Sivasanker , Scientist -F, National Chemial laboratory, Pune, India, for his valuable guidance and encouragement through out the course of this investigation.

I am deeply indebted to Dr. S. Ganapathy for his stimulating discussions and constant professional and personal help rendered during the course of the present investigation. Without his help, it would have been difficult for me to complete my research work suceessfully.

I wish to offer my sincere thanks to Drs. A. V. Ramaswamy, R. Vetrivel, P. R. Rajamohanan, S. Kannan, S. Shinde, V. Ramaswamy and M. Chatterjee for valuable discussions and professional help.

My sincere thanks are to Dr. P. Ganguli, Dr. A. Sarkar, Dr. S. Pal, Dr. P. Ghosh, Binodda, Nikhilda, Ramda, Arnabda, Moloyda and Soumen who helped me to come to NCL; without their encouragement, It was impossible for me to come in this laboratory.

The help and cooperation extended by Drs. A. J. Chandwadkar, S. G. Hedge, A. A. Belhekar, N. E. Jacob, H. S. Soni, C. Gopinathan and all the other staff members in the Catalysis Division, NCL, in completing my research work sucessfully are duly acknowledged.

I take the opportunity to thank my friends Ravi, Debasis, Tapan, Raghavan, Nawal, Asoke, Selvaraj, Anil, Raja, Puyam, Suhas, Shevade, velu, Raju, Venkatathri, Karuna, Sahida, Bhavna, Sindhu, Ranjit, Sushma, Shipra, Asim, Rajib, Selvam, Subratada, Prakash, Manoj, Biswajit, Ramani, Anjan, Adin, Uttam, Babla, Dipak, Meenakshee, Manna, Soumen and ElMekki who constantly provided me a encouraging companionship.

My thanks are to my beloved sister Ms. Sujata and respected Aunty, whose affection, suggestions and advice helped me to perform well of this course,

to Mr. Madhu and Mr. Murugan who personally helped me on various occasions during my stay in NCL and

to my sisters, brother-in-laws, uncle, aunty, and grandmother for their constant encouragement and moral support.

I am thankful to the Director, National Chemical Laboratory, for allowing me to submit this work in the form of a thesis for the award of Ph. D degree. Financial assistance from the University Grants Commision, New Delhi, is gratefully acknowledged.

Date : 24.06.97

TAPAS SEN

CERTIFICATE

Certified that the work incorporated in the thesis entitled "***Synthesis, Characterization and Catalytic properties of some Vanadosilicate Molecular Sieves***" submitted by **Mr. Tapas Sen** for the degree of ***Doctor of Philosophy*** was carried out by the candidate under my supervision at the *National Chemical Laboratory, Pune, India.* Such material as has been obtained from other sources has been duly acknowledged.

Dr. S. SIVASANKER

Supervisor

Contents.....

CHAPTER I

GENERAL INTRODUCTION

1.1 INTRODUCTION

The subject dealing with zeolites is a dynamic and rapidly growing field involving different branches of science, such as inorganic chemistry, organic chemistry, physical chemistry, colloid chemistry, biochemistry, mineralogy, geology, surface chemistry, oceanography, crystallography, catalysis and theoretical physics. Zeolites introduce both unusual activity and selectivity into heterogeneous adsorption and catalytic processes and are the inorganic analogs of enzymes in living systems. These are used on large industrial scale in a great variety of processes from simple drying to complicated catalytic reactions. Zeolites can also act as supports for numerous catalytically active metals.

1.2 ZEOLITES

Zeolites are crystalline aluminosilicates, having stable frameworks, constituted by corner sharing of all four oxygens of the $[SiO_4]^{4-}$ and $[AlO_4]^{5-}$ tetrahedral primary building units. The crystallographic unit cell of a zeolite may be represented as[1] :

$$M_{x/n}[(AlO_2)_x(SiO_2)_y]\ zH_2O$$

Where M is the cation of valence 'n' from group I or II of the periodic table, or a rare earth element or an organic cation. The net negative charge and hence the cation content is governed by the Si/Al (y/x) ratio; y/x can be one to infinity and z is the number of water molecules. The intracrystalline water molecules can be removed by heating or by vacuum. The cations are quite mobile and can be exchanged to varying degrees by other cations.

Replacement of Al^{3+} or Si^{4+} in the zeolite lattice by trivalent and tetravalent metal ions like B^{3+}, Ga^{3+}, Fe^{3+}, Cr^{3+}, $V^{4+/5+}$, Ti^{4+} and Zr^{4+} is possible. The resultant materials are generally called metallosilicate analogs of zeolites or metallosilicate molecular sieves.

1.3 ZEOLITE SYNTHESIS

Milton, in the late 1940's, developed the hydrothermal crystallization of reactive alkali metal aluminosilicate gels at low temperatures and pressures. Later, in the early 1960's, the high silica molecular sieves were synthesized using quaternary ammonium cations and alkali aluminosilicate gels of pH around 12-14.

The variables which have a major influence on the structure crystallized are the gross composition of the reaction mixture, pH of the gel, crystallization temperature and time.[2]

Zeolite synthesis involves the following important events, summarized by Sand[3] :

- precipitation of the gel
- dissolution of the gel
- nucleation of the zeolite structure
- continued crystallization and crystal growth
- dissolution of the initial meta-stable phase
- nucleation of a more stable meta-stable phase
- continued crystallization and crystal growth of the new crystalline phase while the initial crystals are dissolving
- dissolution of the metastable phase
- nucleation of the equilibrium phase and
- crystallization and cyrstal growth of the final crystalline phase

A guest species that is an especially good fit to the zeolite void space is referred to as a template.[4] A template can be charged or neutral or an anionic pair. Moretti *et al.*[5] have reported a wide variety of neutral and ionic organic diamines for the synthesis of various zeolites having different structures. The role of templates may be to :

- act as donors of hydroxyl ions
- increase the solubility of alumnate and silicate ions
- organize the water molecules
- stabilize some structures and
- balancing the framework charge

1.4 CLASSIFICATION

Zeolites have been classified based on morphological characteristics,[1,6-8] crystal structure[1,6,9], chemical composition[1,3,6], effective pore diameter[1,6,10] and natural occurrence.[1,6] Barrer[6] and Sand[3] classified the zeolites based on effective pore diameters into three groups, *viz.*, i) small pore zeolites (d < 5Å), ii) medium pore zeolites (d = 5 - 6.5Å) and iii) large pore zeolites (20Å > d > 6.5Å) with pore openings made up respectively of 8-membered, 10 membered or 12 membered rings of oxygen atoms.

Wilson *et al.*[11] have reported a new class of molecular sieves containing equal moles of Al^{3+} and P^{5+} ions in the lattice, called aluminophosphate ($AlPO_4$) molecular sieves. Davis *et al.*[12] have reported a 18-membered ring large pore molecular sieve of the $AlPO_4$ type, designated as VPI-5 having a pore diameter of 12Å. Esterman *et al.*[13] have recently reported a gallophosphate molecular sieve (cloverite) with a pore diameter of 29-30Å. Besides a new class of mesoporous molecular sieves called MCM-41 and MCM-48 of special interest in catalysis have been syntheisized.[14,15] These posses uniform pores of size ranging from 20 -120 Å . Metal substituted aluminophosphate (MeAlPO) molecular sieves, in which metal ions such as Co, Fe, Mg, Zn, Ga, Cr, Ti, V and Mo have been reported by various authors.[16-18] Silicon substitution in the framework of $AlPO_4$ produces silicoalumnophosphates (SAPO's).[19] These exhibit cation exchange and weak acidic properties.

1.5 ISOMORPHOUS SUBSTITUTION

Substitution of T atoms by bi, tri, tetra and pentavalent metal ions like Be, B, Ga, Fe, Zr, Sn, Ge, V and P in the zeolite framework is called isomorphous substitution. This can be performed either during synthesis or by post synthesis methods. Pauling's theory[20] predicts the possibility of isomorphous substitution and the stability of the particular metal ion in the zeolite tetrahedral framework. According to Pauling criterion, ρ ($\rho = r_c/r_0$, where r_0 is the radius of the ion and r_c is the cationic radius), the metal ion is stable in the tetrahedral framework when it is in the range $0.414 > \rho > 0.225$. Values of Pauling criteria for some metal ions are given in table 1.1.

Table 1.1

Values of Pauling criterion for various elements.

Critical values (ρ_{cr})	Coordination number	Corresponding cations
$\rho > 0.732$	8	Pb^{2+}, Sn^{2+}, Ti^{3+}, Eu^{3+}, Nd^{3+}
$0.732 > \rho > 0.414$	6	In^{3+}, Mn^{2+}, Zn^{2+}, Hf^{4+}, Cu^{2+}, Sn^{4+}, Fe^{3+}, Mo^{6+}, Ti^{4+}, Pt^{4+}, Cr^{3+}, Ga^{3+}, Sb^{5+}, V^{4+}
$0.414 > \rho > 0.225$	4	Al^{3+}, Mn^{4+}, Ge^{4+}, V^{5+}, Si^{4+}, Cr^{6+}, P^{5+}, Se^{6+}, Be^{2+}
$0.225 > \rho > 0.147$	3	B^{3+}

According to Pauling, the cations for which ρ is out of the range for Td-coordination, the substitution in the zeolite lattice is either impossible or could take place only on a limited scale. The first isomorphous substitution in the zeolite framework was reported by Goldsmith[21] in 1952 in the synthesis of germanium containing thomsonite, in which Si was replaced by Ge. Later, Barrer *et al.*[22] reported a number of Ga and Ge substituted zeolites. Isomorphous substitution of Al^{3+} by nontransition metal ions, e.g., B^{3+} and Ga^{3+} and

transition metal ions, e.g., Fe^{3+}, Ti^{4+}, $V^{4+/5+}$ and Cr^{5+} are reported.[23-28] Postsynthesis methods have also been used to incorporate Fe^{3+}, Ga^{3+}, Ti^{4+}, $V^{4+/5+}$ and P^{5+} into the zeolite framework.[29-37] Introduction of metal ions such as Cr^{5+}, Mo^{5+}, and $V^{4+/5+}$ was reported by solid-solid interaction at high temperature (773K).[35-37] Whittington *et al.*[34] have reported that the V-ions can be incorporated at cationic positions of the zeolite (ZSM-5) by chemical vapour deposition method. Recently, Bogdan [38] has reviewed the isomorphous replacement of various metal ions in the zeolite framework.

1.6 CHARACTERIZATION

The techniques normally used to find out whether substitution of metal ions in the framework of molecular sieves has really occurred or not are discussed below.

1.6.1 X-ray diffraction

It is an important technique to study metal substitution in the zeolite lattice. A change in the unit cell volume is a good proof for isomorphous substitution of metal ions in the zeolite lattice. Many refinement procedures such as DLS 76, PDP 11, Reitveld refinement, etc., have greatly improved the usefulness of XRD in the characterization of zeolites. Correlations between the values of unit cell parameters and the extent of incorporation of B, Fe, Ga, Ti, V and Cr have been reported.[39-43,28] Based on the difference between the M-O bond length of the substituted metal and that of Si-O, there could be a shrinkage of the unit cell volume as reported for B-ZSM-5[39] or an expansion, as noticed in Fe, Ti, and V.[40-43] For isomorphous and isovalent substitution, the unit cell volume can be calculated theoretically using Vegard's law[44] by the following equation :

$$V(x) = V(o) - V(o).\ [\ 1 - (d_{M\text{-}O} / d_{Si\text{-}O})^3].x$$

where x (= M / Si +M) is the degree of substitution, V(x) is the observed unit cell volume, V(o) is the unit cell volume of pure silicalite (the all silica isomorph) and d is the average bond length. Comparison between the theoretical and experimental values will give information about the ratio of the framework and nonframework metal ions in the silicate matrix.

1.6.2 Infrared spectroscopy

Infrared spectroscopy is a useful technique for characterizing isomorphous substitution of metal ions in the zeolite lattice.[45,46] The lattice vibrations of the zeolites in the infrared spectrum is observed in the range of 300 -1300 cm^{-1}. These vibrations can be classified into two groups, (i) internal vibrations of the TO_4 units or structure insensitive vibrations and (ii) vibrations due to external linkages of the TO_4 units or structure sensitive vibrations.[45,46] The major infrared band assignments are follows :

<u>Internal tetrahedra</u>	
Asymmetric stretching	1250 - 950 cm^{-1}
Symmetric stretching	720 - 650 cm^{-1}
T-O bending	420 - 500 cm^{-1}
<u>External linkages</u>	
Double ring	650 - 500 cm^{-1}
Pore opening	300 - 420 cm^{-1}
Symmetric stretching	750 - 820 cm^{-1}
Asymmetric stretching	1050 - 1150 cm^{-1}

Isomorphous substitution shifts both the symmetric and asymmetric framework vibrations. The substitution of lighter elements such as B shifts the framework vibrations to higher wave numbers[47], while heavier metal ions such as Fe, Ga and Ti shift the absorption bands to lower wave numbers.[48] In the case of titanium and vanadium silicates an additional asymmetric stretching vibration at around 960 cm^{-1} has been reported. The presence of a 960 cm^{-1} IR band in the case of metallosilicates (e.g., Ti, V and Sn) is a matter of debate. Originally, it was attributed to a stretching vibration of the Si-O bond in Si-O-M bridges.[26,27] Latter on, it has been suggested to the due to M=O (especially Ti=O) and silanol groups (ν Si-O)[50] associated with defect centres.

1.6.3 Electron spin resonance spectroscopy

ESR spectroscopy is a sensitive tool to understand the environmental symmetry of paramagnetic metal ions. ESR spectroscopy is useful in finding out the environment of the metal ions located in the framework or outside the zeolite matrix.[34] The identification of the different species present in the zeolite lattice has been carried out in the case of Cu^{2+}, Cr^{3+}, Fe^{3+} and V^{4+}.[25,35,51,52] ESR technique[35,37] has also been used to characterize solid-solid reactions between the zeolite and metal oxides of elements such as Cu, Cr, Fe, B, V and Mo. Electron spin echo modulation (ESEM) can provide quantitative data on the number of ligands to which the transition metal ion is coordinated and their interaction distances.[53] Recently, Goldfarb *et al.*[54] have reported extensive ESR studies over iron containing sodalite by electron nuclear double resonance technique (ENDOR). The interaction of Cu^{2+} complex has been studied by ESEM.[55] The oxidation state, position, environment and redox property of vanadium in micro and meso porous vanadosilicate molecular sieves with MFI, MEL and MCM-41 structures have been studied by ESR spectroscopy.[26,27,51]

1.6.4 UV-visible spectroscopy

UV-visible diffuse reflectance spectroscopy is a very useful tool for the identification of metal ion environments in the zeolite matrix. The diffuse reflectance bands at different wavelength regions provide information about the environment of the metal ions (e.g. Ti, Sn, V and Cr) in metallosilicate molecular sieves.[56-59]

For example, the position of the absorbance bands in the UV-visible region of some metal ions in different environments are given table 1. 2.

Table 1.2

UV-visible absorption of various metal ions.

Metal ion	Ionic environment	Absorbance (λ; nm)
Ti	Td	212
Ti	Oh	240
V	Td	233 - 285
V	Oh	333 - 500
Sn	SqPy	221 ± 3
Sn	Oh	255 ± 5

1.6.5 Nuclear magnetic resonance spectroscopy

High resolution solid state MAS NMR spectroscopy has emerged as a powerful technique for the investigation of zeolite structures and the location of isomorphously substituted metal ions.[60,61] Isomorphous substitution of metal ions (e.g., Al, Sn, Ti and V) in the lattice of silicalite has been monitored by NMR.[58,62-63]. ^{27}Al and ^{51}Sn MAS NMR have been used to obtain information regarding the coordination of Al and Sn in the silicalite lattice.[62,63] Both static and MAS NMR of ^{51}V provide information regarding the coordination and the location of vanadium in vanadium containing molecular sieves.[58,64]

MAS NMR of low silica zeolites can provide information regarding the connectivity of silicon with aluminium such as the number of (0,1,2,3 or 4) nearest neighbor Al^{3+} ions.[65] Recently, high resolution ^{29}Si MAS NMR has been used to obtain evidence about the connectivity of silicon with titanium in the lattice of ETS-10.[66] Broadening of ^{29}Si MAS NMR spectral lines of vanadosilicates has been attributed to the presence of vanadium in the lattice.[64]

^{1}H MAS NMR is a very useful technique to obtain the information regarding the different types of protons present in molecular sieves. Recently, the presence of Ti-OH and V-OH groups in titanium and vanadium containing molecular sieves has been identified by this technique.[67,64b]

Liquid state ^{29}Si NMR provides information regarding the interaction of titanium or vanadium with the silicate species in the gel phase during the synthesis of TS-1[68] and VS-2.[69]

1.6.6 Sorption and diffusion studies

Zeolites and porous crystalline materials possess the ability to sorb selected molecules inside the channels and cavities. Studies on the sorption characteristics of zeolites can provide accurate information about diffusion properties and pore blockages due to metal substitution in the zeolite lattice. In liquid phase oxidation over metallosilicate molecular sieves, adsorption and diffusion properties control the overall rate of the chemical reaction at the catalytic site. Barrer,[70] Ruthvan,[71] and Palekar[72] have reviewed the sorption properties of the molecular sieves with special emphasis on catalytic properties. Sorption of various gases and vapours on both natural and synthetic zeolites has been extensively studied.[70,73,74]

1.7 OXIDATION PROPERTIES

The catalytic properties of zeolites in selective oxidation reactions have been reviewed by Tagiev.[75] The liquid phase oxidation of various organic molecules over metallosilicates, especially those containing Ti and V are of current interest in the synthesis of fine chemicals.[76,77] Hydroxylation of phenol is already being carried out in a commercial process using TS-1 as the catalyst. Prasad Rao *et al.*[78] have reported the liquid phase oxidation of various organic molecules such as the oxyfunctionlization of n-alkanes and cyclohexane, hydroxylation of benzene and phenol, oxidation of toluene, aniline and sulfides over vanadosilicate molecular sieves (VS-2). Recently, tin silicate[57,63] and chromium silicate[79] molecular sieves have also been used for the liquid phase oxidation of organic compounds using dilute H_2O_2 as the oxidant.

The vapour phase oxidation of methane to carbondioxide over metal ion exchanged X zeolite has been reported.[80] Vanadium containing mordenite has been claimed to have very high activity in the oxidation of H_2S to sulfurdioxide.[81] Wan *et al.*[82] and Bellusi *et al.*[83] have studied the vapour phase oxidation of ethanol over transition metal incorporated microporous aluminophosphate molecular sieves. Recently, the selective oxidation of propane[84] and oxidative dehydrogenation of ethanol[85] have been reported over vanadium containing molecular sieves using molecular oxygen as oxidant.

1.8 TOPOLOGY OF MFI, MEL AND BEA STRUCTURES

ZSM-5 (MFI)[86] and ZSM-11 (MEL)[87] are two extreme members of the "pentasil" family of zeolites. The secondary building units are five membered rings. The X-ray diffraction patterns of the two molecular sieves are shown in figure 1.1.

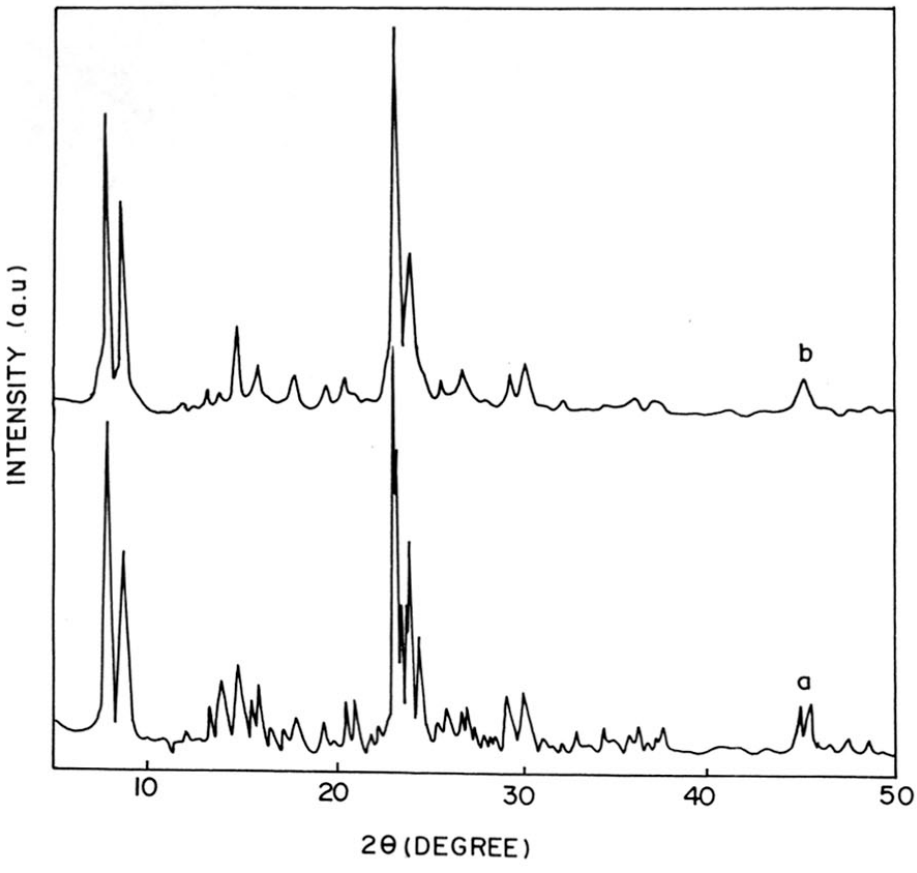

Fig. 1.1 X-ray diffraction patterns of the calcined forms of ZSM-5(MFI) (a) and ZSM-11(MEL) (b).

The structures of ZSM-5 and ZSM-11 have been reported by Kokotailo and coworkers.[86,87] The characteristic structural properties of MFI and MEL types are presented in table 1.3. In ZSM-5 and ZSM-11 structures, the five membered ring secondary building units (Fig.1.2a) are joined along [100] to form chains (Fig. 1.2b), which pack laterally along the [100] plane. The ZSM-5 structure is generated when the adjacent [100] sheets (Fig. 1.2c) are related to one another by inversion (I) and ZSM-11 structure is formed when the [100] sheets are related to one another by mirror symmetry (σ). Infinite series of intermediate structures may be obtained by applying reflection transformations (σ) to ZSM-5 or inversion transformations (I) to ZSM-11. The transformations lead to the channel system. This results in two types of intersecting channels in ZSM-5, with 10-membered ring openings, one with an elliptical (0.51 x 0.53 nm) and the another with a circular (0.55 nm) cross section. In ZSM-11, both the channels are identical (0.51 x 0.55 nm). The cavities formed in ZSM-5 by the intersection of these channels are equivalent, having a maximum diameter of 0.9 nm. Two types of intersections exist in ZSM-11 one possessing the same volume as that present in ZSM-5 and the other one with a larger volume (30% excess). The calculated channel length (based on theoretical crystallographic data) for ZSM-5 and ZSM-11 are 8.8 and 8.0 nm, respectively.[88,89]

Zeolite beta (β; BEA) is a large pore crystalline material and is a highly intergrown hybrid of three distinct but closely related structures, possessing a three-dimensional pore system with 12-membered rings (Fig. 1.3).[90-92] It belongs to a family of zeolites, the end members of which have tetragonal (polytype A) and monoclinic (polytypes B & C) symmetries (table 1.4). In both the crystallographic systems, 12-membered ring straight channels are present in two crystallographic directions, while the 12-membered ring channel in the third crystallographic direction is sinusoidal. The main difference between the

Table 1.3

Comparison of structural data of MFI and MEL topologies.

Structural parameters	MFI	MEL
Secondary Building units	Complex 5-1	Complex 5-1
Framework density (No. of T-atoms per 1000 $Å^3$)	17.9 (Si +Al)	17..6 (Si +Al)
Channels	Three dimensional intersecting 10-membered rings 5.2 x 5.6 A and 5.1 x 5.5 A	10 membered ring, intersecting 5.3 x 5.4 A
Fault planes	[100]	[100]
No. of T-atoms (Si + Al) per unit cell	96	96
No. of non equivalent T atoms	12	7
unit cell composition	$Na_nAl_nSi_{96-n}O_{192}$, $16H_2O$ (with $n < 27$ and typically about 3)	$Na_nAl_nSi_{96-n}O_{192}$, $16H_2O$ (with $n < 16$ and typically about 3)
crystal symmetry / space group symmetry	orthorhombic / P_{nma}	Tetragonal / 14m2
unit cell dimensions	a = 20.1 Å, b = 19.9 Å, c = 13.4 Å,	a = b = 20.1 Å, c = 13.4 Å,

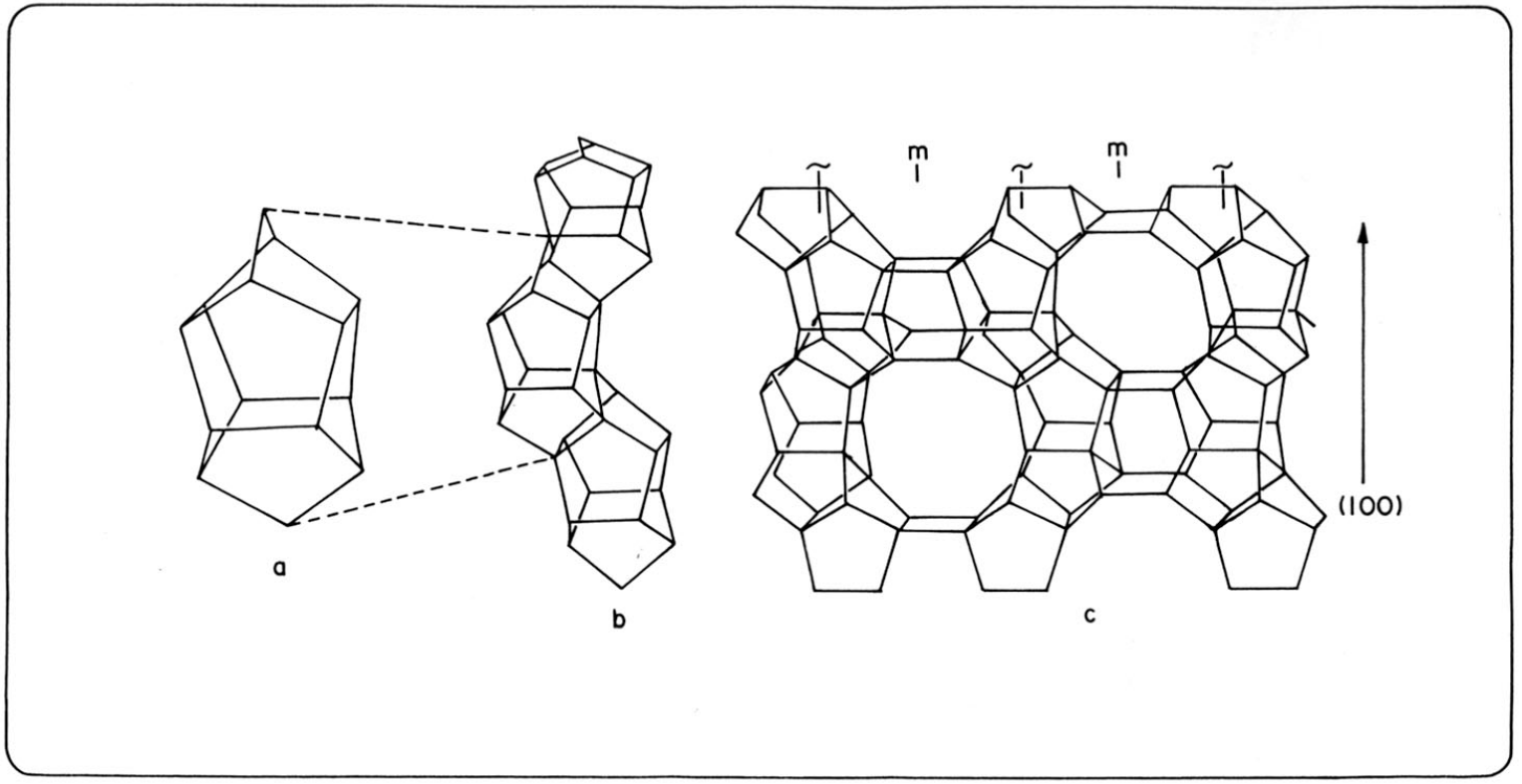

Fig. 1.2 Building blocks of pentasil structures : a : pentasil unit (PU), b : secondary building unit (SBU), c: pentasil layer.

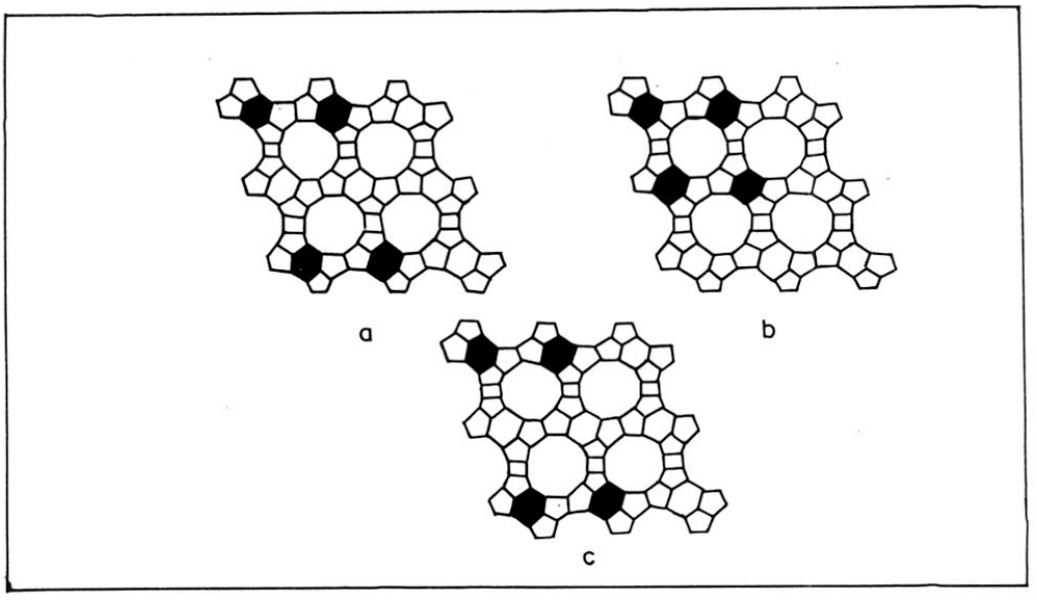

Fig. 1.3 Structure of zeolite β : a) Polytype A (110), b) Polytype B (110), and c) Polytype C (110).

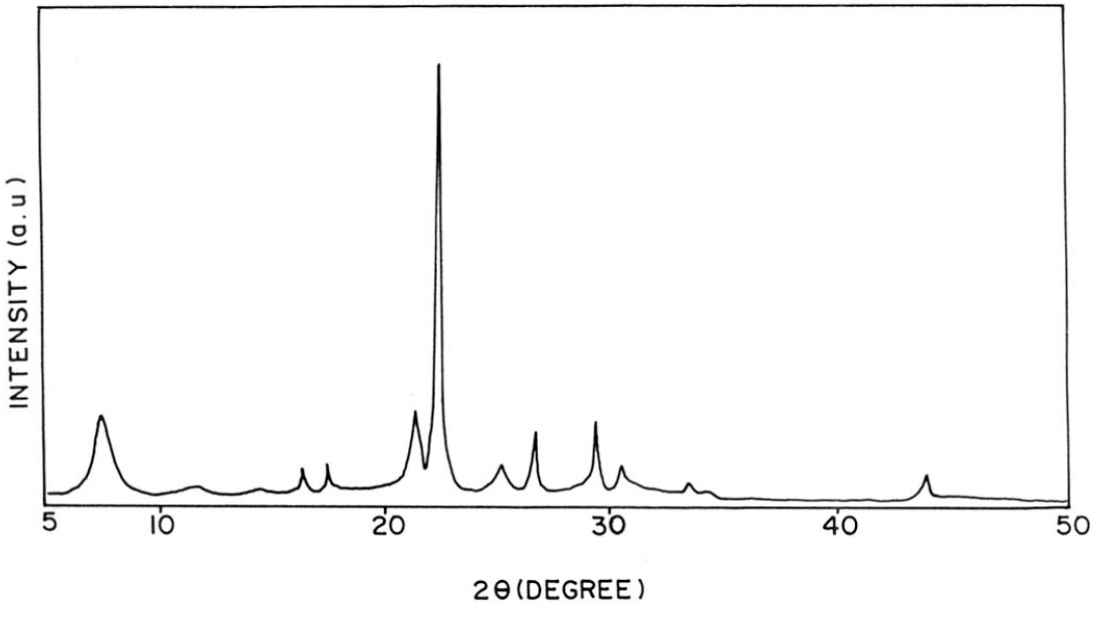

Fig. 1.4 X-ray diffraction pattern of Al-β.

Table 1.4

Structural data of zeolite β (BEA) structure.

Structural parameters	Polytype A	Polytype B	Polytype C
Secondary building units	4(S5R) ↔ D6R ↔ 2(S4R)	4(S5R) ↔ D6R ↔ 2 (S4R)	4 (S5R) ↔ D6R ↔ 2 (S4R)
Channels	12 membered ring, intersecting.	12 membered ring, intersecting	12 membered ring, intersecting
No. of non equivalent T-atoms	9	9	32
Crystal symmetry / space group symmetry	Tetragonal, P_{4122}	Monoclinic, $C_{2/c}$	Monoclinic, $P_{2/c}$
Unit cell dimensions	a = b = 12.469Å, c = 26.330 Å. $\alpha = \beta = \gamma = 90^0$	a = 17.634 Å, b = 17.635 Å, c = 14.416 Å. β = 107.52 [chiral structure]	a = b =12.470 Å, c = 27.609 Å, β = 114.04

polytypes is in the pore dimensions of the straight channel, which is narrower for the tetragonal structure. Moreover, the sinusoidal channels are more tortuous in the tetragonal compared to those in the monoclinic structure. The characteristic structural properties of zeolite β are presented in table 1.4. The X-ray diffraction pattern of Al-β is presented in figure 1.4.

1.9 VANADIUM CONTAINING MOLECULAR SIEVES

Vanadium containing ZSM-5 was first synthesized by Marosi in 1978.[93] The resulting zeolite (V-ZSM-5) was claimed to be a useful catalyst in cracking and isomerization reactions. Xu Renen *et al.*[94] showed the possibility of vanadium being present in three different oxidation states (V^{3+}, V^{4+} and V^{5+}) in zeolite molecular sieves. Kucherov and Slinkin[35] reported the introduction of V^{4+} ions into extrafrmework cationic positions by solid state reaction. Recently, El.Malki *et al.*[37] have reported the synthesis of V-Al-β by solid state reactions of Al-β with V_2O_5 at high temperatures. Miyamoto *et al.*[95] have reported the hydrothermal synthesis of vanadium containing molecular sieves in the presence of aluminium. These vanadosilicates have been reported to have high catalytic activity and selectivity in the oxidative dehydrogenation of propane to propylene when compared to other metallosilicate molecular sieves.[96] These were also found to be good in the selective ammoxidation of xylenes and propane[97,98] and in the oxidation of butadiene to furan.[99]

Fejes *et al.*[100] and Rigutto *et al.*[27a] have reported the hydrothermal synthesis of aluminium containing VS-1 and their characterization by various physicochemical techniques (e.g., XRD, IR, UV-VIS, ESR, NMR and TPR). It was reported that V ions are present as V^{4+} in a square pyramidal environment in the as-synthesized samples and in tetrahedral coordination in calcined samples. Kornatowski *et al.*[101] have reported that both V^{4+} and V^{5+} ions are present in the as-synthesized KVS-5 molecular sieves. Prasad Rao *et al.*[27b] have

reported aluminium free vanadium containing medium pore molecular sieves of MEL structure (VS-2). Tuel *et al.*[102] and Chatterjee *et al.*[103] have reported the incorporation of vanadium in other medium pore zeolites (ZSM-48, EU-1 and ZSM-22)

Vanadium incorporation in a large pore molecular sieve (V-NCL-1) was reported for the first time by Reddy and coworkers.[104] After that, the incorporation of vanadium was achieved in two large pore molecular sieves V-ZSM-12 (MTW)[64a] and Mordenite.[105] The incorporation of vanadium in extralarge pore molecular sieves (VPI-5) has recently been published.[106] Synthesis of mesoporous molecular sieves are at present of interest in the field of catalysis, as large organic molecules can diffuse easily through the large pores of these materials. The incorporation of vanadium in mesoporous molecular sieves (MCM-41) has been also reported.[107] Reddy *et al..*[108] reported the room temperature synthesis of mesoporous vanadium containing molecular sieves. Recently, Morey *et al.*[109] has incorporated vanadium in MCM-48 lattice by a post synthesis method. Centi *et al*[58] have reported that at least two different V-species could be identified in vanadium silicalite with MFI structure by different physicochemical techniques. It has been claimed that vanadium is well dispersed in the solid matrix but it was not clear whether vanadium was incorporated in the framework positions or not. Recently, Moudrakovski *et al.*[64a] reported based on ESR and NMR studies) that V is connected to three silicon atoms through oxygen and it is located near the defect sites in V-ZSM-12 molecular sieves.

The liquid phase oxidation of various organic molecules using H_2O_2 as the oxidant was reported for the first time over VS-2.[78] Subsequently, several reports have appeared on liquid phase oxidation over microporous (medium and large) and mesoporous molecular sieves.[77,107] The reactivity has been suggested to be due to the easy reducibility of the framework V-species.[78]

1.10 SCOPE OF THE THESIS

Although there are plenty of reports available on vanadosilicate molecular sieves, no detailed reports are available, on how and in which form the vanadium species enter the lattices of silicalite molecular sieves during hydrothermal synthesis. Two basic considerations helped to plan the present studies : i) The nature of V-species depends on the pH, the vanadium concentration and the nature of the atmosphere (aerobic/anaerobic) and ii) the Pauling radius ratio rule should prefer the smaller V^{5+} (r = 0.046 nm) rather than V^{4+} (r = 0.059 nm) in the Si^{4+} (r = 0.026 nm) lattice. The excess charge may be compensated by the presence of a stable V=O bond. Based on these considerations, the synthesis of vanadosilicate molecular sieves (with different topologies, MFI, MEL and BEA) were carried out at different pH, different vanadium concentration and aerobic/anaerobic conditions. The role played by the different V-species in the molecular sieve on its catalytic activity and selectivity has not been reported in detail. The work presented in this thesis is aimed at the identification of the different vanadium species in the gel and crystalline phases in two medium pore vanadium containing molecular sieves (V-MFI and V-MEL) and a novel large pore V-Al-β molecular sieve. The catalytic activities and selectivities of the different V-species present in the vanadium containing molecular sieves has been investigated.

The major objective of this thesis is to study (i) the effect of pH on the incorporation of V in V-MFI (VS-1), (ii) the effect of synthesis atmosphere and vanadium concentration (at high pH) on the synthesis of V-MEL (VS-2), (iii) the synthesis of novel large pore vanadium containing molecular sieves (V-Al-β) of the BEA structure and (iv) the activities of various vanadium containing molecular sieves in liquid and vapour phase oxidation reactions.

Chapter II describes the methodologies adopted in the synthesis of vanadium containing medium pore molecular sieves belonging to the MFI (VS-1) and MEL (VS-2) structure types and the large pore molecular sieve of BEA structure (V-Al-β). The experimental procedures used in characterization and in catalytic reactions are also discussed.

Chapter III deals with the physicochemical characterization of (a) V-MFI (VS-1) synthesized in acidic and alkaline media, (b) V-MEL (VS-2) synthesized in inert and ambient atmosphere with different vanadium concentrations and (c) V-Al-β (BEA) synthesized with different vanadium concentrations. The influence of synthesis parameters such as the effect of Si/V, H_2O/SiO_2, R/SiO_2, SiO_2/Al_2O_3 ratios and temperature on the crystallization are also discussed in this chapter.

Chapter IV describes the liquid phase oxidation of phenol and toluene using H_2O_2 as the oxidant, the influence of the promoter (pyridine α-carboxylic acid; picolinic acid) on the reaction and the vapour phase oxidative dehydrogenation of ethanol in air over three different molecular sieves (V-MFI, VMEL-2 and V-Al-β).

Chapter V summarizes the present investigation and presents the conclusions drawn from these studies.

1.11 REFERENCES

1. Breck, D. W., in "*Zeolite Molecular Sieves*", Wiley Pub., New York, 1974.
2. Szostak, R., Molecular Sieves : Principles of synthesis and identification, Van Nostrand Rheinhold, New York (1989).
3. Sand, L. B., *Ecom. Geol.*, 191 (1967).
4. Flanigen, E. M., *ACS Symp. Ser.*, **121,** 119 (1973).
5. Moretti, E., Contesa, S., and Padovan, M., *Chim. Ind.*, 671 (1985).
6. Barrer, R. M., Hydrothermal Chemistry of Zeolites, Academic press, New York (1982).
7. Meier, W. M., and Olson, D. H., Atlas of zeolitic structure types, 2nd Ed. (1987).
8. Bragg, W. L., The atomic structure of Minerals, Cornell University press, Ithaca, New York (9137).
9. Meier, W. M., Molecular Sieves, *Soc. Chem. Ind., London*, p.67 (1968).
10. Flanigen, E. M., Proc. of 5th Int Zeolite Conf. Ed. L. V. C. Rees, Heydon London, p.760 (1980).
11. Wilson, S. T., Lok, B. M., Messina, C. A., Cannan, T. R., and Flanigen, E. M., *J. Amer. Chem. Soc.*, **104,** 1146 (1982).
12. Davis, M. E., Saldarriage, C., Montes, C., Graces, J., and Crowder, C., *Nature,* **331,** 968 (1988).
13. Estermann, M., Me Cusker, L. B., Bacrlocher, Ch., Morrouche, A., and Kessler, H., *Nature,* **352**, 320 (1991).
14. Beck, J. S., Vartuli, J. C., Roth, W. J., Leonowicz, M. E., Kresge, C. T., Schmidt, K. D., Chu, C. T. W., Olson, D. H., Sheppard, E. W., Mac Cullen, S. B., Higgins, J. B., Schlenker, J. L., *J. Am. Chem. Soc.*, **114,** 10834 (1992).
15. Monnier, A., Schuth F., Huo, Q., Kumar, D., Margolese, D., Maxwell, R. S., Stucky, G. D., Krishnamurty, M., Petroff, P., Firouzi, A., Janicke, M., Chmelka, B. F., *Science* 261 (1993).
16. Wilson, S. T., and Flanigen, E. M., *ACS Symp. Ser.*, **298,** 329 (1988).
17. Kraushaar, C. B., Horgervorst, W. G. M., Andrea, P. R., emeis, C. A., and Stork, W. H. J., *Stud. Surf. Sci. Catal.*, **69**, 231 (1991).
18. Montes, C., Davis, M. E., Murray, B., wasw and Narayana, M., *J. Phys. Chem.*, **94,** 6431 (1990).
19. Lok, B. M., Messina, C. A., Patton, R. L., Gayek, R. T., Cannan, T. R., and Flanign, E. M., US Pat. 4,400,870 (1984).

20. Pauling, L., in "The Nature of Chemical Bond", Gaskhimizdat, Moscow (1947).
21. Goldsmith, J. R., *Min. Mag.*, **28**, 952 (1952).
22. Barrer, R. M., Baynham, J. W., Bultitride, F. W., and Meier, W. M., *J. Chem. Soc.*, 195 (1959).
23. Chu, C. T. W., Kuhl, G. H., Lago, R. M., and Chang, C. D., *J. Catal.*, **93,** 451 (1985).
24. Dyer, A., in "An Introduction to Zeolite Molecular Sieves", *Soc. Chem. Ind. London* 186 (1967).
25. Ratnasamy, P., and Kumar, R., *Catal. Today,* **9**, 329 (1991).
26. a) Notari, B., *Stud. Surf. Sci. Catal.*, **37,** 413 (1988).
    b) Kornatowski, J., Sychev, M., Goncharuk, V., and Baur, W, H., *Stud. Surf. Sci. Catal.*, **135**, 581 (1990).
27. a) Rigutto, M. S., and Van Bekkum, H., *Appl. Catal.*, **68**, 21 (1991).
    b) Prasad Rao, P. H. R., Ramaswamy, A. V., and Ratnasamy, P., *J. Catal..*, **137,** 225 (1991).
28. a) Klotz, M. R., US. Pat., 4,299,808 (1981).
    b) Pastore, H. O., Stein, E., Davanzo, C. U., Vichi, E. J. S., Nakamura, O., Baesso, M., Silva, E., and Vargas, H., J. C. S., Chem. Commun.., 772 (1990).
29. Rschetlowski, W., Einicke, W. D., Meier, B., Brunner, E., and Ernst, H., *Stud. Surf. Sci. Catal.*, **69**, 119 (1991).
30. Hamder, H., and Klinowski, J., *ACS Symp. Ser.*, **398,** 329 91988).
31. Yashima, T., Yamagishi, K., Namba, S., Nakata, S, and Asaoka, S., *Stud. Surf. Sci. Catal.*, **37,** 175 (1988).
32. Endoh, A., Nishimiya, K., Tsutsumi, K., and Takaishi, T., *Stud. Surf. Sci. Catal.*, **46,** 779 (1989).
33. Kraushar, C. B., and Van Hoof, J. H. C., *Catal. Lett.*, **1**, 81 (1988).
34. Whittington, B. I., and Anderson, J. R., *J. Phys. Chem.*, **95,** 3306 (1991).
35. a) Kucherov, A. V., and Slinkin, A. A., *Zeolites* **7**, 38 (1987).
    b) Kucherov, A. V., and Slinkin, A. A., *Zeolites* **7,** 4 (1987).
    c) Kucherov, A. V., and Slinkin, A. A., *Zeolites* **8**, 110 (1988)
36. Sass, C. E., Chem, X., Kevan, L., *J. Chem. Soc., Faraday, Trans.*, **86**, 189 (1990).
37. El.Mekki El.Malki, Davidson, A., Massiani, P., Barthomeuf. D., Che, M., *Am. Chem. Soc.,*

Div, Pet, Chem., **40**, 114 (1995).

38. Bogdan, S., *Heterog. Chem. Rev.*, **3(3),** 203 (1996).
39. Mayers, B. L., Wly, S. R., Kutz, N. A., Kaduk, J. A., and VanderBossche, E., *J. Catal.*, **91**, 352 (1985).
40. Szostak, R., and Thomas, T. L., *J. Catal.*, **100**, 555 (1986).
41. Simmons, D. K., Szostak, R., Agrawal, P. K., and Thomas, T. L., *J. Catal.*, **106,** 287 (1967).
42. Perego, G., Bellusi, G., Corno, C., Taramasso, M., Buonomo, F., and Esposito, A., *Stud. Surf. Sci. Catal.*, **28**, 119 (1986).
43. Ratnasamy, P., Kotasthane, A. N., Shiralkar, V. P., Thangaraj, A., and Ganapathy, S., *ACS Symp. Ser.* **398,** 405 (1989).
44. L. V. Azaroff., "Introduction of solids", McGraw-Hill, New York, p. 290, 1960.
45. Zeolite Chemistry and Catalysis, Ed, Rabo *et al.* **171,** 181 (1976).
46. Zeolite Chemistry and Catalysis, Ed, Rabo *et al.* **171**, 80 (1976).
47. Kutz, N. A., Heterogeneous Ctalysis-II, Ed. Shapiro *et al.* P.121 (1984).
48. Szostak, R., and Thomas, T. L., *J. Catal.*, **101**, 549 (1986).
49. Huybrechts, D. R. C., Buskens, P. A., Jacobs, P. A., *J. Mol. Catal.*, **71**, 129 (1992).
50 Camblor, M. A., Corma, A., and Perez-Pariente, J., *J. Chem. Soc., Chem. Commun.*, 557 (1993).
51. Fejes, P., Marsi, I., Kirisci, I., Halasz, J., Hannus, I., Rockenbauer, A., Tasi, Gy., Korecz, L., and Schobel, Gy., *Stud. Surf. Sci.Catal.*, **69,** 173 (1991).
52. Sass, C. E., and Kevan, L., *J. Phys. Chem.*, **92,** 14 (1988).
53. Kevan, L., In time domain electron spin resonance, Ed. L. Kevan and R. N. Schwartz (Wiley-Interscience, New York, 1979) Chap.8.
54. a) Goldfarb, D., Bernado, M., Strohmaier, K. G., Vaughen, D. E. W., Thomann, H., *Stud. Surf. Sci. Catal.*, **84,** 403 (1994).

    b) Goldfarb, D., Bernado, M., Strohmaier, K. G., Vaughen, D. E. W., Thomann, H., *J. Am. Chem. Soc.*, **116**, 6344 (1994).
55. a) Poeppl, A., Baglione, P., Kevan, L., *J. Phys. Chem.*, **99,** 14156 (1995).

    b) Peppl, A., Kevan, L., *Langmuir*, **11**, 4486 (1995).
56. a) Boccuti, M. R., Rao, K. M., Zecchina, A., Leofanti, G., and Petrini, G., *Stud. Surf. Sci. Catal.*, **48,** 133 (1989).

    b) Thangaraj, A., Kumar, R., Mirajkar, S. P., and Ratnasamy, P., *J. Catal.*, **130,** 1 (1991).

57. Ph..D thesis submitted to "The University of Poona", India, by Nawal Kishor Mal on Jan'97.

58. Centi, G., Perathoner, S., Trifiro, F., Abousaus, A., Aissi, C. F., Guelton, M., *J. Phys. Chem.*, **96,** 2617 (1992).

59. Inoe, K. G., Vostrikova, L. A., Ptrova, A. V., and Mastikhin, V. M., in proceedings 8th Int. Cong. on Catal., Berlin, Vol.4., p.519 (1984), Verlag. Chemie, Weinheim.

60. Klinowski, J., *Progress in NMR spectroscopy, (Ed. Emsley, et al.) Pregamon Press, GB.* **17,** 237 (1984).

61. Englehardt, G., and Michel, D., High resolution solid state NMR of Zeolites and related systems, John Wiley and Sons., London, (1987).

62. Muller, D., Gessner, W., Behrens, H. J., and Scheler, G., *Chem. Phys. Lett.*, **79,** 59 (1981).

63. Mal, N. K., Ganapathy, S., and Ramaswamy, A. V., *J. Chem. Soc., Chem. Commun.*, 1933 (1994).

64. a) Moudrakovski, I., Sayari, A., Ratcliffe, C. I., Ripmeester, J. A., and Preston, K. F., *J. Phys. Chem.*, **9**, 10895 (1994).

b) Sen, T., Rajamohanan, P. R., Ganapathy, S., and Sivasanker, S., *J. Catal.*, **163,** 354 (1996).

65. Van Hoof, J. H. C., and Roelofsen, A., *Stud. Surf. Sci. Catal.*, **58,** 242 (1992).

66. Anderson, M. W., Terasaki, O., Ohsuma, T., Philippou, A., *Nature,* **367,** 347 (1994).

67. Hauka, S., Lakomaa, E. L., and Root, A., *J. Phys. Chem.*, **97,** 5085 (1993).

68. Thangaraj. A., Sivasanker, S., *J. Chem. Soc., Chem. Commun.*, 123 (1992).

69. Sen, T., Ramaswamy, V., Ganapathy, S., Rajamohanan, P. R., and Sivasanker, S., *J. Phys. Chem.*, **100,** 3809 (1996).

70. Barrer, R. M., *Proc. Roy. Soc. A.*, **167,** 392 (1938).

71. Karger, J., and Ruthven, D. M., *Zeolites,* **9,** 267 (1989)

72. Palekar, A., and Rajadyaksha, R. A., *Catal. Rev. Sci. Eng.*, **28,** 371 (1986).

73. Barrer, R. M., *Pure Appl. Chem.*, **52,** 2143 (1980).

74. Vadrine, J. C., Auroux, A., and Coudurier, G., Catalysic Materials, Relationship between Structure and Reactivity., Ed. Whyte, *Amer. Chem. Soc., Washington, D. C.*, 253 (1984).

75. Tagiev, D. B., and Minachev, Kh. M., *Russ. Chem.. Rev.*, **50,** 1009 (1981).

76. Notari, B., *Stud. Surf. Sci. Catal.*, **37,** 413 (1988).

77. Ramaswamy, A. V., Sivasanker, S., and Ratnasamy, P., *Microporous, Mater.*, **2(5),** 451 (1994).

78. a) Prasad Rao, P. R. H., Ramaswamy, A. V., *J. Chem. Soc., Chem. Commun.*, 1245 (1992).

b) Prasad Rao, P. R. H., Ramaswamy, A. V., and Ratnasamy, P., *J. Catal.*, **141(2),** 604 (1993).

c) Prasad Rao, P. R. H., Ramaswamy, A. V., and Ratnasamy, P., *Appl., Catal., A* **93 (2),** 123 (1993).

d) Prasad Rao, P. R. H., Belhekar, A. A., Hedge, S. G., Ramaswamy, A. V., and Ratnasamy, P., *J. Catal.*, **141(2),** 595 (1993).

79. a) Chem, J. D., Lempers, H. E. B., and Sheldon, R. A., *Stud. Surf. Sci. Catal.*, **92,** 754 (1995).

b) Joseph, R.., Sasidharan, M., Sudalai, A., and Rabindranathan, T., *J. Chem. Soc., Chem. Commun.*, 1523 (1995).

c) Jayachandran, B., Sasidharan, M., Sudalai, A., and Rabindranathan, T., *J. Chem.Soc., Chem. Commun.*, 1523 (1995).

80. Rudham, R., and Sanders, M. K., *J. Catal.*, **27,** 287 (1972).

81. Hass, R. H., Hansford, R. C., Hennig, H., US. Pat.. 4,088,743 (1978).

82. Wan, B. Z., Huang, K., Yang, T. C., and Tai, C-Y., *J. Chin. Insti. Chem. Engg.* **22,** 17 (1975).

83. Bellusi, G., and Rigutto, M. S., in "Advance Zeolite Science and Applications", *Stud. Surf. Sci. Catal.*, **85**, 179 (1994).

84. a) Fejes, P., Halasz, J., Kiricsi, I., Kele, Z., Tasi, Gy., Hannus, I., Fernandez, C., Nagy, J. B., Rockenbaur, A., and Schobel, Gy., Proceedings of 10th inter. Cong. on Catalysis., 19-24 July, 1992, Budapest, Hungary, 1993. Elsevier Science Publishers.

b) Centi, G., and Trifiro, F., *Appl. Catal., A.* **143(1),** 3 (1996).

85. Kannan, K., Sen, T., and Sivasanker, S., *J. Catal.*, (in press).

86. Kokotailo, G. T., Chu, P., Lawton, S. L., and Meier, W. M., *Nature,* **272,** 437 (1978).

87. Kokotailo, G. T., Chu, P., Lawton, S. L., and Meier, W. M., *Nature,* **275,** 119 (1978).

88. Gabellica, Z., Derouane, E. G., and Blom, M., *ACS Symp Ser.*, **248,** 219 (1984).

89. Jacobs, P. A., Beyer, H. K., and Vaylon, J., *Zeolites,* **1**; 161 (1981).

90. Treacy, M. M. J., and Newsam, J. M., *Nature,* **332,** 249 (1988).

91. Newsam, J. M., Treacy, M. M. J., Koetsier, W. T., and deGruyter, C. B., *Proc. R. Soc. London, A* **420,** 375 (1988).

92. Higgings, J. B., Lapierre, R. B., Schlenker, J. L., Rohrman, A. C., Wood, J. D., Kerr, G. T., and Rohrbaugh, W. J., *Zeolites,* **8**, 446 (1988).

93. Marosi, L., Stabenow, J., and Schwarzmann, M., Ge. Pat.., 2,831,631 (1978).

94. Renen, Xu., Wenguin, P., *Stud. Surf. Sci. Catal.,* **24**, 27 (1985).

95. Miyamoto, A., Medhanavyan, D., and Inui, T., Proc. 9th inter. Cong. on Catalysis., (M. J. Philip and M. Ternan, Eds.).

96. Zatorski, L. W., Centi, G., Neito, J. L., Trifiro, F., Bellusi, G., and Fattore, V., *Stud. Surf. Sci. Catal.,* **49B**, 1243 (1989).

97. Cavani, F., Trifiro, F., Habersberger, K., and Tvaruzkova, Z., *Zeolites,* **8**, 12 (1988).

98. Miyamoto, A., Iwamoto, Y., Matsuka, H., and Inui, T., *Stud. Surf. Sci. Catal.,* **49B**, 1233 (1989).

99. Tvaruzkova, Z., Centi, G., Jiru, P., and Trifiro, F., *Appl. Catal.,* **19,** 307 (1985).

100. Fejes, P., Halasz, J., Kiricsi, I., Halasz, J., Hannus, I., Rockenbaur, A., Tasi, Gy., Korecz, L., and Schobel, Gy., *Stud. Surf. Sci. Catal.,* **69**, 173 (1991).

101. a) Kornatowski, J., Sychev, M., Gouchoruk, V., and Baur, W. H., *Stud. Surf. Sci. Catal.,* **69,** 173 (1991).

b) Kornatowski, J., Wichterlova, B., Rozwadowski, M., Baur, W. H., *Stud. Surf. Sci. Catal.,* **84**, 117 (1994).

102. Tuel. A., and Ben Taarit, Y., *Zeolites* **14,** 18 (1994).

103. Chatterjee, M., Bhattacharya, D., Venkatathri, N., and Sivasanker, S., *Catal. Lett.,* **35,** 313 (1995).

104. Reddy, K. R., Ramaswamy, A., V., Ratnasamy, P., *J. Catal.,* **143,** 275 (1993).

105. Geon-Joong, K., Dong-Sucho, Kwang-Ko, K., Wan-Suk, K., Jong-Ho, K., and Hiroshi, S., *Catal. Lett.,* **31**, 91 (1995).

106. Chaudhari, K., Das, T. K., Chandwadkar, A. J., Chandwadkar, J. G., and Sivasanker, S., *Stud. Surf. Sci. Catal.,* **105,** 253 (1997).

107. Reddy, K. M., Moudrakovski, I., Sayari, A., *J. Chem. Soc., Chem. Commun.,* 1049 (1994).

108. Reddy, J. S., and Sayari, A., *J. C. S. Chem. Commun.,* 2231 (1995).

109. Morey, M., Davidson, A., Eckert, H., and Stucky, G., *Chem. Mater.,* **8,** 486 (1996).

CHAPTER II

EXPERIMENTAL

2.1 SYNTHESIS

The reactants used in the synthesis of the vanadosilicates, V-MFI (VS-1), V-MEL (VS-2) and the vanadoalumnosilicate V-Al-β (BEA), silicalite-1, silicalite-2 and Al-β are listed in table 2.1.

Table 2.1

Specification of the chemicals used in synthesis of molecular sieves.

Sr. No.	Chemical name	Chemical formula	Purity (%)
1.	Tetraethyl orthosilicate, TEOS (Aldrich)	$Si(OC_2H_5)_4$	98
2.	Fumed silica (Sigma)	SiO_2	100
3.	Cab-o-sil (Sigma)	SiO_2	100
4.	Tetrabutyl ammonium hydroxide (Aldrich)	$(C_4H_9)_4NOH$	40% aqueous solution
5.	Tetraethyl ammonium hydroxide (Aldrich)	$(C_2H_5)_4NOH$	40 % aqueous solution
6.	Tetrapropyl ammonium hydroxide (Aldrich)	$(C_3H_7)_4NOH$	1M aqueous solution
7.	Tetrapropyl ammonium bromide (Aldrich)	$(C_3H_7)_4NBr$	100
8.	Aluminum sulfate (Loba Chemie, India)	$Al_2SO_4,16H_2O$	99.2
9.	Vanadyl sulfate trihydrate (Aldrich)	$VOSO_4, 3H_2O$	99.9
10.	Ammonium metavanadate (Loba Chemie, India)	NH_4VO_3	99.5
11.	Vanadium pentoxide (Aldrich)	V_2O_5	99.9
12.	Ammonium fluoride (Loba Chemie, India)	NH_4F	98.2

The hydrothermal synthesis were carried out using 100 ml capacity stainless steel autoclaves (Fig. 2.1) under static conditions. Before use, the reactors were thoroughly cleaned with 35% HF and scraped and polished with a carbon brush to minimize the seeding effect of residual crystalline products. Synthesis in acidic medium was carried out in a teflon-lined autoclave.

2.1.1 Vanadosilicate, V-MFI (VS-1)

Synthesis in alkaline medium :

Synthesis of VS-1 in alkaline medium, V-MFI (B; basic) was carried out by hydrothermal methods following reported procedures[1-5] using gels of the following molar composition: SiO_2 : 0.0125 VO_2 : 0.33 TPAOH : 22 H_2O (TPAOH = tetrapropyl ammonium hydroxide). In a typical preparation, the following procedure was adopted : 40 ml of 1M tetrapropyl ammonium hydroxide was added slowly to 25g of tetraethyl orthosilicate solution. The mixture was stirred for about 1h. A solution of 0.65g of $VOSO_4$, $3H_2O$ in 6 ml water was added to the above mixture. The resultant mixture was stirred for the another 3h. The pH of the light green gel was 11.1. The gel was allowed to crystallize at 443K for 2 days under static conditions. The crystalline material was filtered, washed with deionized water, dried (383K), and calcined (823K for 12h). The calcined material was white under dehydrated conditions and pale yellow in the hydrated form.

Synthesis in acidic medium :

Synthesis of VS-1 in acidic medium, V-MFI(A; acidic) was carried out using the following molar composition: SiO_2 : 0.0125 VO_2 : 0.25 TPABr : NH_4F : 70 H_2O. In a typical preparation, the following procedure was used: NH_4F (2.47g) and tetrapropy

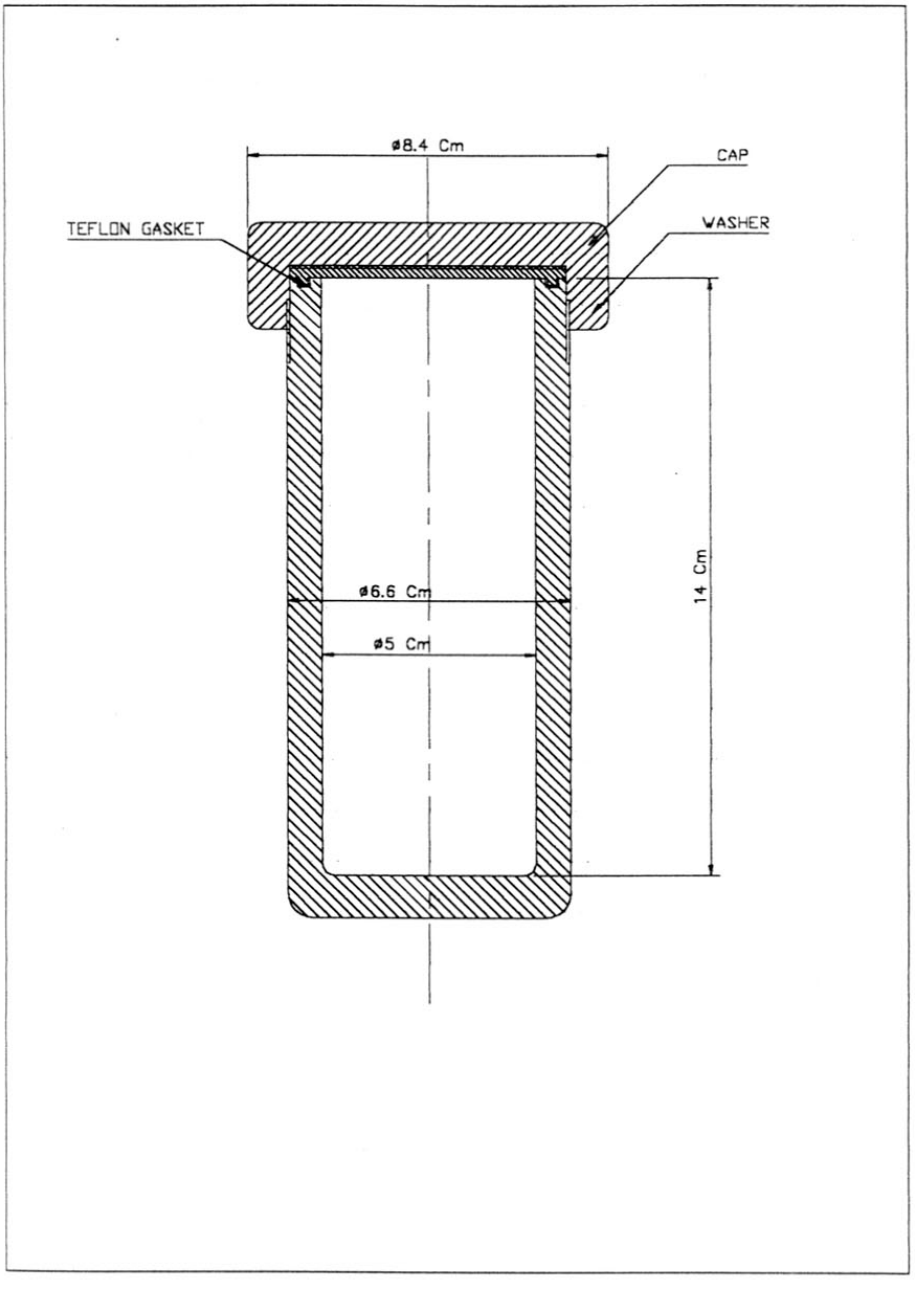

Fig. 2.1 Stainless steel autoclave used in the synthesis of vanadosilicate molecular sieves.

ammonium bromide (TPABr; 4.44g) were dissolved in water (40g) and mixed with an aqueous solution of $VOSO_4$, $3H_2O$ (0.18g in 44g water). The resultant solution was blue in colour. Fumed silica (4g) was added slowly to the above solution over a period of 1h with vigorous stirring. After complete addition of the fumed silica, the resultant gel was gray in colour. This was stirred for another 1h. The pH of the gel was 6.8. The gel was allowed to crystallize at 473K for 7 days under static conditions in a teflon lined autoclave. The grayish white material was dried at 373K and calcined at 823K for 12h. The calcined material was white under dehydrated conditions and on hydration it became dark yellow.

2.1.2 Vanadosilicate, V-MEL (VS-2)

i) V-MEL(1 to 4); normal synthesis

Synthesis of V-MEL samples (1 to 4) was carried out by hydrothermal methods following published procedures[6] using gels of the following molar composition : SiO_2 : 0.2 TBAOH : x VO_2 : 30 H_2O, where x = 0.025, 0.0125, 0.0091 and 0.00625 (respectively for samples 1 to 4). In a typical preparation, the following procedure was used : 18g of tetrabutyl ammonium hydroxide (TBAOH) was added slowly at RT to 45.5g of tetraethyl orthosilicate. To the resultant mixture, an aqueous solution of the required quantity of vanadyl sulfate trihydrate ($VOSO_4$, $3H_2O$) in 10g of distilled water was added very slowly under vigorous stirring. The mixture was then stirred at RT for 30 mins before adding to it 9g TBAOH in 50g of distilled water. The final clear liquid reaction mixture was then stirred at 323K for 6h before transferring it into an autoclave. The crystallization was carried out under static conditions at 443K for 4 days.

ii) V-MEL(1-He); synthesis excluding air

The synthesis procedure of V-MEL(1-He) was similar to V-MEL(1) excepting that the gel preparation and crystallization were carried out under anaerobic conditions in a helium atmosphere.

2.1.3 Vanadoalumnosilicate, V-Al-β (BEA)

The synthesis of V-Al-β samples (a to c) was carried out using the following molar composition : SiO_2 : x Al_2O_3 : y VO_2 : 0.52 is TEAOH : 21 H_2O. $x > 0.025$, $y < 0.033$, TEAOH = tetraethyl ammonium hydroxide. In a typical preparation, 17.1g tetraethyl ammonium hydroxide was added to 20.6g tetraethyl orthosilicate at 295K. After stirring the mixture for 40 mins, an aqueous solution of the required amount of $VOSO_4$, $3H_2O$ in 10ml deionized water was added slowly to the above gel. This mixture was stirred for 30 mins. Then 0.16g of Al_2 SO_4, $3H_2O$ in 6 ml deionized water was added slowly to the above gel. The resultant mixture was stirred for 2h. 10ml of deionized water was added to the resultant gel and stirred for another 2h. The pH of the final gel varied from 12.6 to12.8. The gel was allowed to crystallize at 413K for 8 days under static conditions.

2.1.4 Vanadium impregnated materials

15 mg of $VOSO_4$,$3H_2O$ was dissolved in 1ml distilled water and the solution was mixed with 1g aluminosilicate of BEA structure (zeolite β, Si/Al = 78) synthesized following published procedures.[7] The mixture was dried at 373K for 2h and calcined at 723K for 6h. The Si/V ratio of the resultant solid was 250.

36 mg of $VOSO_4$, $3H_2O$ was dissolved in 1ml distilled water and the solution was mixed with 1g Cab-o-sil. The mixture was dried at 373K for 2h and calcined at 773K for 6h.

The Si/V ratio of the resultant solid was 98. The same procedure was adopted for the preparation of V-impregnated silicalite-1 (V-imp-sil-1) and silicalite-2 (V-imp-sil-2) synthesized following published procedures.[8]

2.1.5 Pretreatment procedure

All the molecular sieve materials synthesized above contained organic templates inside the channels. In order to characterize and use these materials in catalytic reactions, it was necessary to remove the organic material from the zeolite pores. The as-synthesized zeolites were dried at 373K (for 8h) and subsequently calcined. The V-MFI samples were calcined at 823K for 12h and the V-MEL and V-Al-β samples were calcined at 773K for 10h.

The calcined materials were then treated with 1N ammonium acetate solution (20 ml / g zeolite, 353K for 12h) in order to remove the extralattice V-species. After the exchange, the material was filtered, washed thoroughly with deionized water and dried at 393K for 10h. The resultant material was calcined at 723K for 6h. The extracted V-MEL(1-He) was treated with 1N $NaNO_3$ solution at 333K for 12h, filtered, washed, dried and calcined at 723K (4h) to get the Na-form.

2.2 CHARACTERIZATION

2.2.1 Chemical analysis

An exact amount of the sample was taken in a platinum crucible with lid and ignited to get the dry weight of the sample. The sample was then cooled in a desiccator and weighed. The difference in weights gave the loss on ignition. The anhydrous weight of the sample was noted. The anhydrous sample was treated with hydrofluoric acid and evaporated on a hot plate to remove silicon in the form of SiF_6. This treatment was repeated three times and the

sample was again ignited, cooled in a desiccator and weighed. The loss in the weight of the sample was determined to get the silica content. The residue was fused with potassium pyrosulfate and dissolved in water. It was then analyzed by ICP (Jobin Yvon. JYU - 38 VHR) and atomic absorption spectroscopy (Hitachi) for estimating V and Al. An X-ray fluorescence spectrometer (Rigaku 3700) was also used to obtain the Si/V ratios.

Titrimetric method for the estimation of V^{4+} and V^{5+}: An exact amount of the gel or the solid samples was stirred in a 1M HCl solution in O_2 free CO_2 atmosphere (using $NaHCO_3$) to avoid the transformation of V^{4+} to V^{5+}. The mixture was then titrated with 0.05 N $KMnO_4$ solution for the estimation of V^{4+}. Similarly, another mixture was titrated with 0.05 N Mohr's salt solution using sodium diphenyl amine sulfonate as the indicator for the estimation of V^{5+}.[9] The $KMnO_4$ solution was standardized by standard oxalic acid solution. The Mohr's salt solution was standardized by standard $KMnO_4$ solution.[10] The titrimetric procedure was standardized by the analysis of a series of silicalite-2 samples impregnated with known quantities of V^{4+} ($VOSO_4$) and V^{5+}(NH_4VO_3) ions.

2.2.2 X-ray diffraction (XRD)

The samples synthesized during the course of the work under different conditions and different crystallization times were analyzed for qualitative and quantitative phase identification by X-ray powder diffraction (Rigaku, Model D MAX-IIIVC; Ni filtered Cu-K_α radiation; λ = 1.5406Å; and graphite monochromator). For calculating the X-ray cystallinity, XRD patterns were recorded in the 2θ range of 21 to 25 degrees, where the most intense peaks characteristic of the specified zeolite structure occur.

The X-ray crystallinity was then calculated from the following equation:

$$\% \text{ X-ray crystallinity} = \frac{\text{(Peak area between } 2\theta = 21\text{ -}25^0 \text{ of sample)}}{\text{(Peak area between } 2\theta = 21\text{ -}25^0 \text{ of the standard sample)}}$$

The sample with the most intense X-ray pattern obtained during the studies was used as the standard sample.

For V-MEL samples, the data were collected in the 2θ range of 5 to 50 degrees, in a step-scan mode with a step size of 0.01^0. The observed interplaner 'd' spacings were corrected with respect to an internal standard (Si). The tetragonal unit cell parameters were refined using two different least square fitting programs (HOCT and PDP11).

2.2.3 Scanning electron microscopy (SEM)

The morphology of MEL samples was investigated using a scanning electron microscope (JEOL, JSM 5200). The sample was dusted on alumina and coated with a thin film of gold to prevent surface charging and to protect the zeolite material from thermal damage by the electron beam. In all the analyses, a uniform film thickness of about 0.1 mm was maintained.

2.2.4 Electron spin resonance spectroscopy (ESR)

ESR spectra of the liquids and solids were recorded in a Bruker ER 200D model spectrometer at 9.73 GHz (X band) with a rectangular cavity (ST 8424). A standard sample (weak pitch, Varian, g = 2.0029) was used for calibration purposes. A modulation frequency of 100 kHz with an intensity of 1.25 GPP and a time constant of 10^3 msec were used. The spectra were recorded at 298K at a constant gain (2×10^{-5}) using the same amount of sample (0.2g). The estimation of V^{4+} in the gel as well as in the solid phases was performed by

integrating the ESR spectra and comparing the areas obtained for a series of V-impregnated silicalite-2 samples (standard) containing known quantities of V^{4+} and V^{5+} ions. The total area of the spectrum was calculated by adding the areas of the hyperfine peaks; a plot of the areas of the standard samples was made against the concentration of the paramagnetic V^{4+} species (Fig. 2.2). The V^{4+} concentration in the unknown materials was estimated using this calibration plot.

2.2.5 Infrared spectroscopy (IR)

The infrared spectra were recorded with a PC based FT-IR (Perkin Elmer; PC16) spectrometer in the frequency range 400 - 1300 cm^{-1} using KBr pellets. The samples and KBr crystals were dried at 423K for 6h before making the pellets. The same amount of the sample (1mg) and KBr (300 mg) used for all the pellets.

2.6 UV-Visible diffuse reflectance (DR) spectroscopy

Diffuse reflectance spectra were recorded in the UV-Visible region (UV-2101, Shimadzu) with barium sulfate as the reference sample. The spectra were recorded in air at 300K.

2.2.7 Nuclear magnetic resonance spectroscopy (NMR)

The liquid state ^{51}V NMR spectra were recorded in a Bruker MSL-300 spectrometer. The solid state ^{51}V MAS NMR spectra were recorded using the same instrument operated at 78.9 MHz. The samples were packed in a 7 mm o.d zirconia rotor and the spectra recorded using a spectral width of 125 kHz, pulse length of 1.5 μsec and repetition time of 0.5 sec. The data were accumulated using quadrature phase cycling with three different spinning

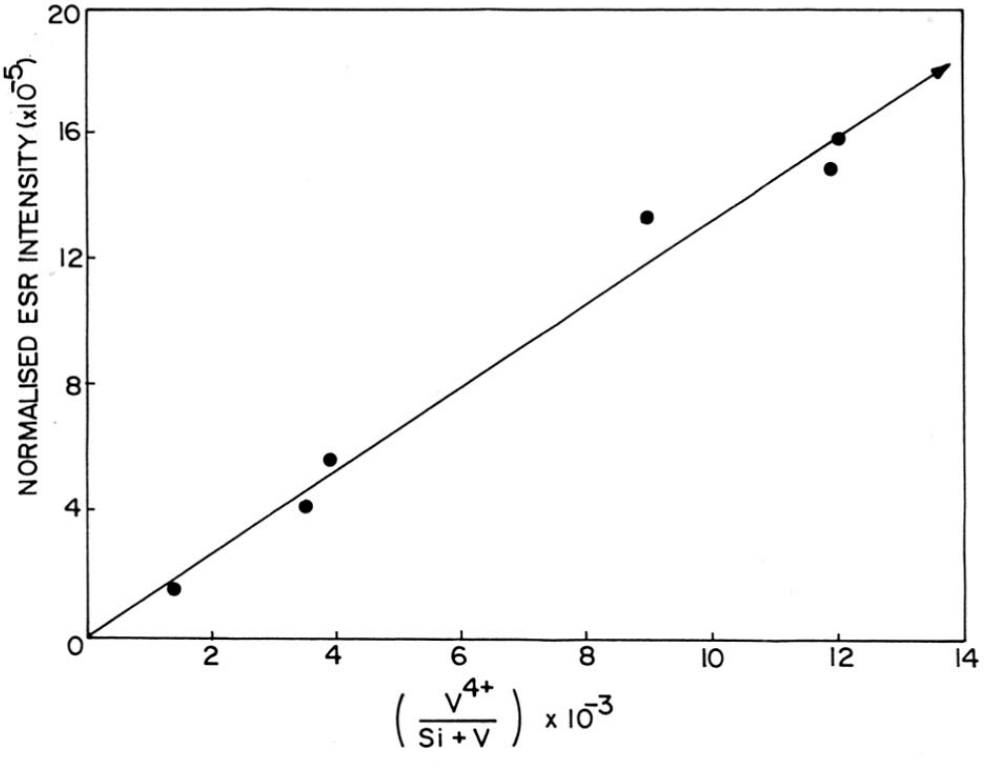

Fig. 2.2 Normalized ESR intensity *vs.* actual concentration of V^{4+} (V^{4+}/Si+V) in the standard samples.

speeds (3.3, 4.1 and 4.3 kHz). The chemical shift values are reported with respect to $VOCl_3$. The nutation of ^{51}V magnetization was studied by varying the pulse duration of the exciting r.f pulse proceeding the Π pulse in the Curr-Purcell-Meiboom-Gill (CPMG)[11] sequence. This way, the nutation behavior of two chosen regions of the ^{51}V spectrum, one at the centre of the spectrum and the other at a distant frequency in the powder pattern could be monitored. The 90^0 pulse was typically of 7.0 μsec duration for the $VOCl_3$ liquid sample.

^{29}Si NMR spectra of liquids and solids (using MAS) were recorded in the same instrument. Tetramethyl silane was used as the standard.

^{1}H MAS NMR spectra were recorded at 300 MHz using the same instrument mentioned above. A spectral width of 125 kHz was employed and the data were collected using quadrature phase cycling using 2.0 sec relaxation delay. The spinning speed employed was 3 - 4 kHz.

^{13}C MAS NMR were recorded at 75.47 MHz using CP pulse spectrum. The Hartman Hann match conditions were established using adamantane (typically a match condition of 50 kHz was employed). The chemical shift were referred w.r.t to the CH peak of adamantane (38.7 ppm). A spinning speed of ~ 3 kHz was used.

2.2.8 Thermal analysis

Simultaneous TG-DTA-DTG analysis of the as-synthesized and dried vanadium containing molecular sieves were performed on an automatic instrument (Setaram, TG-DTA 92). The thermograms of the samples were recorded under the following conditions.

Weight of the sample = 30 mg.

Heating rate = 10K min^{-1}

Air flow = 16 ml /min at atm. pressure

Sensitivity :

TG = 10 μg

DTG = 0.2mV

DTA = 0.1mV

Preheated and finely powdered α-alumina was used as the reference material. Detailed analysis of the weight loss due to decomposition of the template and accompanying heats of decomposition were calculated from stored data of each TG-DTA analysis using the software program available with the instrument.

2.2.9 Surface area measurements

A commercial adsorption unit (Omnisorb 100CX; COULTER corporation USA) was used for the measurement of nitrogen adsorption to determine the surface areas. The samples were activated at 673K for 12h in a high vacuum. After the treatment, the anhydrous weight of the sample was recorded. The samples were then cooled to 94K in liquid nitrogen and the samples allowed to adsorb nitrogen gas. Finally, knowing the amount of N_2 adsorbed at different equilibrium pressures, the BET surface area was calculated.[12]

2.2.10 Adsorption measurements

The sorption measurements for water, n-hexane and cyclohexane were carried out gravimetrically in a recording electromicrobalance (Model : Cahn-2000G). The zeolite sample of about 60 mg was pressed into a pellet and weighed into an aluminium bucket which was attached to the balance. The system was evacuated down to a pressure of 10^{-6} torr at 673K. After 2h, the temperature was lowered to the required value. The adsorbate vapours were admitted into the sample compartment at a constant pressure and temperature and the

weight gain was recorded as a function of time. After the experiment was over, the catalyst was evacuated and heated to 673K at 10^{-6} torr and used for the next experiment.

2.3 CATALYTIC PROPERTIES

The chemicals used in the various reactions are listed in table 2.2

Table 2.2

Chemicals used in the catalytic reactions.

Sr. No.	Name	Source	Further purification
1.	Phenol (AR grade)	s.d. fine-chem. Ltd, India	Nil
2.	Toluene (AR grade)	do	do
3.	Acetonitrile (AR grade)	do	do
4.	Ethanol (AR grade)	do	double distilled
5.	Hydrogen peroxide (30% W/V aqueous solution)	Loba Chemie, India	Nil

2.3.1 Liquid phase oxidation

a. Hydroxylation of phenol and oxidation of toluene

The catalytic reactions were carried out in a two-necked glass R.B flask (100 ml capacity) kept in an oil bath. One neck was fitted with a chilled water condenser, while the other neck was fitted with a thermometer. Aqueous H_2O_2 (26 wt %) was used as the oxidant.

Acetonitrile was used as the solvent for toluene oxidation and water was used for phenol hydroxylation. The reactant (1g), solvent (10 ml) and the catalyst (0.1g) were

taken in the reaction flask and the temperature maintained at 353K while stirring with a magnetic stirrer. The required amount of aqueous of H_2O_2 was introduced and the products were taken out periodically with a glass syringe before analysis.

b. Promoter induced catalysis

The hydroxylation of phenol and the oxidation of toluene were carried out in the presence of the catalyst and the required quantity of promoter (α-pyridine carboxylic acid; picolinic acid) at identical conditions mentioned above.

2.3.2 Vapour phase oxidation

The reactor system employed for the vapour phase oxidative dehydrogenation of ethanol was a bench top reaction system (BTRS, Autoclave Engineers, USA) which was a fixed bed continuous down-flow reactor (5cc) operating under steady state conditions. Ethanol was fed through a HPLC liquid injection pump (Alcott, Model-760) and air was passed using a mass flow controller (Brooks, Model-5896). The reactants were mixed and vaporized in a preheated oven maintained at 393K and passed through the reactor (6 mm i.d). The temperature around the reactor was maintained by a temperature controlled furnace. The outlet of the reactor was directly connected to a gas chromatograph (HP-5890 series II) through a heated transfer line which was maintained at 393K. A 8 port sampling valve was used to inject a known amount of the product mixture or reactant (250 μl) onto the GC column using nitrogen as the carrier gas.

Air after drying through a trap containing molecular sieve (4A) and doubly distilled ethanol (>99%) were used for the reaction. A reactant gas mixture of 3 vol % C_2H_5OH in air [5.3 cc / 170cc; WHSV of ethanol (mass of ethanol passed in 1h / mass of catalyst) = $2.6h^{-1}$]

was used. The concentration of ethanol in air was well below the lower explosion limit. 250mg of the catalyst (ASTM mesh size 22 - 30) was employed for the reaction. The catalyst was initially activated at 673K for 3h in air and cooled to the reaction temperature. A stable activity without much deactivation was observed for a long time period (~ 10h). Carbon and oxygen mass balances of 100 ± 5 % were obtained for most of the experiments. Rate, when expressed as turn over rate, was calculated as the number of molecules of ethanol converted per vanadium atom per second.

2.3.3 Product analysis

The products from hydroxylation of phenol and oxidation of toluene were analyzed in a gas chromatograph (HP 5880A) equipped with a capillary column (50 m x 0.25 mm cross linked methyl silicone gum). The products were identified by GC-MS (Shimadzu QCMS - QP 2000A). Since the GC response of different compounds vary, standard samples were injected to determine the response factors. The product analysis was normalized using GC response factors.

The products of the vapour phase oxidation of ethanol were analyzed in a GC (HP 5880A) using a capillary column (cross-linked methyl silicone gum, 50 m x 0.25 mm) and a FID. The carbon oxides in the samples were estimated separately using another GC (Shimadzu, 15-A) using a Poropak-Q column (2 m x 3 mm) and a TCD.

2.4 REFERENCES

1. Miyamoto, A., Medhanavyn, D., and Inui, T., *Appl. Catal.* **28**, 89 (1986); in "Proceedings, 9th International Congress on Catalysis, Calgary, 1988" (M. J. Phillips and M. Ternan, Eds), vol.1, p. 437. Chem. Inst. of Canada, Ottawa, Ontario, 1988.
2. Zatorski, L. W., Centi, G., Nieto, J. L., Trifiro, F., Bellusi, G., and Fattore, V., *Stud. Surf. Sci.Catal.* **B 49**, 1243 (1989)
3. Trifiro, F., and Jiru, P., *Catal. Today* **3**, 519 (1991)
4. Rigutto, M. S., and Van Bekkum, H., *Appl. Catal.*, **68**, L1 (1991)
5. Centi, G., Perathoner, S., Trifiro, F., Aboukais, A., Aissi, C. F., and Guelton, M. J., *J. Phys.Chem.*, **96**, 2617 (1992)
6. Prasad Rao, P. R. H., Ramaswamy, A.. V., Ratnasamy, P., *J. Catal.*, **143,** 275 (1993)
7. Perez-pariente, J., Martens, J. A.., and Jacobs, P. A.., Appl. Catl., 31, 35 (1987).
8. a) Flanigen, E. M., Bennett, J. M., Grose, R. W., Cohen, J. P., Patton, R. L., Kirchener, R. M., and Smith, J. V., *Nature* **271,** 512 (1978).

   b) Bibby, D. M., Milestone, N. B., and Aldridge, L. P., *Nature* **280,** 664 (1979).
9. Kolthoff, I. M., Treatise on Analytical Chemistry, Part II, Vol. 8; Interscience : New york - London, p 226, **260** (1963).
10. Vogel, A. I., "Text Book of Quantitative Inorganic Analysis," London, Longmens, Ed. 1961.
11. Meiboom, S., Gill, D., Rev. Sci. Instrum., 29, 688 (1958).
12. Brunauer, S., Emmett, P. H., and Teller, E., *J. Am. Chem. Soc.*, **60**, 309 (1938).

CHAPTER - III

PHYSICOCHEMICAL CHARACTERIZATION

1.1 INTRODUCTION

The introduction of vanadium into zeolite lattices was first attempted by Marosi *et al.*[1] in 1978. Later on, Xu. Renen *et al.*[2] reported the possibility of isomorphous substitution of vanadium in three (III, IV and V) different oxidation states. Miyamoto *et al.*[3] have reported the hydrothermal synthesis of aluminum containing vanadosilicate. Kucherov *et al.*[4] and later Sass *et al.*[5] introduced V^{4+} ions into framework cationic positions, by solid state interactions. Recently, ElMalki *et al.*[6] reported the incorporation of vanadium in zeolite β, where VO^{2+} ions are located near the aluminum sites. Anderson *et al.*[7] reported a post synthesis method of vanadium incorporation in ZSM-5 by vapour phase deposition using $VOCl_3$. Several reports have appeared on the synthesis of vanadium containing medium pore molecular sieves (V-MFI[8], V-MEL[9], V-ZSM-48[10] and V-Eu-1[11]). It has been reported that the incorporation of vanadium occurs as V^{4+} in the zeolite lattice during hydrothermal synthesis and then transforms to V^{5+} during calcination. Kornatowski *et al.*[12] have reported the possibility of incorporation of V^{5+} in the zeolite lattice. Das *et al.*[13] have reported the formation of Si-O-V bonding with isolated tetrahedral vanadium environments containing V=O during impregnation using vanadium (5+) triisopropoxide oxide. Because of the severe restrictions to diffusion of large molecules in the pores of medium pore zeolites, particularly in the liquid phase, a strong need exists for the development of transition metal modified large pore zeolites. Vanadium containing large pore zeolites, such as V-NCL[14], V-ZSM-12[15], V-Mordenite[16] and V-Al-β[17] have been reported recently. Vanadium containing mesoporous molecular sieve, V-MCM-41[18] has been reported and recently Luan *et al.*[19] identified both V^{4+} and V^{5+} in the as-synthesized materials (V-MCM-41). Recently, Morey *et al.*[20] identified two and three legged Si-O-V dispersed in ultralarge pore cubic mesoporous MCM-48

synthesized by grafting. The chemistry of vanadium, its redox behavior in the presence of air/hydrogen, its pH dependence are already well established.[21]

This chapter describes the detailed physicochemical characterization of (a) gel and crystalline phases of medium pore V-MFI (VS-1) synthesized in acidic and alkaline medium,[22] (b) gel and crystalline phases of medium pore V-MEL (VS-2) synthesized in inert and normal atmosphere and at various vanadium concentrations at alkaline pH,[23] and (c) gel and crystalline phases of the novel large pore molecular sieve (V-Al-β[17]) of the BEA type by analytical methods, XRD, ESR, FT-IR, UV-Vis, NMR, TG-DTA, surface area and sorption techniques.

3.2 RESULTS AND DISCUSSION

3.2.1 Part a - Physicochemical characterization of V-MFI (VS-1)

This section examines the influence of pH of the synthesis gel on the incorporation of V in V-MFI samples.

i) Analytical Data

Both the samples V-MFI(A) and V-MFI(B) were prepared using $VOSO_4$, $3H_2O$ possessing only V^{4+} ions. Table 3.1 presents the V^{4+} and V^{5+} breakup in the gel and crystalline samples of V-MFI. The acidic gel is found to contain more V^{4+} ($12.2x10^{-3}$), while the alkaline gel contains more V^{5+} ($8.4x10^{-2}$) than V^{4+} ($4.1x10^{-3}$) ions. The aerial oxidation of V^{4+} to V^{5+} is known to occur in alkaline media.[18] The as-synthesized crystalline sample, V-MFI(A) contains mostly V^{4+} ($10.2x10^{-3}$), whereas sample V-MFI(B) contains mostly V^{5+} ($4.2x10^{-3}$). When the as-synthesized samples are calcined, only V^{5+} species are present in sample V-MFI(B), whereas sample V-MFI(A) retains a small amount of V^{4+}. On extraction

Table 3.1

V^{4+} and V^{5+} break up in the gel and crystalline samples of V-MFI samples.

Sample	pH of gel	V-concentration ($\times 10^{-5}$)								
		Gel			Crystalline material					
					As-synthesized			Calcined		Ext[d]
		V / Si +V	V^{4+} / Si+V	V^{5+} / Si+V	V / Si +V	V^{4+} / Si+V	V^{5+} / Si+V	V^{4+} / Si+V	V^{5+} / Si+V	Si / V
A	6.8	12.5	12.2 (11.8)[a] (11.4)[b]	0.3	10.2	10.2 (9.5)	-	0.5 -	9.7	1.1
B	11.1	12.5	4.1 (11.9)[a] (3.9)[b]	8.4	5.4	1.2 (0.9)	4.2	- (3.7)[c]	5.4	3.9 (3.4)[c]

Values within brackets have been estimated from ESR.

a → initial concentration of V^{4+} in gel.

b → Final concentration of V^{4+} in gel.

c → concentration of V^{4+} in reduced samples.

d → Calcined sample extracted with 1N NH_4OAc solution.

with 1N NH_4OAC solution, most of the vanadium (89%) is extracted out from V-MFI(A), while a much smaller amount of vanadium (28%) is extracted out from V-MFI(B).

ii) XRD studies

The as-synthesized forms of both the samples were highly crystalline with an orthorhombic structure (Figs. 3.1a and 3.1b). Upon calcination, V-MFI(A) changes its symmetry to monoclinic (revealed by the splitting of the line at $2\theta = 24.38^{\circ}$)[24], while V-MFI(B) retains the orthorhombic symmetry (Fig. 3.1; compare a, a′ and b, b′). Earlier workers[25] have reported that silicalite-1 and TS-1 containing less than 1 Ti/UC change symmetry on calcination, while TS-1 containing more Ti did not. In the case of V-MFI(B), no change in symmetry is observed even though it contains only about 0.5 V / UC. While a change in symmetry need not be an evidence for non-incorporation (as in V-MFI(A)), the absence of symmetry change in V-MFI(B) does suggest that V-ions are probably present in the framework positions in V-MFI(B). However, the presence of extraneous matter in the zeolite pores, such as adsorbates[26] and the presence of faults (defects)[27] could prevent such a symmetry change. When silicalite-I was loaded (by impregnation) with 1 wt% V and calcined, the symmetry change took place. The above observation and the observation of a symmetry change in sample V-MFI(B) suggests that the reason for the absence of symmetry change of V-MFI(B) is probably due to the presence of V in the framework (and not due to the V being present as occluded oxides). However, the simultaneous creation of the defect sites along with vanadium incorporation could also explain the absence of the symmetry change. Moreover, a slight shift in the position of the 100% peak ($2\theta = 23.2^{\circ}$) for the calcined V-MFI(B) is noticed, when compared to pure silicalite-1 indicating a small increase in the unit cell size of V-MFI(A). As V-ions are much larger than Si^{4+} ions, an increase in the

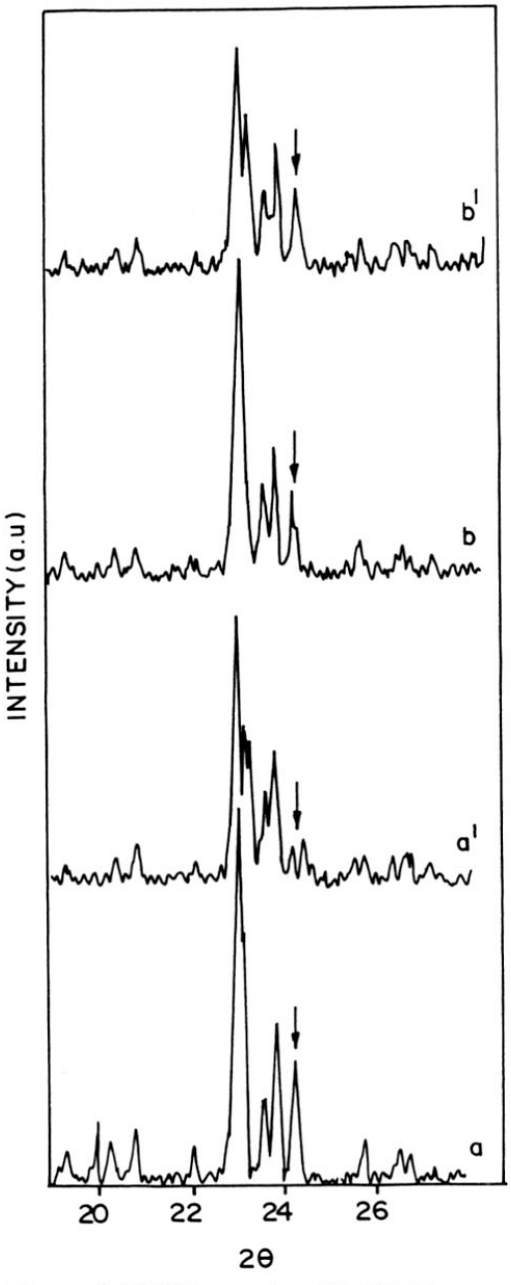

Fig. 3.1 XRD pattern of V-MFI samples. V-MFI-(A) : as-synthesized (a) and calcined (a/); V-MFI(B) : as-synthesized (b) and calcined (b/).

unit cell size is expected if V-ions are present in the framework. In fact, earlier studies[9,10] have shown that the expansion of the unit cell volume is related to the concentration of the framework vanadium in the samples. The XRD studies suggest that while a few or no V-ions are present in the framework of V-MFI(A), V-MFI(B) contains significant quantities of framework V-species.

iii) SEM

The SEM micrograph of V-MFI(A) (Fig. 3.2a) reveals mostly large (6 - 8 μm) twinned hexagonal crystallites. V-MFI(B) crystallites are spheroidal (0.1- 0.2 μm; Fig. 3.2b).

iv) ESR spectroscopic studies

The ESR spectra of the precursor gels of samples V-MFI(A) and V-MFI(B) reveal eight hyperfine lines without anisotropy (g =1.963 and A = 92.8G; Fig. 3.3a and 3.3b) immediately after preparation (0h). On aging the acidic gel at 298K for 2h, the spectrum is similar to the fresh one (Fig. 3.3a), while the spectrum of the gel of V-MFI(B) after aging for 4h reveals eight hyperfine lines with anisotropy (g_{11} = 1.923, $g_{\perp}$ = 1.981, A_{11} = 1.852G, $A_{\perp}$ = 79.8G; Fig. 3.3b). The ESR spectra suggest that free VO^{2+} ions are present in the fresh and aged gels of V-MFI(A) (Figs. 3.3a and 3.3a′)[28] and that they are present in an axially symmetric environment in the aged gels of V-MFI(B) (Figs. 3.3b and 3.3b′). The intensity of the spectrum of the final alkaline gels is less than that of the final acidic gel (Figs. 3.3 a and 3.3a′), although the same amount of V^{4+} was added during the preparation of the gels, due to transformation of the V^{4+} ions into V^{5+} ions in the alkaline medium.[21]

The as-synthesized sample V-MFI(A) exhibits an eight-line hyperfine spectrum (Fig. 3.4a) with a broad background. The ESR parameters (g_{11} = 1.935, $g_{\perp}$ = 1.982,

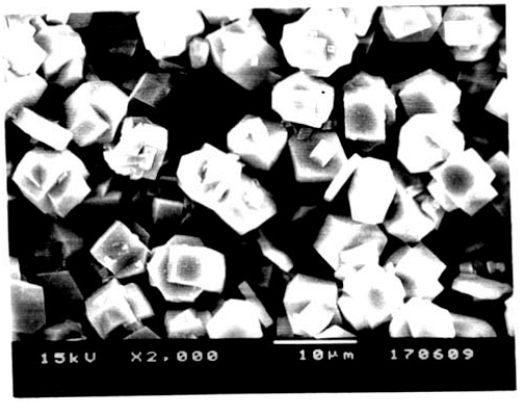

(a)

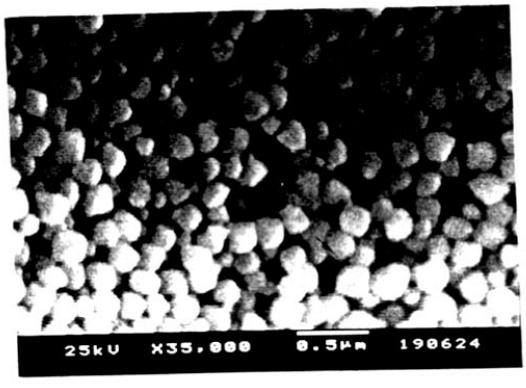

(b)

Fig. 3.2 SEM photographs of the V-MFI samples. V-MFI(A) (a) and V-MFI(B) (b).

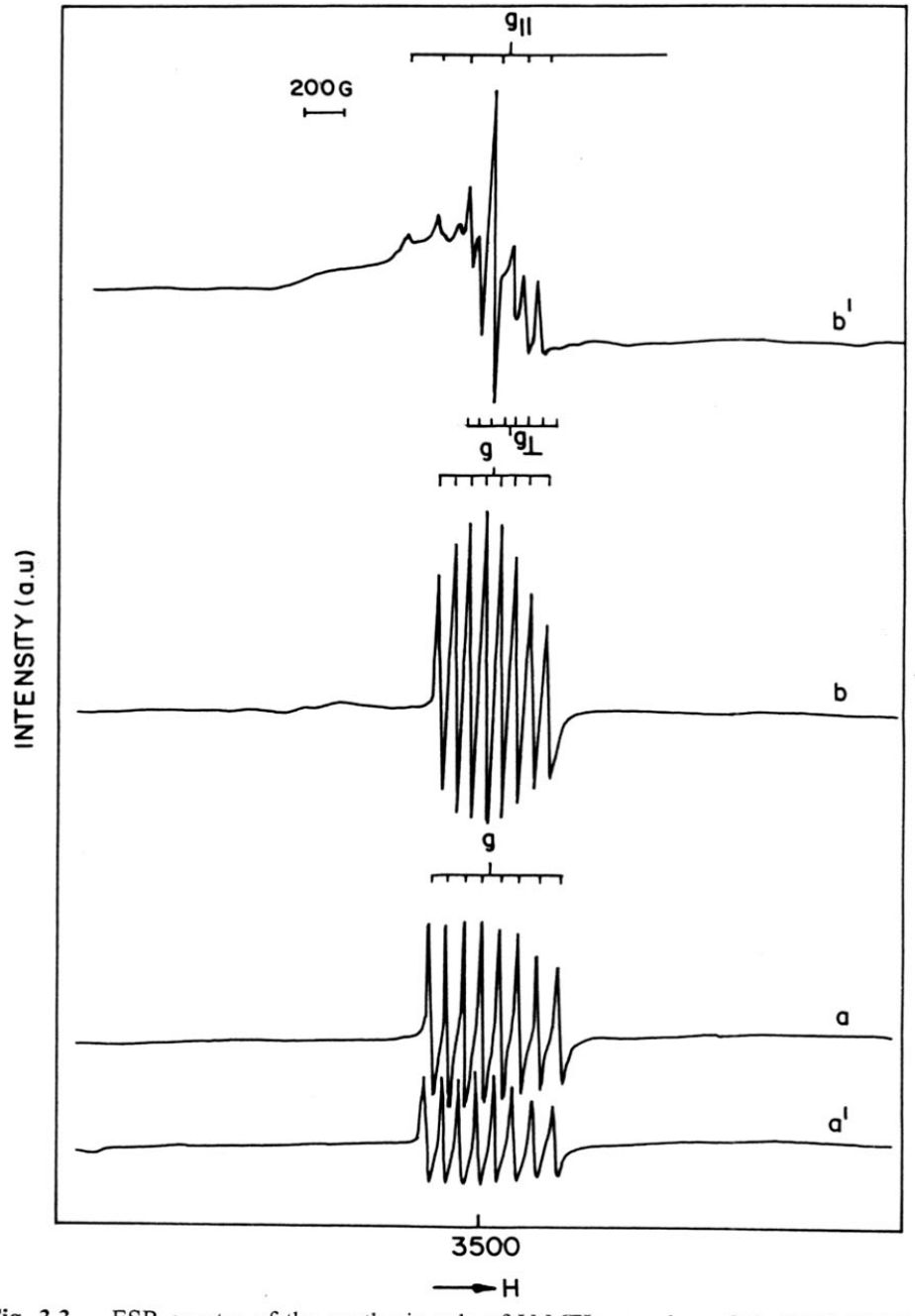

Fig. 3.3 ESR spectra of the synthesis gels of V-MFI samples. Gel of V-MFI(A) : initial, 0h (a) and final, 2h (a/); gel of V-MFI(B) : initial, 0h (b) and final, 4h (b/).

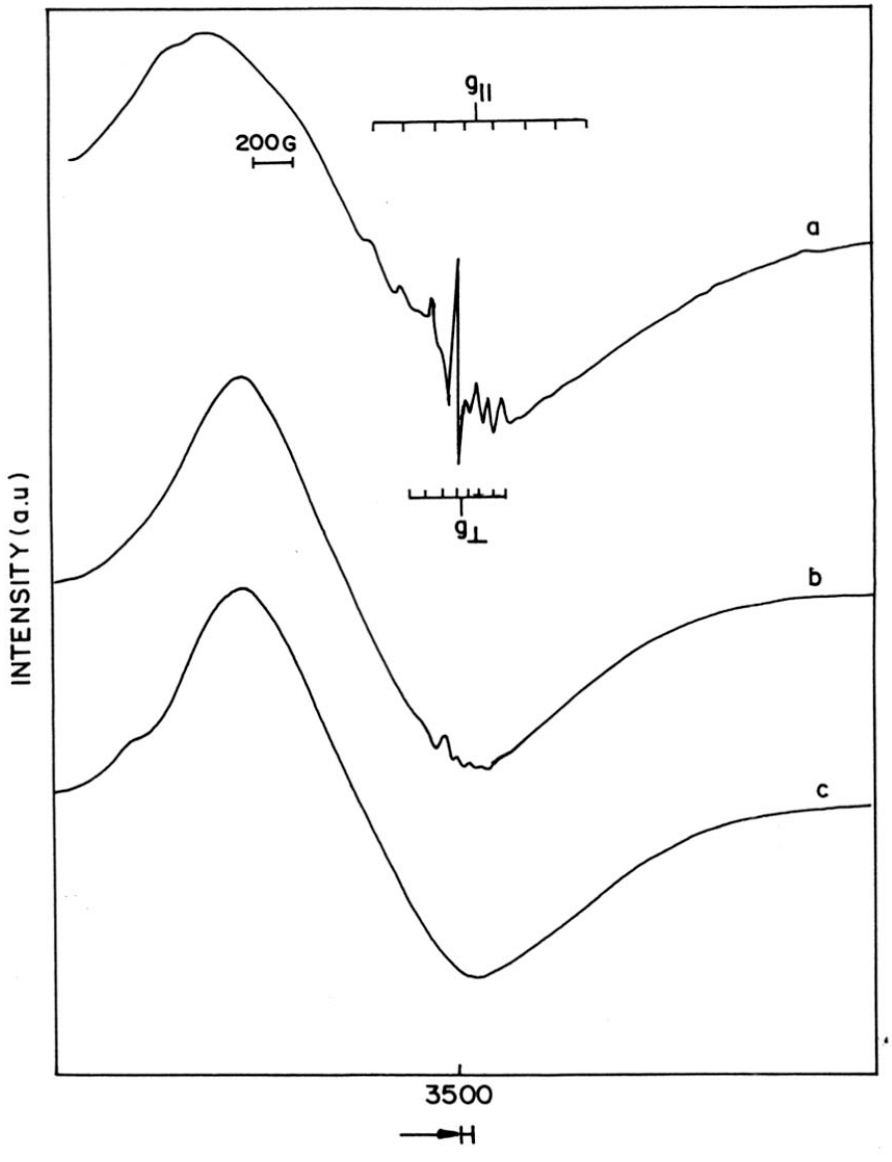

Fig. 3.4 ESR spectra of the V-MFI synthesized in acidic medium. V-MFI(A) : as-synthesized (a), calcined (b) and reduced (c).

A_{11} = 188.5G, $A_{\perp}$ = 82G) indicate that the V-species are in a distorted octahedral (Oh) environment.[29,30] It is possible that the broad band is associated with agglomerated V^{4+} ions. However, this does not appear likely as even the calcined sample (in which all the V^{4+} ions are expected to be transformed into V^{5+}) exhibits the band with about the same intensity (Fig. 3.4b). The intensity of the sharp hyperfine lines attributed to better dispersed V^{4+} becomes very small on calcination suggesting the near total oxidation of the V^{4+} ions into V^{5+}. Upon reduction in H_2 at 573K (6h), the V^{4+} hyperfine lines do not reappear (Fig. 3.4c), suggesting that the V^{4+} species which exhibited the lines in the as-synthesized V-MFI(A) have become irreversibly oxidized.

The results of the quantitative analysis of the ESR spectra of the crystalline samples using a calibration graph (Fig. 2.2) reveal that the V^{4+} contents of the samples estimated by ESR and chemical methods are of similar magnitude. The sample V-MFI(B) exhibits an eight line ESR signal (Fig. 3.5a) with a weak broad background. The ESR parameters (g_{11} = 1.932, $g_{\perp}$ = 1.982, A_{11} = 185.1 G, $A_{\perp}$ = 73.2 G) indicate that V^{4+} is present in a distorted octahedral (Oh) environment.[29,30] Upon calcination, no ESR signal attributable to V^{4+} ions is observed (Fig. 3.5b) due to the complete conversion of V^{4+} to V^{5+}. On reduction in H_2 (at 573K for 6h), an intense eight line hyperfine spectrum (Fig.3.5c) is obtained, indicating that the vanadium in sample V-MFI(B) is easily reduced. The ESR parameters of the reduced sample of V-MFI(B) (g_{11} = 1.931, $g_{\perp}$ = 1.991, A_{11} = 180.5G, $A_{\perp}$ = 69.5G) correspond to V^{4+} in a square pyramidal (SqPy) environment.[31] The reduced forms of both the calcined and extracted samples of V-MFI(B) contain about the same amount of V^{4+} ions (Table 3.1) as the V^{5+} ions present before reduction, showing the easy reducibility of these framework ions.

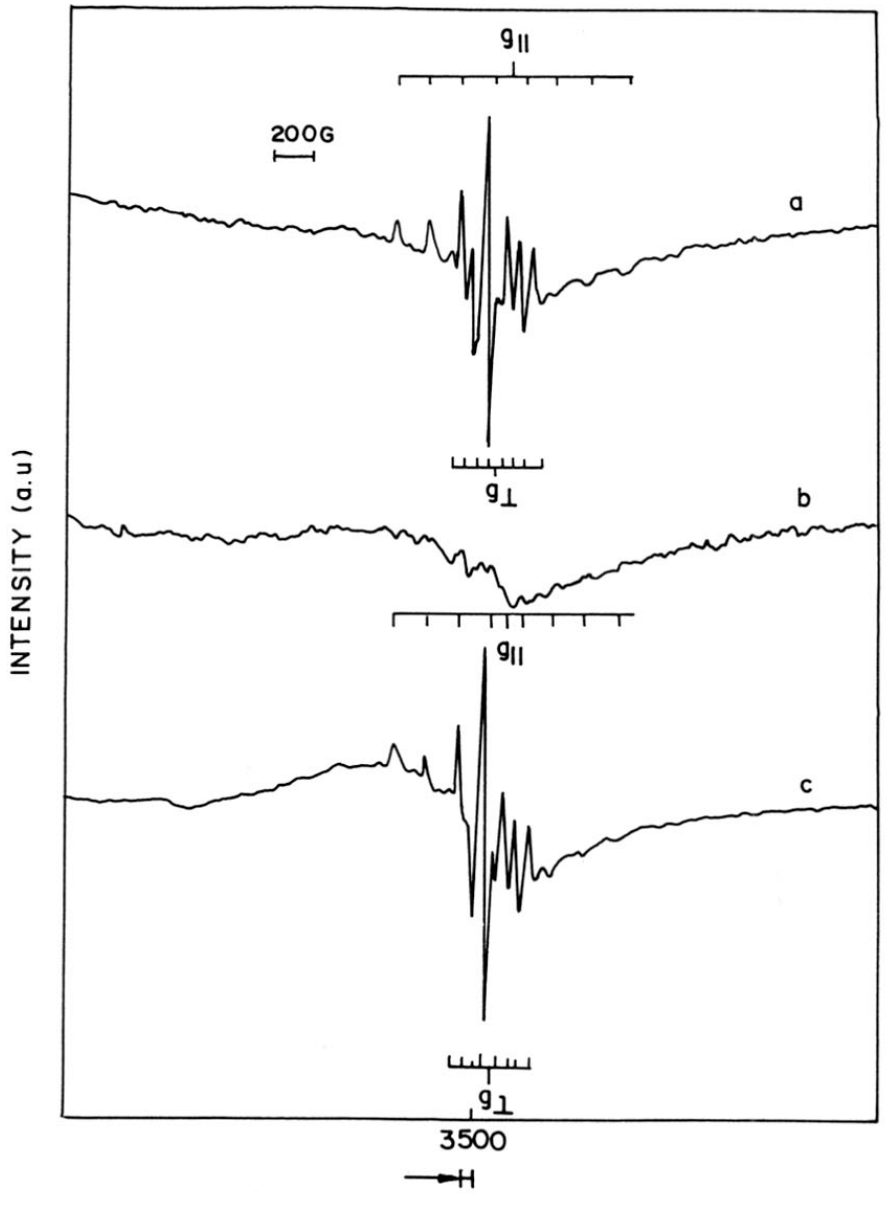

Fig. 3.5 ESR spectra of the V-MFI synthesized in alkaline medium. V-MFI(B): as-synthesized (a), calcined (b) and reduced (c).

v) FT-IR spectroscopic studies

The framework IR spectra of calcined V-MFI(A) and V-MFI(B) are shown in figure 3.6. The sample V-MFI(B) exhibits a band at 969 cm^{-1} but it is absent in the case of sample V-MFI(A). The framework spectra of the titanium silicalites TS-1[32], TS-2[33] and vanadium containing zeolites V-ZSM-48[10], VS-2[9] have already been reported. In all the cases, an IR band at around 967 cm^{-1}, not present in the Ti (or V) free analog, is noticed. The band has been attributed to Si-O^- vibrations[34] and is believed to be a proof for the presence of the metal (M) ions in the framework.[35] This indicates that in V-MFI(B), the V-ions are present in the framework.

vi) UV-visible (DR) spectroscopic studies

Figure.3.7 presents the UV-visible diffuse reflectance (DR) spectra of as-synthesized and calcined samples of V-MFI(A), V-MFI(B) and V-impregnated Cab-o-sil (V-imp-cab-o-sil). Assignments for the absorptions in the UV-visible region based on solid vanadium compounds and V-silicates are shown in table 3.2. Recently, Kornatowski *et al.*[11] have reported the presence of 340 and 295 nm DR bands in the as-synthesized forms of the V-silicate, KVS-5 and have attributed them to Td-V^{5+} species. The as-synthesized form of V-MFI(A) does not exhibit any band in the region 250-340 nm (Fig. 3.7a), indicating the presence of V^{5+} in tetrahedral (Td) environments. The calcined form of V-MFI(A) exhibits intense bands at 280 and 402 nm (Fig. 3.7a$^{/}$) corresponding to Td and Oh-V^{5+} species. V-imp-Cab-0-sil exhibits intense DR bands (Fig. 3.7c) at 286 and 402 nm. The positions of these bands are similar to those of the calcined V-MFI(A). This indicates that the V-species present in V-MFI(A) (after calcination) are similar to those present in the impregnated

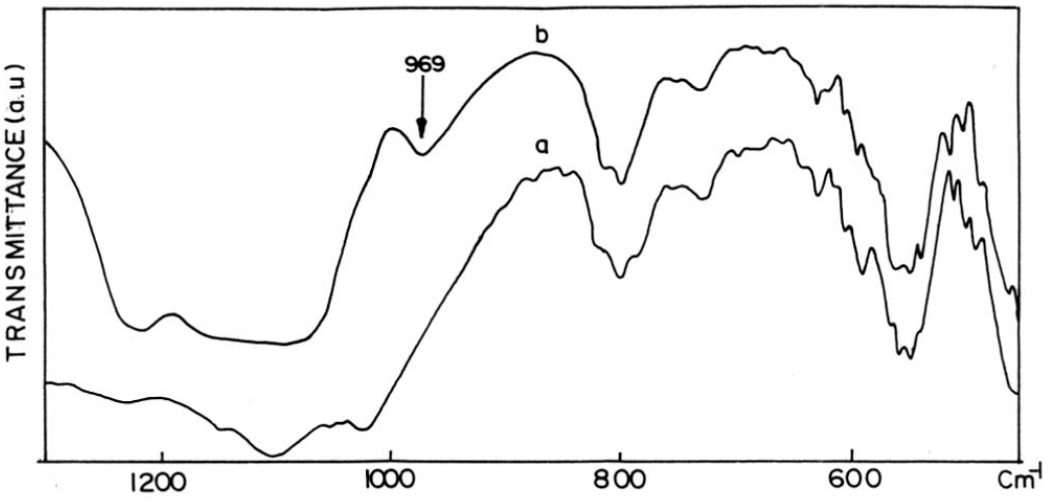

Fig. 3.6 Framework IR spectra of the calcined V-MFI samples. V-MFI(A) (a) and V-MFI(B) (b).

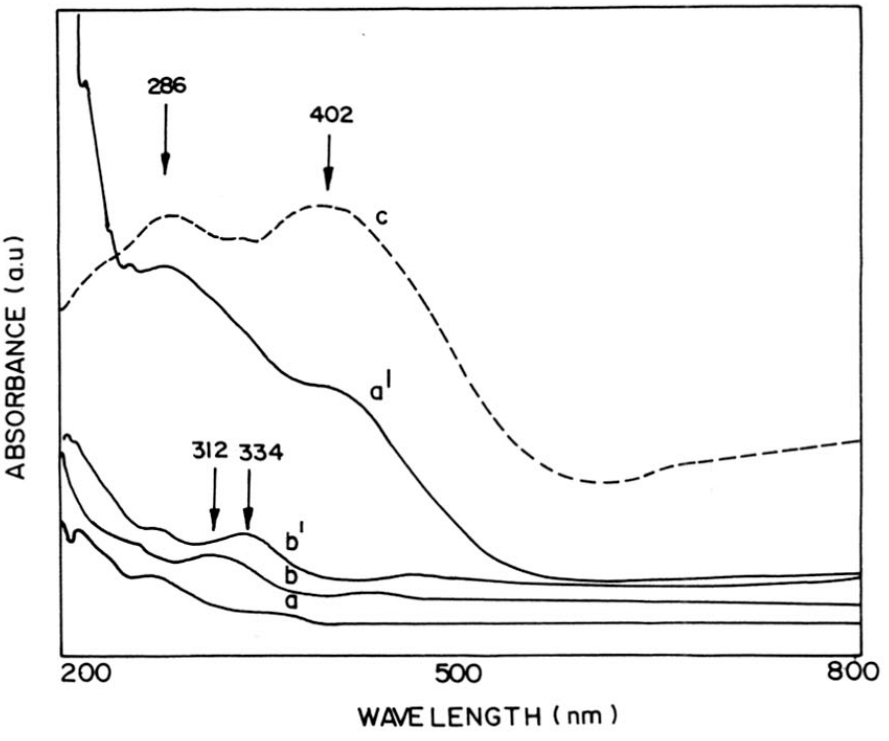

Fig. 3.7 UV-Visible DR spectra of the V-MFI samples. V-MFI(A) : as-synthesized (a) and calcined (a′); V-MFI(B) : as-synthesized (b) and calcined (b′); V-impregnated cab-o-sil (c).

Table 3.2

Assignment of UV-Vis absorption bands of V-ions.

Metal oxidation state	Transition energy (nm)	Type of transition	Ionic environment	Ref.
V^{5+} (pure compounds)	333-500	charge transfer O→V	T_d	55
V^{5+} (pure compounds)	285-333	charge transfer O→V	T_d	55
V^{4+} (pure compounds)	769	d-d	-	56
V^{4+} (VO^{2+})	250-285	charge transfer O→V	-	56
V-MFI	384	charge transfer O→V	T_d	57
V-MEL	333	charge transfer O→V	T_d	23
KVS-5	340	-	T_d	12

sample. The calcined form of the sample V-MFI(B) exhibits a band at 334 nm (Fig. 3.7b'), corresponding to Td-V^{5+} species.

vii) NMR spectroscopic studies

The liquid-state ^{51}V NMR spectrum of the gels of sample V-MFI(A) and V-MFI(B) are shown in figure 3.8. The gel of V-MFI(A) does not exhibit any NMR signal indicating the absence of detectable amounts of V^{5+} ions (Fig. 3.8a). The gel of V-MFI(B) produces an intense signal at δ = -533 ppm along with weak signals at δ = -558 and -565 ppm (Fig. 3.8b). The signal at δ = -533 ppm corresponds to HVO_4^{2-} species.[36,37] This is the major V^{5+} species suggested to be present at pH > 10.[21] The signals at δ = -558 and -565 ppm are probably due to $V_2O_7^{4-}$ and its protonated form, $HV_2O_7^{3-}$, respectively.

The solid state ^{51}V static NMR spectra of calcined V-MFI(A) and V-MFI(B) are presented in figure 3.9. V-MFI(A) exhibits a strong signal (Fig. 3.9a) at -502 ppm (δ_2) along with weaker signals at -284 ppm (δ_1) and -975 ppm (δ_3). Earlier workers[38] have attributed the signals at -284 and -975 ppm to Oh V-species similar to V_2O_5, and the signal at -502 ppm to vanadium in a Td environment as in polymeric NH_4VO_3. The static ^{51}V NMR spectrum of a sample of V-imp-Cab-o-sil is presented in figure 3.9c. The spectrum is distinctly different from those of both V-MFI(A) and V-MFI(B) suggesting that a major amount of the V-species present in V-MFI(A) and V-MFI(B) is different from those in the impregnated sample. After NH_4OAc treatment, the calcined V-MFI(A) does not show any NMR signal due to the extraction of most of the vanadium (see Table 3.1). Sample V-MFI(B) gives a nearly anisotropic spectrum (Fig. 3.9b) with a peak maximum at δ = -555 ppm. The spectrum has been attributed to V in a distorted Td environment similar to the case of VS-12.[15]

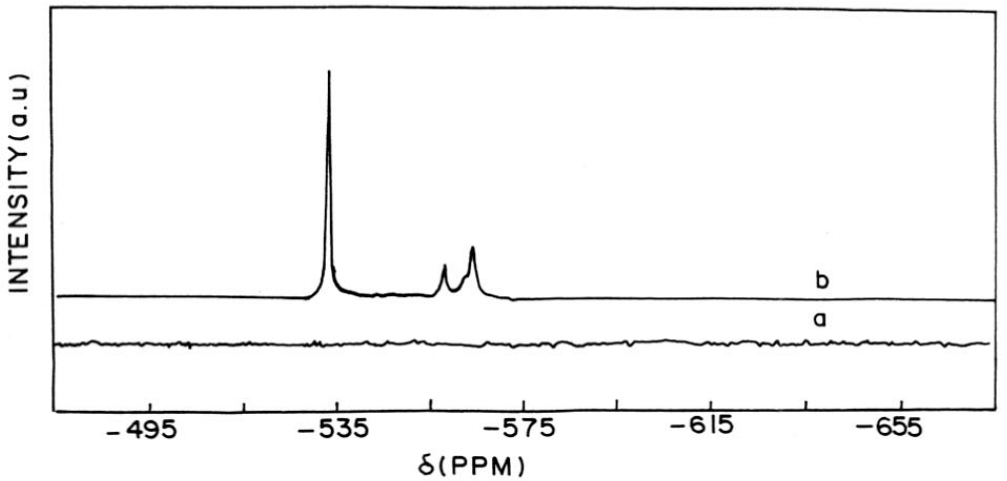

Fig. 3.8 ^{51}V liquid state NMR spectra of the synthesis gels of V-MFI samples after aging. Gel of V-MFI(A) (a) and gel of V-MFI(B) (b).

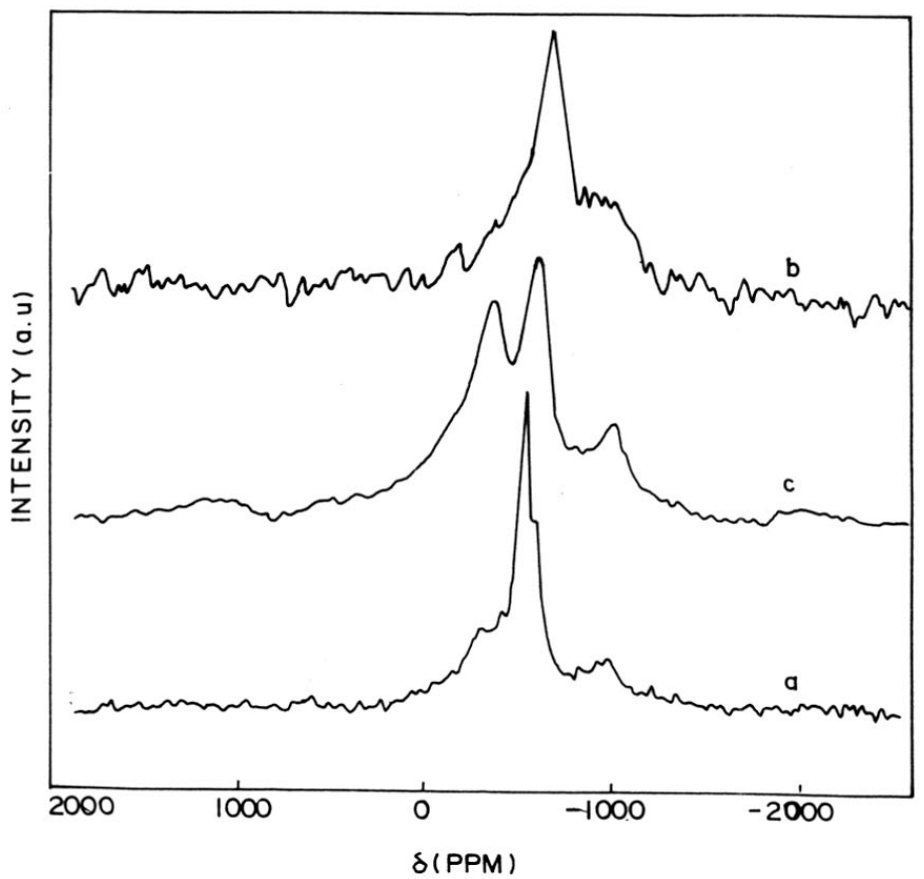

Fig. 3.9 ^{51}V static NMR spectra of the calcined V-MFI samples. V-MFI(A) (a), V-MFI(B) (b) and V-impregnated Cab-o-sil (c).

^{29}Si MAS NMR spectrum of the calcined sample V-MFI(A) shows seven lines (Fig. 3.10a) in the chemical shift range from δ = -111 to -118 ppm, corresponding to Q^4-Si sites.[39] The absence of signals in the range of δ = -98 to -102 ppm indicates the absence of defect sites (Si-OH).[40] Besides, Axon *et al.*[41] have reported a broad spectrum for Fe-silicalite-1 prepared in fluoride medium, the broadness being attributed to the iron-silicon connectivity in the framework. The sharply resolved spectrum of V-MFI(A) (Fig. 3.10) indicates that the vanadium present in it does not have any effect on the silicon environment, presumably due to the lack of V-O-Si linkages in the framework. The ^{29}Si MAS NMR spectrum of the calcined V-MFI(B) shows two broad lines (Fig. 3.10b). The signal at δ = -102 and -114 ppm correspond to the defect silanol and Q^4-Si sites. The broadness of the lines in this spectrum is interesting. According to Moudrakovski *et al.*[15b] the broadening of the lines in the spectrum can be an indirect indication of the statistical distribution of vanadium in the lattice.

^{1}H MAS NMR spectra of the calcined sample V-MFI(A) and V-MFI(B) are presented in figure 3.11. The signal at δ = 4.8 ppm corresponds to adsorbed water. This has been confirmed by the enhancement of signal intensity on stepwise hydration. The peak at 2.5 ppm of sample V-MFI(B) (Fig. 3.11b) is in the chemical shift range of Si-OH.[39] The signal position at 7.1 ppm (V-MFI(A)) may be attributed to V-OH based on a similar assignment for Ti-OH.[42] The signals at 1.6 and 1.2 ppm are probably due to two distinct ^{1}H environments and are present in both the samples, the intensity being more in V-MFI(A). The two peaks can not be assigned to silanol groups as these would have been reflected in the ^{29}Si MAS NMR spectrum of V-MFI(A) (signals would have appeared in the δ = -98 to -102 ppm range). It is therefore possible that these are associated with the extralattice V-ions. Evidence for these being due to V-OH groups is obtained from the ^{1}H NMR spectrum of V-

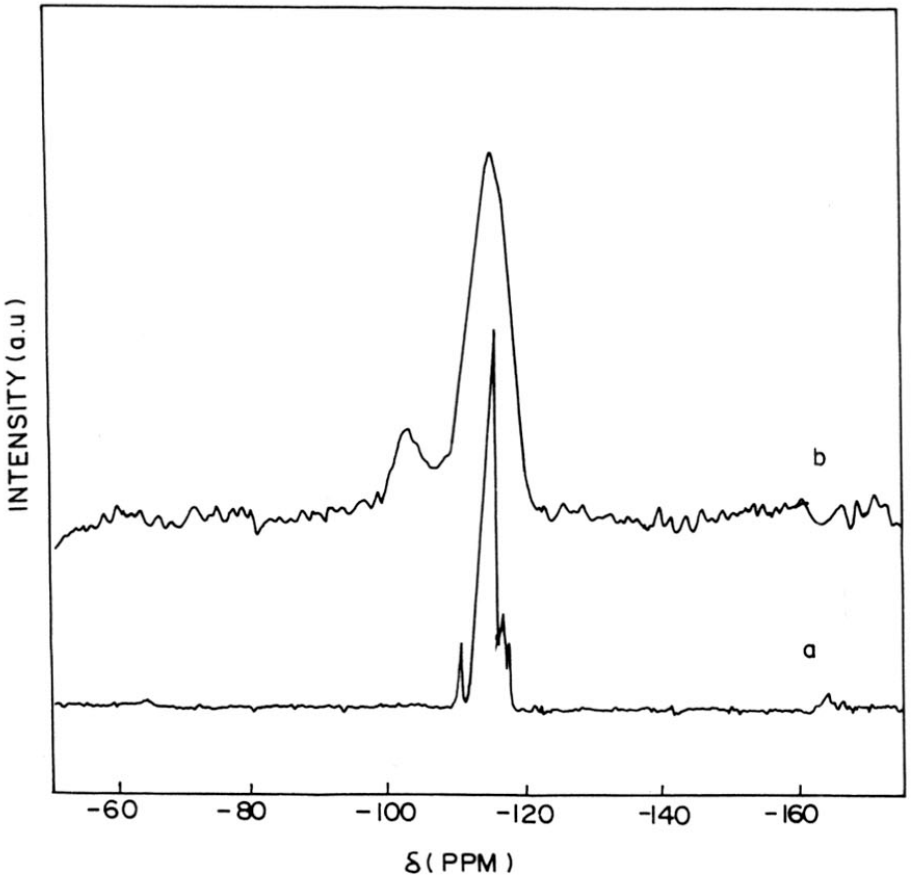

Fig. 3.10 ^{29}Si MAS NMR spectra of the calcined forms of the V-MFI samples. V-MFI(A) (a) and V-MFI(B) (b).

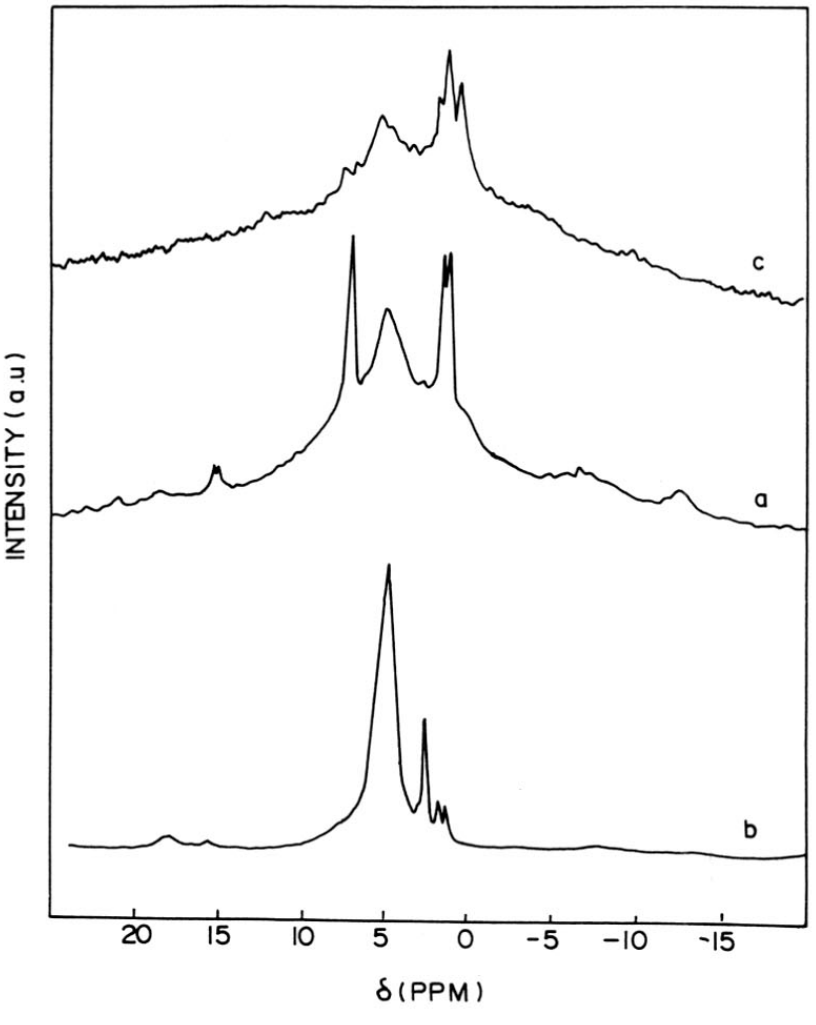

Fig. 3.11 ^{1}H MAS NMR spectra of the calcined forms of the V-MFI samples. V-MFI(A) (a), V-MFI(B) (b) and NH_4OAc extracted V-MFI(A) (c).

MFI(A) after extraction with NH_4OAc (Fig. 3.11c). All the signals attributed to V-OH have decreased significantly. Besides, the ^1H NMR spectrum of silicalite-1 did not reveal these bands. However, interestingly, the bands were also not seen in V-imp-sil-1 sample. The slightly broader spectrum of V-MFI(A) compared to V-MFI(B) is due to the presence of small amounts of paramagnetic V^{4+} ions in the former.

^{13}C MAS NMR spectrum of the as-synthesized V-MFI(A) and MFI(B) are shown in figure 3.12. Such spectra have already been reported for the as-synthesized silicalite-1 prepared in fluoride and alkaline media.[41] The similar type of splitting for C_α, C_β and C_γ indicate that the orientation of the template (tetrapropyl ammonium hydroxide) in silicalite-1 is nearly the same as in vanadium containing silicalite-1.

viii) Thermal analysis

The TG and DTA curves of the as-synthesized samples V-MFI(A) and V-MFI(B) are shown in figure 3.13. A single exotherm is observed for the combustion of the template in the temperature range 723-823K for V-MFI(A), while a more complex (multiple) exotherm is observed for V-MFI(B). Besides, the onset of the exotherm and the occurrence of the peak maximum (of the major exotherm) are earlier in V-MFI(B). These differences suggest that the template interacts significantly with V-ions in V-MFI(B) and not in V-MFI(A). The interaction between the template and V-ions in V-MFI(B) suggests that the V-ions are present in the framework in this sample. Another interesting difference is the presence of a broad and weak exotherm (without weight loss) in the temperature range 513 - 557K in the DTA curve of V-MFI(A), and which is not readily apparent in that of sample V-MFI(B). It is likely that this exotherm is due to the phase transformation of the sample V-MFI(A) from orthorhombic to monoclinic (see XRD Section). Earlier workers[24] have

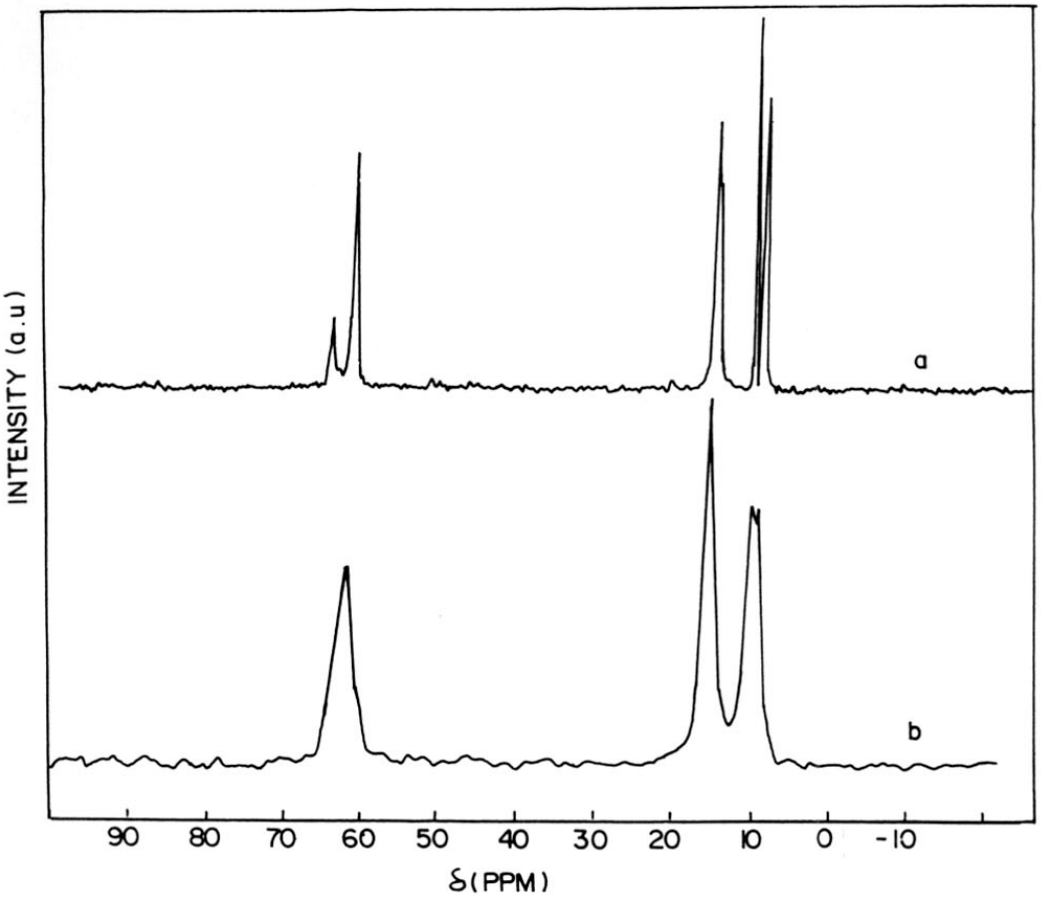

Fig. 3.12 ^{13}C CP MAS NMR spectra of the as-synthesized form of the V-MFI samples. V-MFI(A) (a) and V-MFI(B) (b).

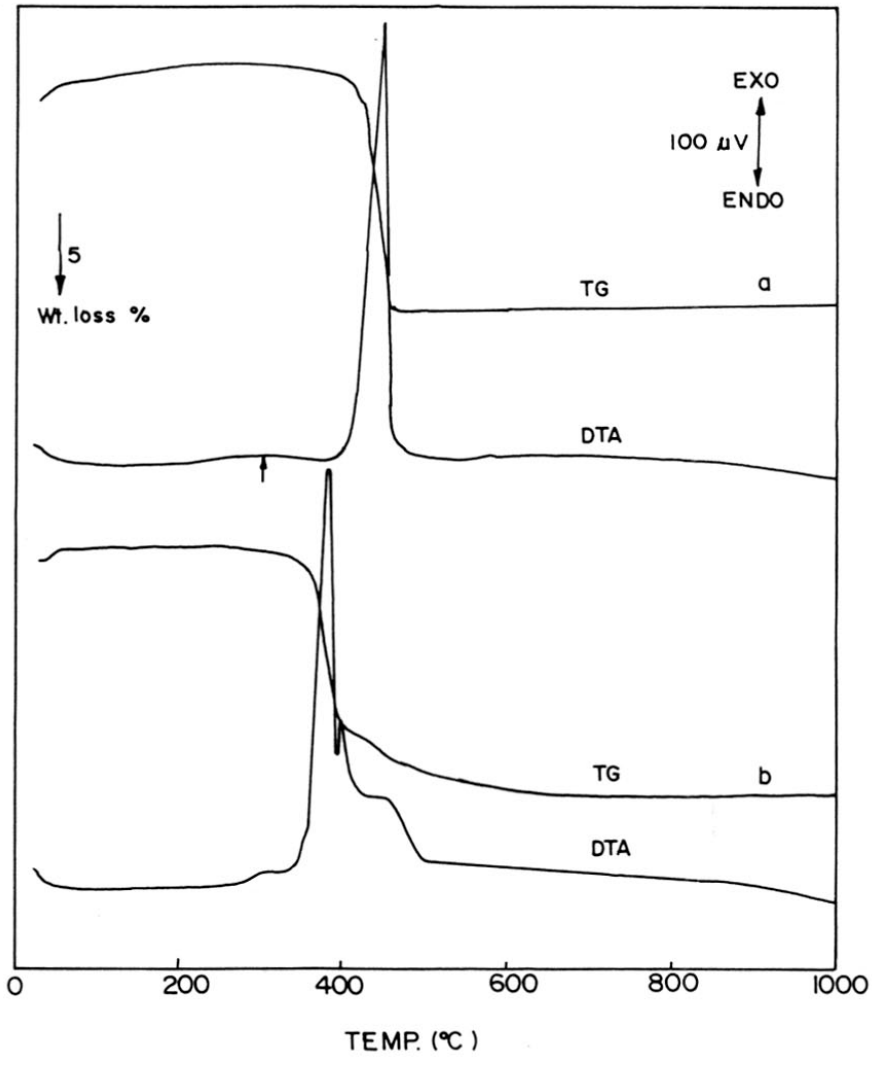

Fig. 3.13 TG-DTA curve of the as-synthesized V-MFI samples. V-MFI(A) (a) and V-MFI(B) (b).

reported (based on XRD studies) that the symmetry change (orthorhombic to monoclinic) occurs in the temperature range 513 - 557K for MFI zeolites.

ix) Surface area and adsorption studies

The total surface areas (S_{BET}) of V-MFI(A) , V-MFI(B) and pure silicalite-1 are respectively, 380, 531 and 386 m^2/g. The mesopore area (t-plot analysis) are 23, 31 and 17 m^2/g. The t-plot areas suggest that the contribution (to total area) from amorphous or external surfaces is similar in all the samples. However, the S_{BET} value is surprisingly large for V-MFI(B). It is possible that the defect sites are responsible for the creation of additional micropore area in V-MFI(B).

n-Hexane and cyclohexane sorption over both the samples were nearly the same (5.2 & 14.1 for V-MFI(A) and 5.3 & 14.4 for V-MFI(B)) whereas water sorption was different (6.0 for V-MFI(B); 6.9 for V-MFI(A)). This larger adsorption of water by V-MFI(A) is probably due to adsorption by the non-framework V-species.

3.2.2. Part b - Physicochemical characterization of V-MEL (VS-2)

The earlier section dealt with the influence of pH on the synthesis of vanadosilicates (typically, MFI). The studies revealed the importance of alkaline pH in vanadium incorporation. The present studies have been undertaken to further evaluate the influence of synthesis parameters in alkaline medium on the incorporation of vanadium and the nature of the species present in the samples. The parameters examined were the atmosphere in which the synthesis was carried out and the concentration of vanadium in the synthesis gel.

Details of the synthesis of V-MEL samples in alkaline medium was presented in Chapter II. Similarly the experimental methods of characterization were also presented in Chapter II. The results of the characterization studies are discussed in this section

i) Analytical data

All the samples V-MEL (1-He and 1 to 4) were prepared using $VOSO_4$ possessing V in the V^{4+} state. However, when the precursor gels were analyzed, both V^{4+} and V^{5+} were present (Table 3.3), the V^{5+} being formed by the aerial oxidation of the V^{4+} in alkaline media (pH > 10.9).[21] When air was excluded by bubbling He through the reactants (V-MEL(1-He)), the amount of V^{5+} formed was lower for the same vanadium input (to be compared with sample V-MEL(1); Table 3.3). In general, both V^{4+} and V^{5+} concentrations in the gel increases with increasing vanadium input (4 to 1-He). The ratio of V^{5+}/V^{4+} increases with decreasing vanadium input (1 to 4). This increase could also be due to the slight increase in the pH values from V-MEL(1) to V-MEL(4) (10.94 to 11.71), though it is probably more due to the shift in equilibrium towards V^{5+} at lower vanadium concentrations in the presence of ambient air (constant excess). Examining the as-synthesized samples, we find that the amount of vanadium incorporated is only about 30 ± 5 % of the vanadium present in the gel (Table 3.3). We also find that while the V^{4+} content increases with increasing total vanadium content, V^{5+} content goes through a maximum (Fig. 3.14).

The V^{4+} content of the as-synthesized samples increases linearly with the V^{4+} content in the gel. The V^{5+} content however, goes through a maximum with increase in the V^{5+} content in the gel (Fig. 3.14). This sharp contrast in the pick-up of V^{4+} and V^{5+} species in the samples could suggest that the two V-species are entering the solid differently. The linearity in the pick-up of V^{4+} with increasing V^{4+} content in the gel is reminiscent of Henry's

Table 3.3

V^{4+} and V^{5+} break up in the gel and crystalline samples of V-MEL samples.

Sam-ple	pH of the gel	color of the gel	V-concentration (x 10^{-5})							
			Gel			As-synthesized			Calc-ined	Ext[b]
			V/ Si+V	V^{4+}/ Si+V	V^{5+}/ Si+V	V/ Si+V	V^{4+}/ Si+V	V^{5+}/ Si+V	V/ Si+V	V/ Si+V
1-He	10.9	dark green	25.0	20.6 (19.9)[a]	4.3	10.2	8.9 (8.4)[a]	1.3	10.2	0.3
1	10.9	green	25.0	12.7 (11.6)	12.2	7.5	6.0 (5.8)	1.5	7.5	0.7
2	11.2	light green	12.5	3.5 (4.2)	8.9	4.1	0.8 (1.2)	3.3	4.1	2.4
3	11.5	color-less	9.1	1.9 (2.3)	7.2	3.5	0.3 (0.5)	3.2	3.5	2.5
4	11.7	color-less	6.3	0.8 (1.0)	5.4	2. 5	0.3 (0.3)	2.2	2.5	1.9

a → Numbers in parentheses indicate V^{4+}/ Si +V from ESR measurements.

b → Calcined and extracted with 1N NH_4OAc solution.

law and suggests that the V^{4+} ions are bound (or adsorbed) on the large surface available (even when the template is present) in the solids. Maximum pick-up of V^{5+} in the samples occurs at an intermediate concentration of V^{5+} in the gel. At high concentrations of V^{5+}, reduced incorporation occurs due to the formation of oligomeric V^{5+} species (which are probably insoluble solids) in the gel.

When the as-synthesized samples were calcined, only V^{5+} ions were present in the samples (Table 3.3). On extraction with 1N NH_4OAc solution, a significant amount of vanadium was lost from the samples. The vanadium contents of the extracted samples were slightly less than the V^{5+} present in the as-synthesized samples (Table 3.3). Based on the vanadium pick-up data and the results of the extraction experiments, one may surmise that the vanadium extracted by the NH_4OAc treatment was mostly what was originally present as V^{4+} ions in the as-synthesized samples, most of the V^{5+} ions which had probably entered the lattice being resistant to extraction. Besides, the small decrease in the V^{5+} content of the extracted samples (2 to 4) could have been due to the loss of oligomeric V^{5+} ions picked up from the gel and which were weakly attached to the lattice.

ii) XRD studies

All the samples (V-MEL(1-He and 1 to 4)) were highly crystalline without any impurity phases, especially MFI. Incorporation of vanadium increases the unit cell (UC) volume of the samples (Table 3.4). A linear correlation exists between the UC volume and the amount of non-extractable vanadium present in the calcined samples (Fig. 3.15). On the other hand, the UC volume goes through a maximum when plotted against total vanadium content in the samples (Fig. 3.15b). The XRD results provide direct evidence that non-extractable V^{5+} ions are in the lattice.

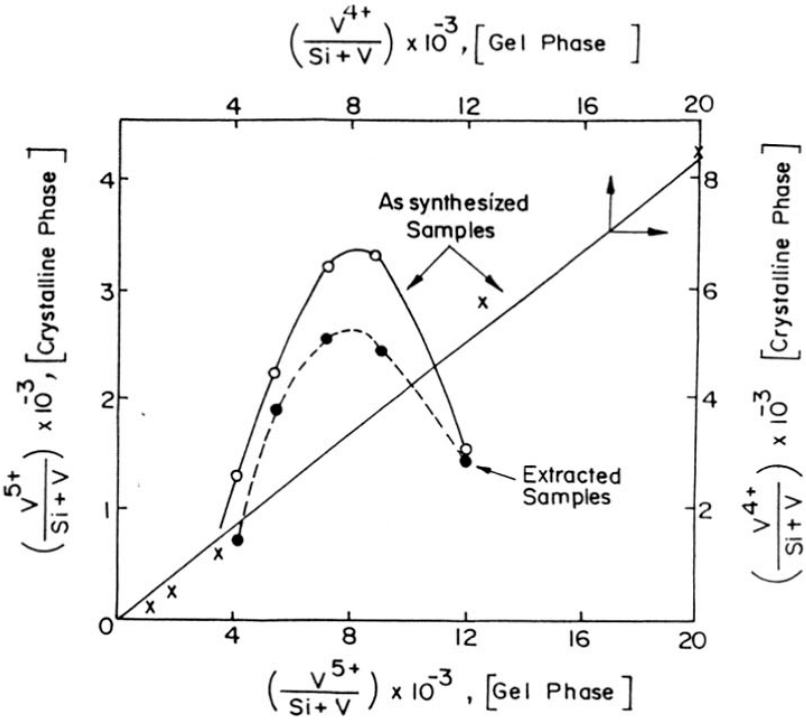

Fig. 3.14 Concentration of V^{4+} and V^{5+} in crystalline samples *vs.* V^{4+} and V^{5+} in the gels of V-MEL samples.

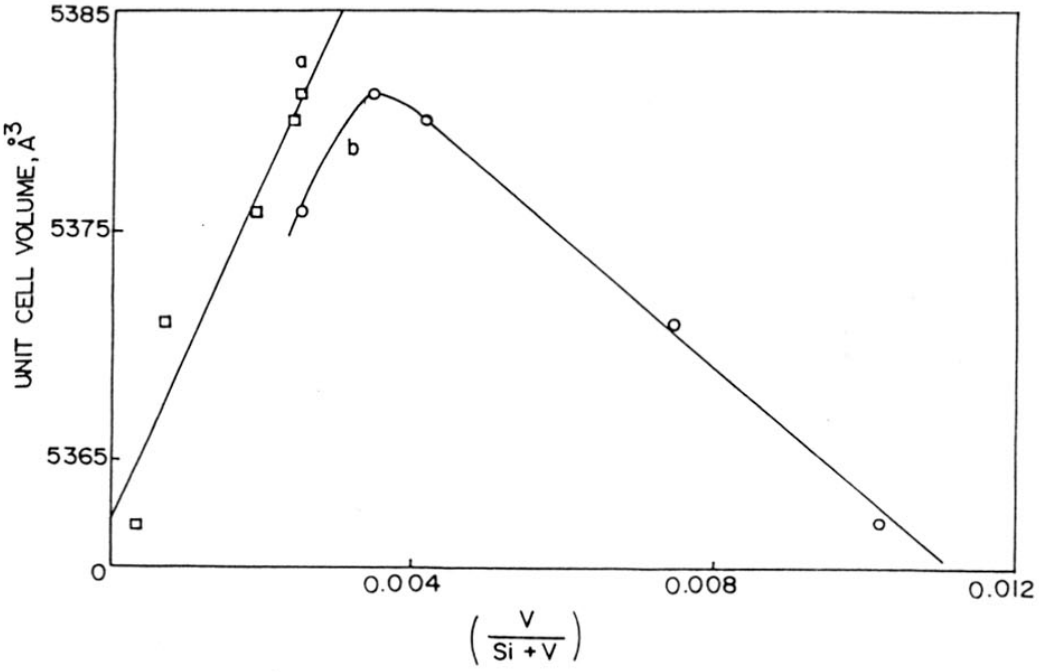

Fig. 3.15 Dependence of unit cell volume of the calcined samples on the vanadium concentration in extracted (a) and calcined (b) MEL samples.

Table 3.4

Physicochemical properties of V-MEL samples.

Sample	Unit cell volume of calcined samples	Surface area (m^2/g)	Sorption capacity* (wt %)		
	($Å^3$)		cyclohexane	n-hexane	water
1-He	5363.5	547	8.3	12.8	6.4
1	5372.6	549	8.1	13.1	6.3
2	5383.3	554	8.5	13.4	5.6
3	5384.7	556	8.4	13.1	5.5
4	5378.4	558	8.4	13.5	5.4
sil-2	5360.2	542	8.1	13.1	2.0

*→ $p/p_0 = 0.5$; temp. = 300K.

iii) *SEM*

Figure. 3.16 shows the SEM photographs of four different samples. The particle size (2-5 μm) decreases with increase in the vanadium incorporation (silicalite-2 to V-MEL(3)).

iv) ESR spectroscopic studies

The gel phase ESR spectra of all the samples at 0h (just after the addition of $VOSO_4$ solution during the gel preparation) consist of eight hyperfine lines (Fig. 3.17a; V-MEL(1)) without anisotropy (g = 1.963 and A=92.8 G) and correspond to free vanadyl (VO^{2+}) ions.[28] The final gels (after 5h stirring) produce again eight line spectra (Fig. 3.17b; sample V-MEL(1)), though, with anisotropy (g_{11} = 1.928, $g_{\perp}$ = 1.977, A_{11} = 187.5, $A_{\perp}$ = 80G). The spectra correspond to V^{4+} ions in an axially symmetric environment. These vanadyl ions are probably $VO(OH)_3$, which are reported to be present at high pH (10-12). The concentration of V^{4+} estimated from the ESR peak intensities are presented in table 3.3. The concentration of V^{4+} ions (based on ESR and analytical data) increases with the total vanadium concentration in the gel, but the lines do not pass through the origin (Fig. 3.18) suggesting that nearly all the V^{4+} ions are converted to V^{5+} at low vanadium inputs.

All the as-synthesized samples exhibit eight line hyperfine spectra (Fig. 3.19a) with anisotropy (g_{11} = 1.932, $g_{\perp}$ = 1.982, A_{11} = 186G, $A_{\perp}$ = 73G) attributed to V^{4+} in an Oh environment .[29,30] The absence of ESR activity (298K and 77K) in the calcined (both dehydrated and hydrated) samples of V-MEL (2, 3 and 4) confirm the absence of paramagnetic V-species. The dehydrated calcined samples of V-MEL(1-He and 1) exhibit a broad single line ESR spectrum attributable to paramagnetic $O_2^{\cdot -}$ (g = 2.002) attached to the vanadium. No signal attributable to V^{4+} ions could be detected in these samples also. Such

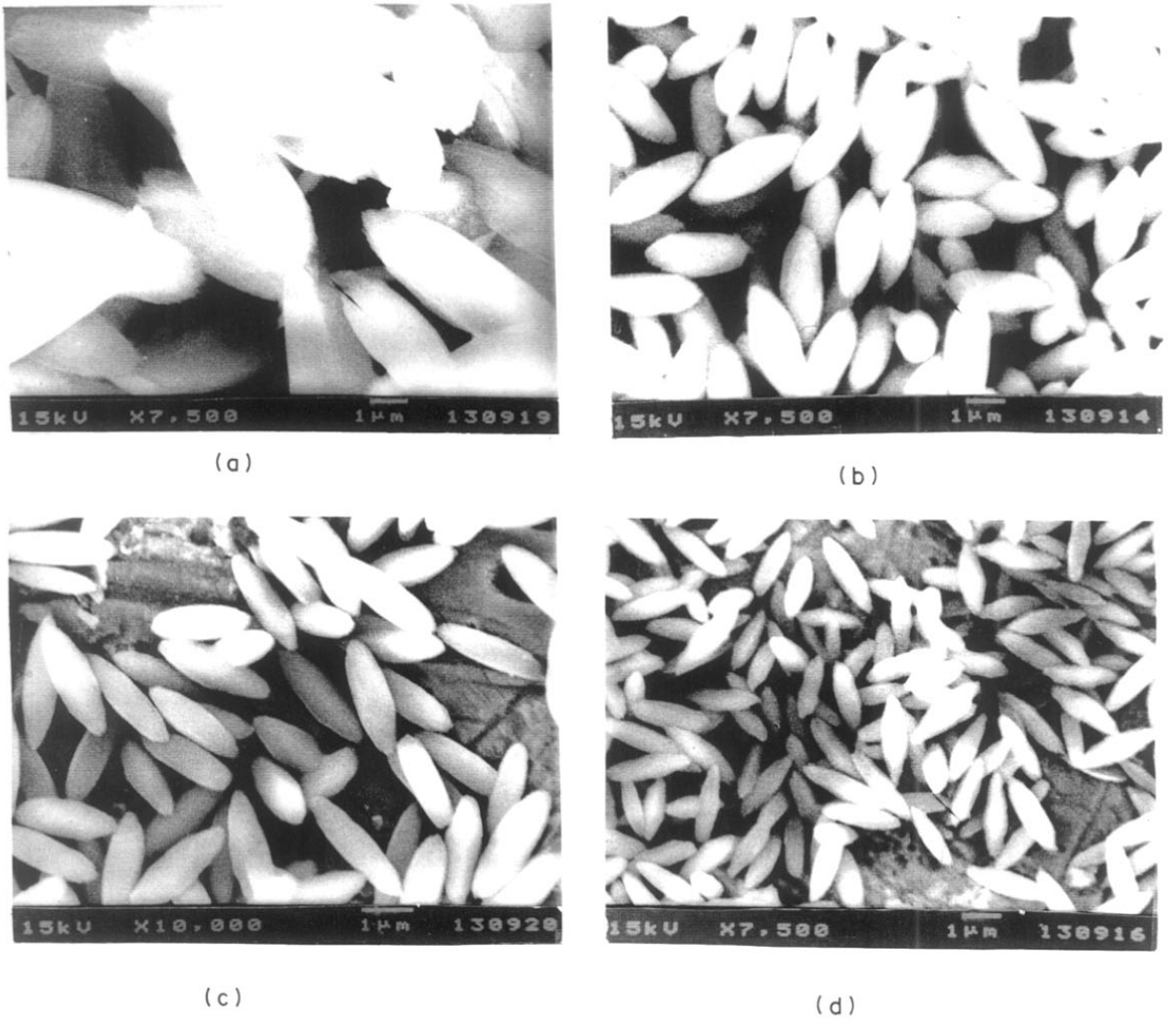

Fig. 3.16 SEM photograph of V-MEL samples. Silicalite-2 (a), V-MEL(1-He) (b), V-MEL(1) (c) and V-MEL(3) (d).

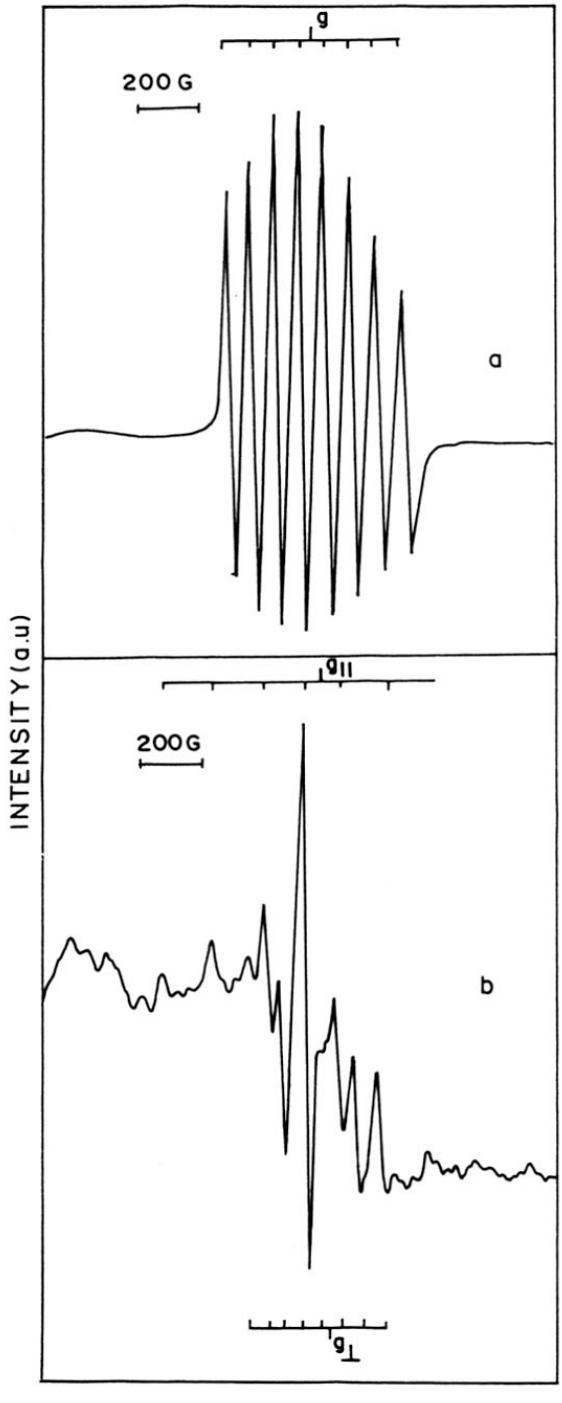

Fig. 3.17 ESR spectra of the synthesis gel of V-MEL sample. V-MEL(1) : initial time, 0h (a) and final time, 4h (b).

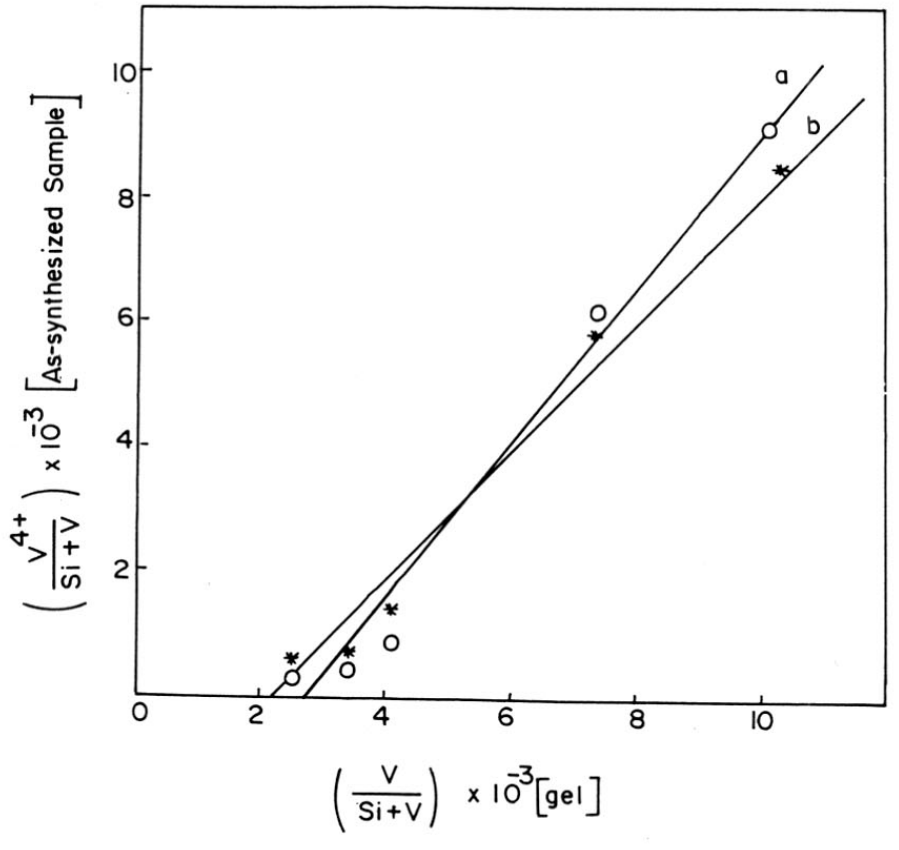

Fig. 3.18 Dependence of V^{4+} concentration (ESR (a) and titrimetric (b)) on the concentration of total V in the as-synthesized V-MEL samples.

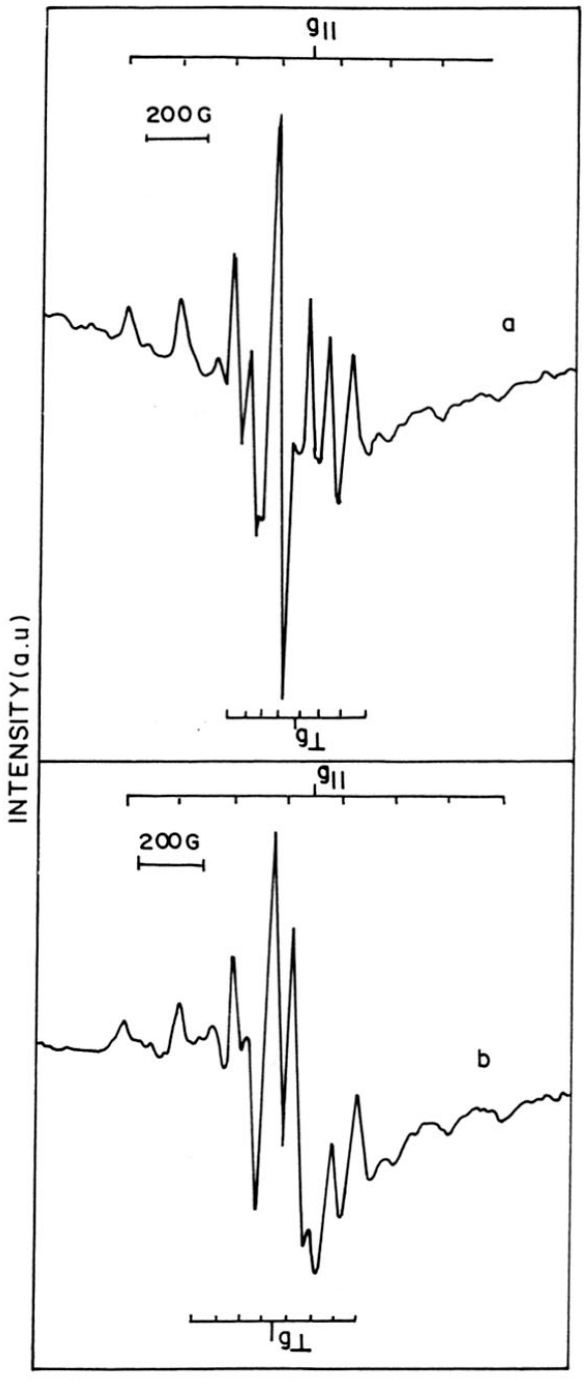

Fig. 3.19 ESR spectra of the as-synthesized (a) and reduced (b) forms of sample V-MEL(2).

an $O_2^{\cdot -}$ species has been reported by Fejes *et al.*[43] in VS-1. Upon hydration, both the samples (V-MEL(1-He) and V-MEL(1)) were yellow and ESR inactive. The vacuum dehydrated (10^{-6} Torr, 543K) sealed samples exhibited an eight line hyperfine spectrum corresponding to paramagnetic V^{4+} species. Cavani *et al.*[44] have reported that TiO_2 supported V^{5+} undergoes reduction to V^{4+} in vacuum (1×10^{-5} Torr) at 623K.

Upon reduction in the presence of H_2 at 573K for 6h, samples 2, 3 and 4 exhibit similar ESR spectra ($g_{11} = 1.935$, $g_\perp = 1.992$, $A_{11} = 182G$, $A_\perp = 70G$) at 77K and 298K (Fig. 3.19b), while the V-MEL(1-He) and V-MEL(1) were ESR inactive. The signals are attributable to V^{4+} ions in a SqPy environment (supporting argument follows).[31] According to Davidson *et al.*[31] the ESR spectra of axially distorted octahedral geometries are generally difficult to distinguish from those of the SqPy ones, because the sixth ligand is weakly bonded and only slightly modifies the unpaired electron distribution. However, ESR spectra of the two geometries are characterized by $g_\perp > g_{11}$ and $A_\perp > A_{11}$. The unpaired electron is assumed to be mainly located in the $3d_{xy}$ orbital of the metal. According to Sharma *et al.*[45], the quantity $B = \Delta g_{11} / \Delta g_\perp$ (where, Δg_{11} and $\Delta g_\perp$ refer to the differences between the g values for a free electron and the observed g values) reflects changes in the tetragonal distortion (C_{4v} symmetry). An increase of B indicates a shortening of the V=O bond, or a lengthening of the distance of the oxygen ligands in the basal plane. The B value for the V^{4+} in the as-synthesized samples (Oh symmetry) is 3.77 and is smaller than the value (8.12) for the species present in the reduced samples. This indicates a shortening of the axial V=O bond in the V^{4+} species in the reduced samples and confirms our assignment of the SqPy symmetry. The V=O bond length in $VOSO_4,5H_2O$ (Oh) is 1.591Å and is larger than 1.560Å observed in the case of $VO(acac)_2$ (SqPy environment).[46]

v) FT-IR spectroscopic studies

Figure 3.20 presents the framework IR spectra of calcined V-MEL(1-He and 1 to 4) samples. An absorption band at around 967 cm^{-1} is present in the framework IR spectra (Fig.3.20). This band has been attributed to the $Si\text{-}O^{\delta-}$ linkages associated with the defect site around a metal ion.[34] The band is absent in silicalite-2 and V-imp-sil-2. The relative intensity of this band [I_{967}/I_{550}] goes through a maximum with increasing vanadium content in the calcined samples, while it increases linearly with the V^{5+} content in the extracted samples (Fig. 3.21). The intensity of the 967 cm^{-1} band is the same in both the extracted and calcined samples indicating that the band originates from the stable V-species in the silicate lattice. In the case of the as-synthesized samples, the relative intensity of the IR band at 967 cm^{-1} increases linearly with the V^{5+} ions (Fig. 3.21) suggesting increasing amounts of V^{5+} ions in the framework and the consequent increasing amounts of defect sites.

vi) UV-visible diffuse reflectance (DR) spectroscopic studies

Figure 3.22 and figure 3.23 present the UV-Visible DR spectra of the as-synthesized and calcined V-MEL samples (1-He and 1 to 4). The as-synthesized forms of the samples V-MEL(1-He and 1) do not exhibit any band in the 250-340 nm region suggesting the absence of detectable amounts of V^{5+} in Td environments (based on the assignment of table 3.2), but the as-synthesized forms of samples V-MEL(2, 3 and 4) exhibit an intense absorption at 333 nm indicating the presence of V^{5+} in Td environments. The calcined forms of the sample V-MEL(1-He) and V-MEL(1) exhibit intense bands at 285 nm and 384 nm (Fig. 3.23) indicating the presence of Td-V^{5+} species with V=O bonds. The calcined forms of samples V-MEL (2, 3 and 4) exhibit an intense band at 333 nm (Fig. 3.23) similar to the as-synthesized samples. Sample V-MEL(1-He) did not exhibit any absorption

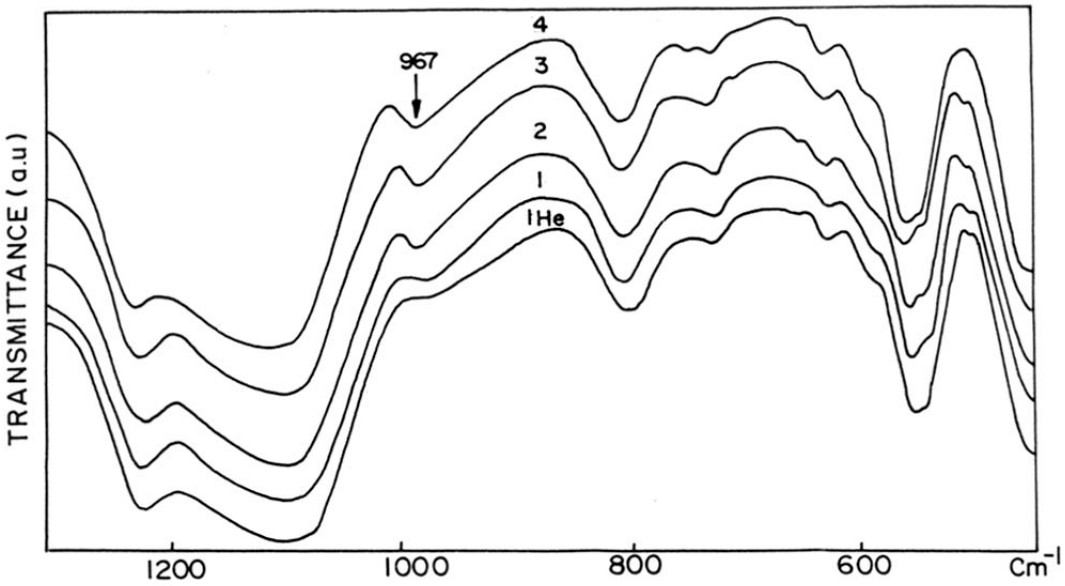

Fig. 3.20 Framework IR spectra of calcined V-MEL samples.

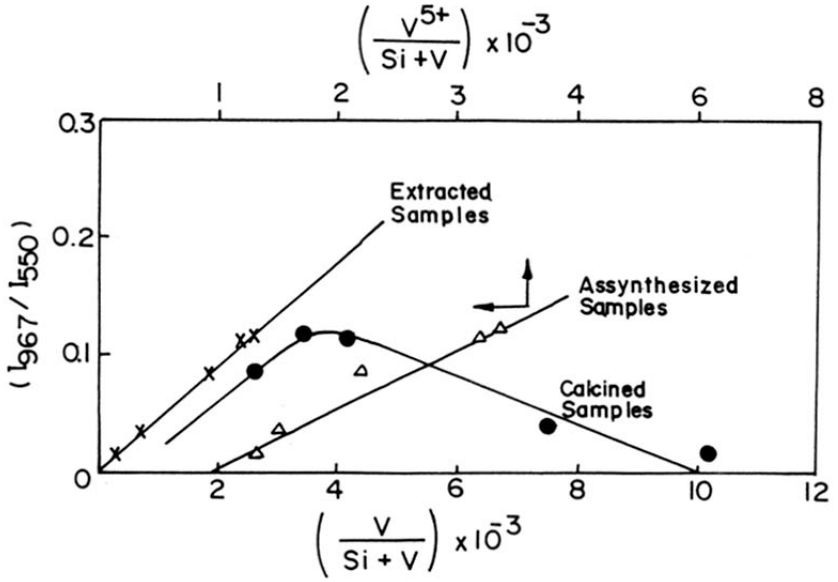

Fig. 3.21 Relative intensity of the 967 cm^{-1} band (I_{967} / I_{550}) as a function of V^{5+} concentration in the as-synthesized, calcined and extracted V-MEL samples.

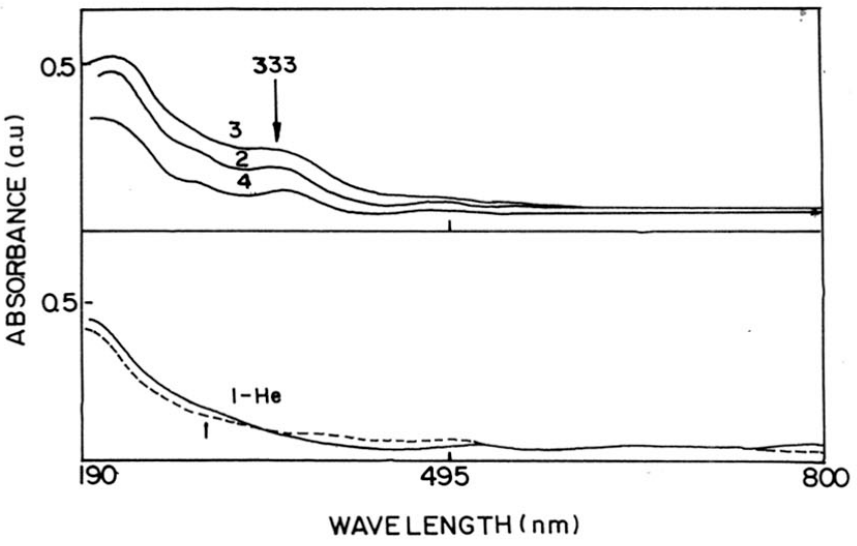

Fig. 3.22 UV-Visible DR spectra of the as-synthesized V-MEL samples.

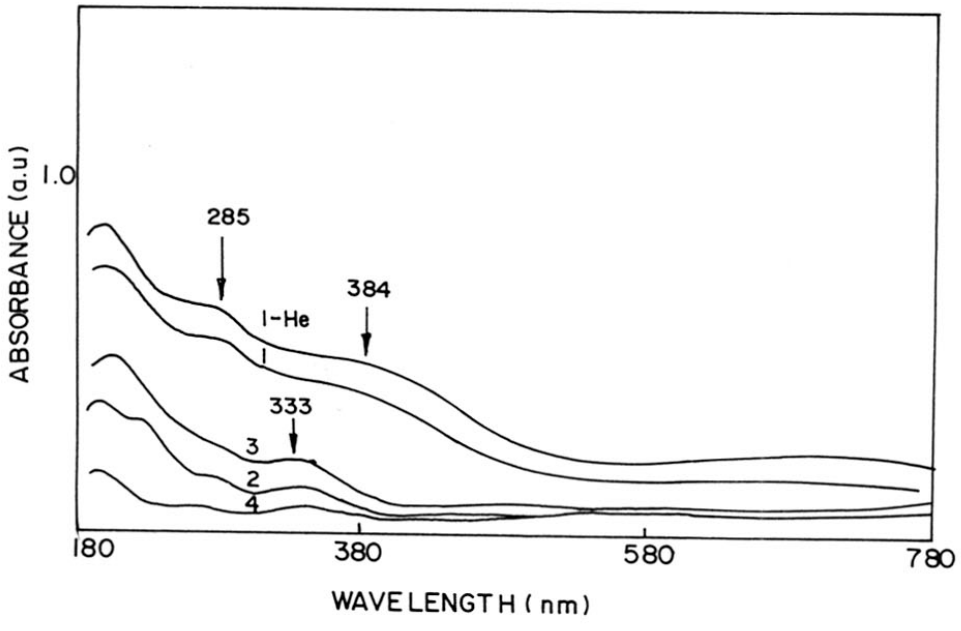

Fig. 3.23 UV-Visible DR spectra of the calcined V-MEL samples.

after extraction with NH_4OAc suggesting the absence of detectable amounts of V, whereas, the absorption spectrum is unchanged in the samples V-MEL(2, 3 and 4). The spectrum of V-MEL(1) after extraction with NH_4OAc is too weak for proper analysis. The above observations indicate that at least two vanadium species with different Td-V^{5+} environments are present in the calcined V-MEL samples. One of the species is easily leached out by NH_4OAc treatment and the other one is stable in the MEL lattice.

vii) NMR spectroscopic studies

Figure 3.24 presents the ^{51}V liquid state NMR spectrum of the final gel (5h) of V-MEL(2). The intense peaks at around δ = -536 ppm and -561 ppm (reference $VOCl_3$), correspond to the monomeric HVO_4^{2-} species (present in equilibrium with VO_4^{3-} species) and dimeric $V_2O_7^{4-}$.[36,37] It has already been reported that these are the two major V^{5+} species present at high pH (9 to 13).[21]

Figure 3.25 presents the solid state ^{51}V MAS NMR spectra of the V-MEL samples. A-E are the spectra of the calcined and hydrated samples, whereas the one shown as D* corresponds to the spectrum of the as-synthesized form of V-MEL(3).

Interpretation of the two line ^{51}V MAS NMR spectrum of the sample V-MEL(1-He) (Fig. 3.25a) requires us to consider anisotropic quadrupole and chemical shielding effects normally encountered in vanadium compounds. In an effort to disentangle these effects, we have recorded ^{51}V NMR spectrum of a static sample at different spectrometer conditions, viz., field strength and pulse sequences. These data are presented in figure 3.26. When the spectral width is small (125 kHz), the ^{51}V NMR spectrum is essentially dominated by an intense resonance at δ = -526.8 ppm (I) flanked by a low field shoulder(II) at -505.8 ppm (Fig. 3.26a), when the spectrum is recorded at 7.05 Tesla. The resolution is clearly increased

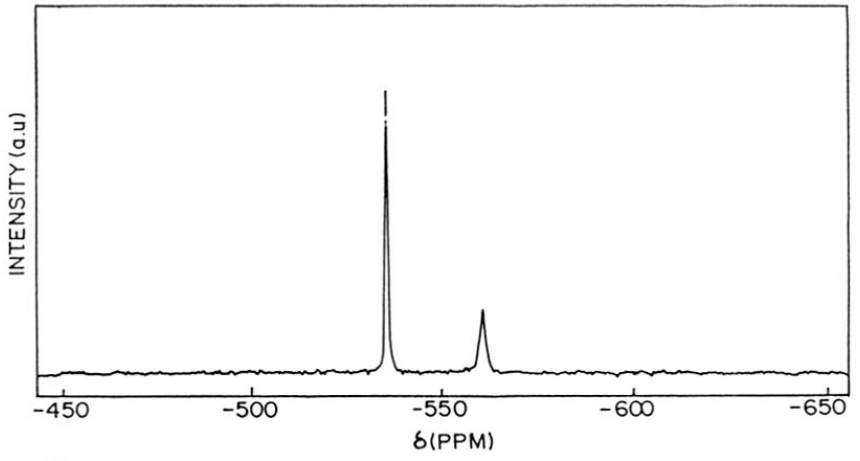

Fig. 3.24 ^{51}V liquid state NMR of the final gel of sample V-MEL(2).

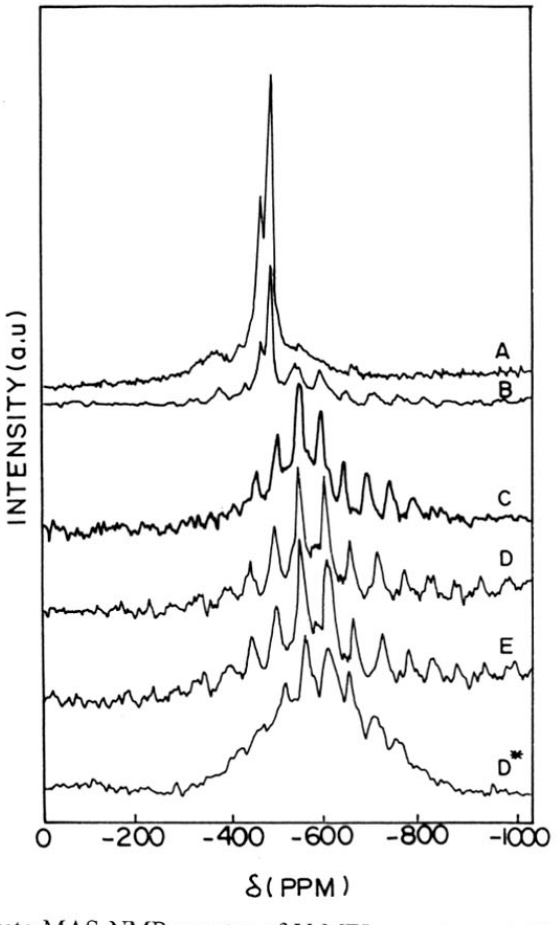

Fig. 3.25 ^{51}V solid state MAS NMR spectra of V-MEL samples : A-E, calcined and hydrated V-MEL(1-He); and V-MEL(1) to V-MEL(4) respectively; D^* , as-synthesized V-MEL(3).

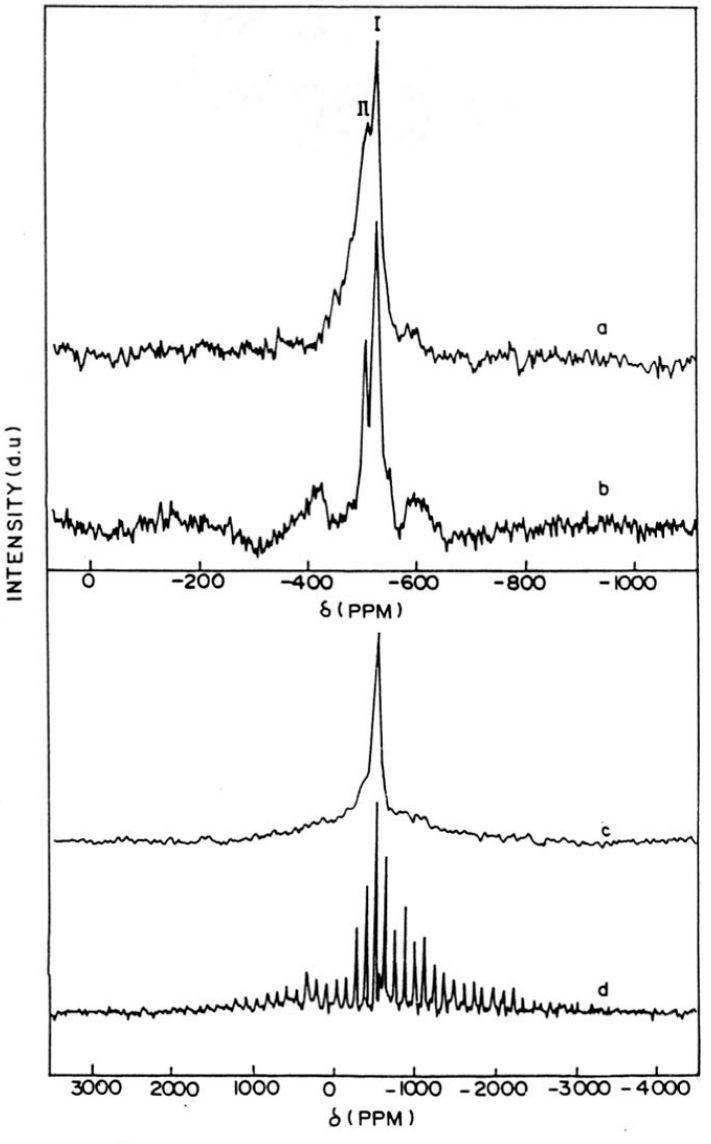

Fig. 3.26 Static ^{51}V NMR spectra of sample V-MEL (1-He) : (a) 7.05 Tesla field, obtained using spin-echo sequence and 125kHz spectral width, 18,300 scans, (b) 9.4 Tesla field, obtained using a CYCLOPS sequence and 125kHz spectral width, 18300 scans, (c) 7.05 Tesla field, obtained using spin-echo sequence and 1.7 MHz spectral width, 29,500 scans. 250 ms recycle delay, τ = 50 μsec. and (d) 7.05 Tesla field, obtained using spin-echo sequence and 1.7 MHz spectral width. This spectrum is the result of Fourier-Transforming the spin-echo train obtained using a CPMG pulse sequence using τ = 50 μsec; 62,000 scans, 200ms recycle delay.

at 9.4 Tesla (Fig. 3.26b), where we observe that the low field resonance experiences a small shift (-2.2 ppm) and also has a smaller line width (1.25 kHz) than at 7.05 Tesla (3.31kHz). It may be noted that the high field resonance position (-526.8 ppm) is independent of the manner in which the spectrum is obtained (static or MAS) or the strength of the main magnetic field (7.05 or 9.40 T). This at once suggests that the high field resonance (I) has negligible anisotropy and therefore corresponds to highly mobile V-species. The anisotropic line broadening for the low field resonance (II) is clearly revealed when the spectral width is increased to 1.67 MHz and a distortionless powder pattern is recorded using the spin-echo technique (Fig. 3.26). Here, the intense central line corresponds to the two line pattern noticed in a and b, the loss of peak resolution attributable to inferior digital spectral resolution. The anisotropic broadening associated with (II) is clearly demonstrated in figure 3.26, where the result of Fourier transforming a Carr-Purcell-Meiboom-Gill (CPMG)[47] echo train is shown. In the CPMG pulse sequence, the application of a non-selective $\Pi/2$ pulse at the beginning of the sequence creates transverse magnetization. The repeated application of Π pulses of spacing 2τ generates an echo train only when internal interactions are inhomogeneous in character and therefore can be refocussed by the Π pulse. The time domain response of the echo train is essentially a convolution of the lineshape function, which leads to the envelope of the powder spectrum (c), by a comb function of spacing 2τ(d). Thus, Fourier transform of this echo train results in spikelets (d) of width 1.6 kHz, spaced ~10 kHz (τ = 50 μsec) apart, showing that the observed broadening in (c) is inhomogeneous in nature. Although the CPMG experiment suggests the presence of quadrupole interactions (Fig. 3.26(c,d)), the experiment by itself does not intensify the specific species (I or II) which experiences strong quadrupole interaction.

Nutation experiments will identify the species experiencing quadrupole interaction. In the nutation experiment, the response of the ^{51}V nucleus experiencing a quadrupole interaction to an applied magnetic field is monitored by varying the duration of the exciting pulse. When the quadrupole interaction is absent or very weak, the nutation behavior is expected to be similar to that of an equivalent spin 1/2 system. In the presence of quadruple interactions however, the observed magnetization nutates faster, the nutation frequency being determined by the strength of the quadrupole interaction and the spin transition being excited. Hardcastle *et al.*[48] have discussed a similar experiment in the case of V-Bi system. The observed nutation behaviour for I and II, are shown in figure 3.27 and compared with the data obtained on liquid $VOCl_3$ sample. The nutation behavior of I is similar to that of $VOCl_3$ liquid and therefore suggests that the quadrupolar effects are negligible for this V-species. This reinforces our view that type I environment is highly mobile and may be associated with their presence in the zeolite channel. Similar observation of highly mobile V-species in V-impregnated Al_2O_3 surfaces at pH = 10 has been reported.[49] The faster nutation of magnetization for species II at once suggests that quadrupolar interactions dominate the observed spectral broadening. The observation of a narrower line in the high field (9.4 Tesla) static and 7.05 Tesla MAS spectra are indicative of weak to moderate quadruple couplings for this V-species. Recently, Reddy *et al.*[19] have reported a similar two line pattern in the ^{51}V MAS NMR spectrum (7.05 Tesla) of V-MCM-41 and have tentatively assigned this to two different Td V-species.

The fully dehydrated sample V-MEL(1-He) is NMR inactive. The reason may be due to the presence of paramagnetic $O_2^{\cdot-}$ (g = 2.002, ESR evidence) bonded to the V^{5+} in the freshly calcined sample in air. On dehydration under similar conditions in vacuum, the vacuum sealed sample V-MEL(1-He) is also NMR inactive, while it exhibits an eight line

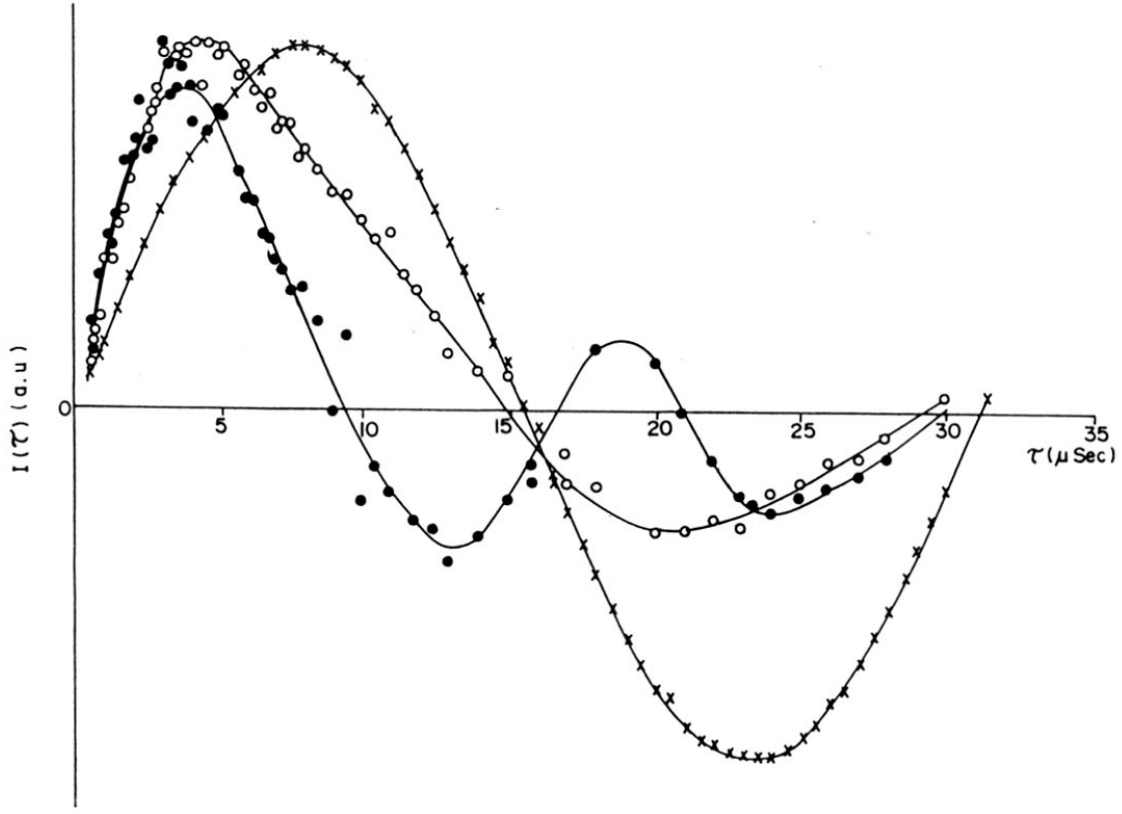

Fig. 3.27 ^{51}V signal intensity as a function of the length of exciting r.f pulse showing the nutation of ^{51}V magnetization under the influence of an applied r.f field. (X) $VOCl_3$ neat liquid; (0) Central ^{51}V resonance (~ 505) ppm; (0) ^{51}V resonance at (~-1100) ppm.

hyperfine ESR spectrum corresponding to paramagnetic V-species. After NH_4OAc treatment and calcination, sample V-MEL(1-He) exhibits no NMR signal due to the absence of detectable amounts of V^{5+} ions (Table 3.3). This observation suggests that these NMR active V-species are easily extracted by NH_4OAc. These are probably mostly the nonframework V-species.

The calcined form of the samples V-MEL (2, 3 and 4) exhibits NMR spectra with a typical anisotropic pattern (isotropic chemical shift δ = -621.1 ppm) with negligible contribution from quadrupolar effects of I = 7/2 ^{51}V nucleus. Reddy *et al.*[15a] and Moudrakovski *et al.*[15b] have also reported similar spectra for VS-12 and have suggested that V-species are present in distorted Td environments. No change in the NMR spectra is observed upon hydration/dehydration or NH_4OAc treatment indicating that the spectra are those of stable V-species. These species are probably the framework V-species. Sample V-MEL(1) exhibits a NMR spectrum containing both the environments (framework and nonframework). After NH_4OAc treatment, sample V-MEL(1) exhibits a weak NMR signal with an isotropic chemical shift at δ = -621.1 ppm. The intensities of the NMR peaks due to the non-framework V-species (a two line NMR pattern) are related to the amount of extractable vanadium species. Sample V-MEL(1-He) and V-MEL(1) do not exhibit any NMR signal in the as-synthesized form due to the absence of any significant amount of V^{5+} ions.

The as-synthesized forms of the samples V-MEL (2, 3 and 4) exhibit similar broad intense NMR spectra (Fig. 3.25D$^{\bullet}$) corresponding to V^{5+} species. The isotropic chemical shift at δ = -621.1 ppm is similar to that observed in the calcined samples and has been attributed to the distorted Td environments.[15] The broadness may be due to the presence of diamagnetic V-ions (V^{5+}) in close proximity to the paramagnetic V-ions (V^{4+}).

^{29}Si NMR spectra of the gels of V-MEL samples and silicalite-2 (without vanadium) are shown in figure 3.28. The gel sample of the silicalite-2 exhibits a NMR spectrum containing a sharp peak at δ = -109 ppm corresponding to Q^4 species, $[(SiO)_4Si]$.[39] The intensity of this peak decreases with increasing vanadium concentration in the gel. This indicates a definite interaction between the monomeric HVO_4^{2-} species with the silicate species in the gel. Thangaraj *et al.*[50] also made a similar observation in the case of TS-1.

viii) Thermal analysis

Simultaneous TG-DTA (in air) of V-MEL(3) shows the exothermic combustion of the template in the as-synthesized samples (Fig. 3.29). The decomposition around 600 - 630K, coincides with a weight loss due to template decomposition. The decomposition of template of pure silicalite-2 occurs at around 623 - 633K. The exotherm of V-MEL(3) occurs at a lower temperature compared to silicalite-2, probably due to V acting as a combustion promoter.

ix) Surface areas and adsorption studies

The low pressure nitrogen adsorption isotherms of the samples at liquid nitrogen temperature are typical of microporous materials. The surface areas of the V-MEL samples with different Si/V ratios and silicalite-2 are given in table 3.4. The surface areas show a marginal decrease with increase in the vanadium content of the calcined samples. The mesoporous areas (t-plot analysis) are quite small (20 to 60 m^2/g) and increase with increasing vanadium content. silicalite-2 possess a lower area than the others.

The sorption capacities of the samples for water, n-hexane and cyclohexane are also presented in table 3.4. The sorption capacity for water decreases with an increase in

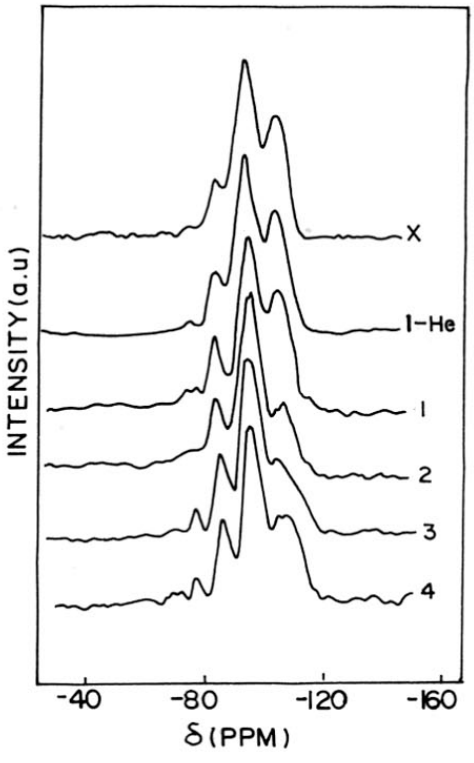

Fig. 3.28 ^{29}Si liquid state NMR of the gels of V-MEL samples and silicalite-2 (x).

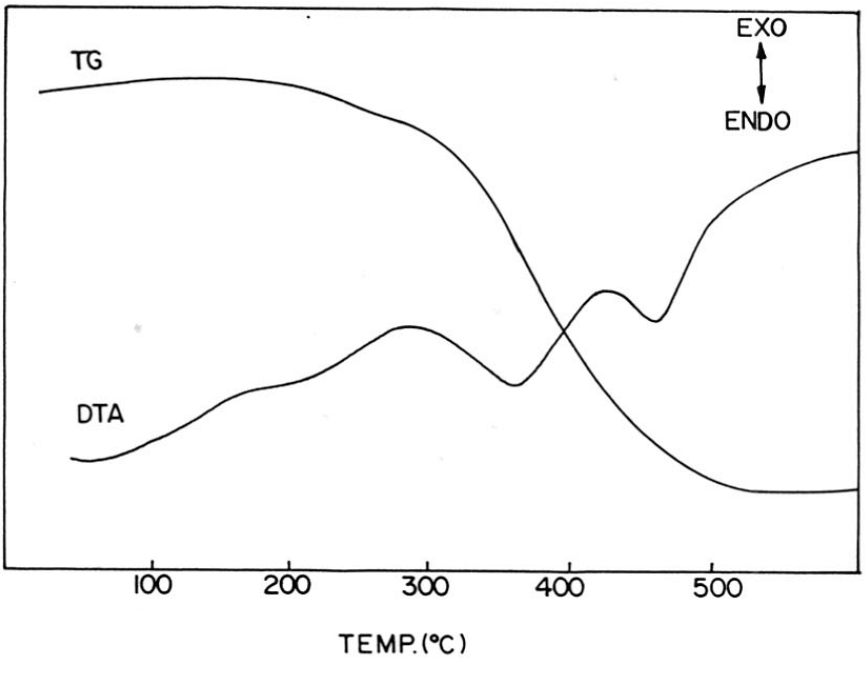

Fig. 3.29 TG-DTA curve of the as-synthesized V-MEL(3).

Si/V ratio. The sorption capacity for water is indicative of the relative hydrophobicity / hydrophilicity of the molecular sieves. The hydrophobicity can be expected to increase with the Si/V ratio. The equilibrium sorption capacities for the bulkier cyclohexane are lower than for the linear n-hexane. The sorption capacities for cyclohexane and n-hexane are similar for all the samples.

Probable V-species in the samples

Based on the above data, the plausible structures for the V-species present in the gels, the as-synthesized, calcined (hydrated/dehydrated) and reduced V-MEL samples are presented in Scheme 3.1. The two major V-species present in the precursor gels (identified by ESR and NMR) are HVO_4^{2-} (V^{5+}; I) and H_3VO_4 (V^{4+}; II). During synthesis, the HVO_4^{2-} species interact with the silicate species (^{29}Si NMR data) and produce framework V-species (III) present in a distorted Td environment (NMR and UV-VIS data). Simultaneously, V^{4+} ions (IV) are picked up by samples as extra lattice ions. These possess an Oh environment and are ESR active. These appear to exist as discrete V^{4+} species as their concentrations estimated by ESR and titrimetric methods match (Table 3.3). On calcination, these species (IV) are oxidized to the V^{5+} species (VA) and (VB); (VA) is mobile and (VB) is loosely bound to the surface. These are, however, NMR inactive due to their association with $O_2^{\cdot -}$ ions (ESR of $O_2^{\cdot -}$ observed). On hydration these transform into NMR active species (VI A) and (VI B). These V^{5+} species are extracted by NH_4OAc and are catalytically inactive. On evacuation, these undergo reduction into ESR active species (VII A and B). The V^{5+} species (III) originally present in the as-synthesized samples change symmetry into distorted Td (VIII) on calcination (dehydration). Hydration of this sample does not alter its symmetry as

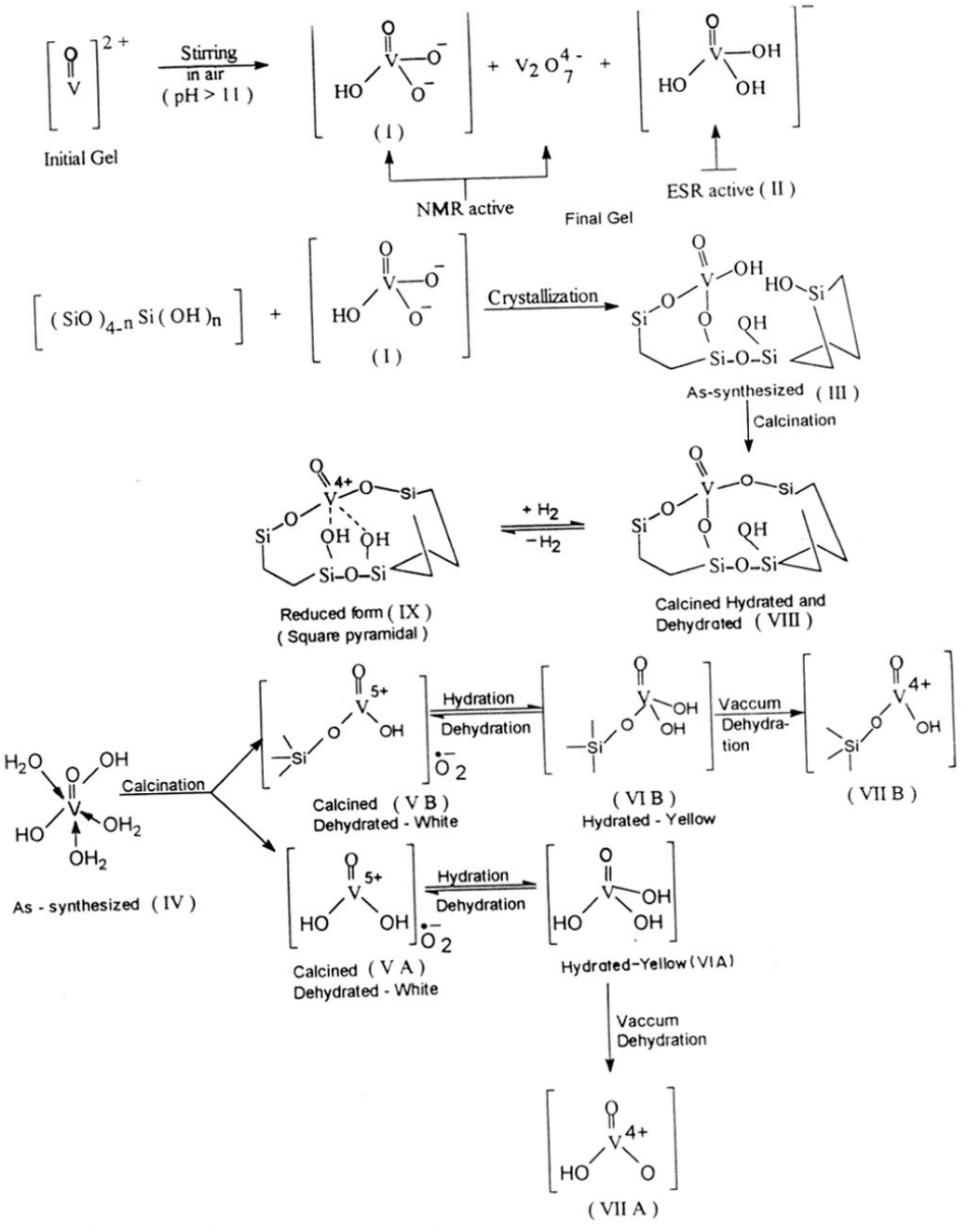

SCHEME-3.1 Plausible structures of the different V-species in the gel, as-synthesized, calcined (hydrated / dehydrated) and reduced samples.

the Si-O-V bonds are stable. Upon reduction, the V-species (VIII) go into SqPy environments (IX).

3.2.3 Part c - Synthesis and characterization of V-BEA (V-Al- β)

The V-Al-β studied in this thesis is reported for the first time.[17] Whenever newer materials are synthesized, it is important to understand the synthesis in detail and to establish the influence of the various process parameters so that an optimal synthesis procedure may be developed. In this section, the influence of process parameters on the synthesis of V-Al-β will be discussed. Besides, the results of the characterization studies of these samples will also be presented.

The general procedures used in the synthesis of V-Al-β and in the characterization of the samples were presented in Chapter II

a. Crystallization Kinetics

The various gel compositions used in this study, their pH and the pH of the mother liquor after crystallization are presented in table 3.5.

i) Effect of temperature

These studies were carried out with a gel of composition :

SiO_2 : 0.0025 Al_2O_3 : 0.0125 VO_2 : 0.52 TEAOH : 22 H_2O

Figure 3.30 shows the influence of temperature on the nucleation and crystallization of V-Al-β samples at 383, 413, 423K (curves a to c). The crystallization of V-Al-β depends significantly on the temperature. The crystallization rate is faster at 423K and slower at 388K. It is clearly observed that the formation of nuclei (induction period) is

Table 3.5

Gel compositions of V-Al-β used in the study of crystallization kinetics.

Gel composition	pH of the gel before auto-claving	pH of the mother liquor after crystallization
SiO_2 : 0.0025 Al_2O_3 : 0.0250 VO_2 : 0.52 TEAOH : 22 H_2O	12.3	12.7
SiO_2 : 0.0025 Al_2O_3 : 0.0170 VO_2 : 0.52 TEAOH : 22 H_2O	12.5	12.7
SiO_2 : 0.0025 Al_2O_3 : 0.0125 VO_2 : 0.52 TEAOH : 22 H_2O	12.7	12.9
SiO_2 : 0.0250 Al_2O_3 : 0.0125 VO_2 : 0.52 TEAOH : 22 H_2O	12.7	12.9
SiO_2 : 0.0083 Al_2O_3 : 0.0125 VO_2 : 0.52 TEAOH : 22 H_2O	12.7	12.9
SiO_2 : 0.0050 Al_2O_3 : 0.0125 VO_2 : 0.52 TEAOH : 22 H_2O	12.7	12.9
SiO_2 : 0.0025 Al_2O_3 : 0.0125 VO_2 : 0.60 TEAOH : 22 H_2O	13.1	13.2
SiO_2 : 0.0025 Al_2O_3 : 0.0125 VO_2 : 0.35 TEAOH : 22 H_2O	12.0	12.3
SiO_2 : 0.0025 Al_2O_3 : 0.0125 VO_2 : 0.52 TEAOH : 15 H_2O	12.8	12.9
SiO_2 : 0.0025 Al_2O_3 : 0.0125 VO_2 : 0.52 TEAOH : 35 H_2O	12.4	12.6

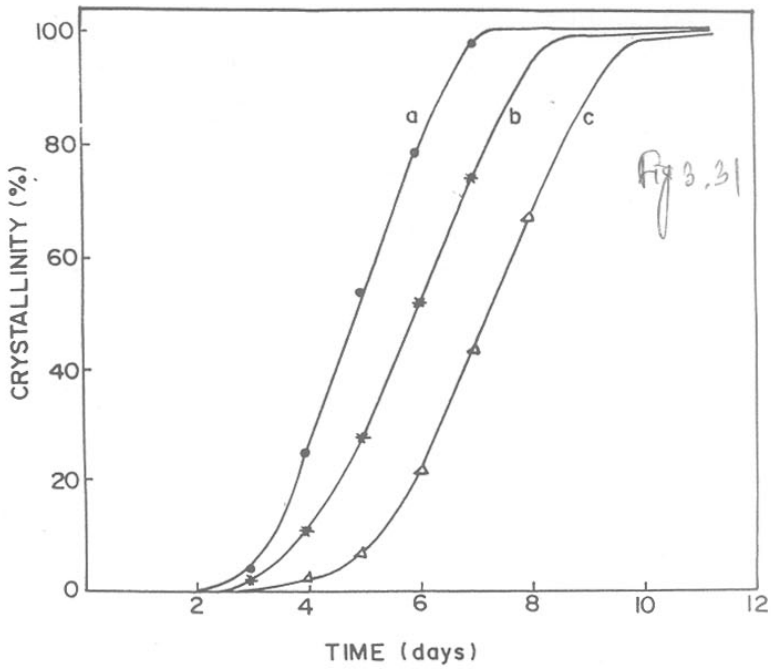

Fig. 3.30 Effect of temperature on the rate of crystallization of V-Al-β. Curves 'a' to 'c' represent crystallization at temperature 423, 413 and 383K respectively.

Gel composition : SiO_2 : 0.0025 Al_2O_3 : 0.0125 VO_2 : 0.47 TEAOH : 22 H_2O.

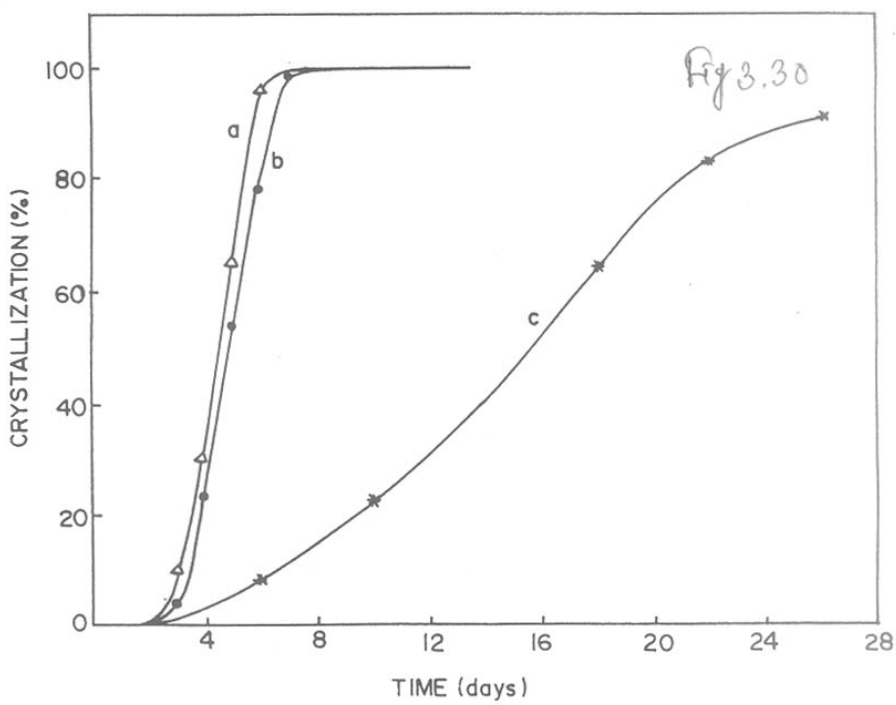

Fig. 3.31 Influence of Si/V molar ratio on the crystallization . Curves 'a' to 'c' correspond to Si/V molar ratios 80, 60 and 40, respectively.

Gel composition : SiO_2 : 0.0125 Al_2O_3 : x VO_2 : 0.47 TEAOH : 22 H_2O.

basically independent of temperature, whereas crystal growth rate changes significantly with temperature. Maximum crystallization (100%) takes place after 5-6 days at 423 and 413K, whereas maximum crystallization (92%) takes place after 27 days at 383K.

ii) Effect of Si/V molar ratio

These experiments were carried out at 413K with synthesis gels of typical composition : SiO_2 : 0.0025 Al_2O_3 : x VO_2 : 0.52 TEAOH : 22H_2O, where x = 0.025, 0.017, 0.0125.

The effect of increasing vanadium concentration in the initial reaction mixture (gel) on the crystallization is shown in figure 3.31. The crystallization becomes faster at higher Si/V molar ratios (Fig. 3.31a). Curves 'a' to 'c' represent crystallization rate of reaction mixtures of Si/V ratios = 80, 60 and 40. Both the induction period and crystal growth rate change with the Si/ V molar ratio.

iii) Effect of SiO_2 /Al2O_3 ratio

These studies were carried out at 413K with a gel of typical composition :

SiO_2 : x Al_2O_3 : 0.0125 VO_2 : 0.52 TEAOH : 22H_2O, where x = 0.025, 0.0125, 0.0083, 0.0050

Figure 3.32 shows the influence of SiO_2 /Al_2O_3 molar ratio on the crystallization of V-Al-β samples. Higher SiO_2/Al_2O_3 ratios in the synthesis gel decrease the rate of production of the zeolite, but the induction period remains roughly the same. Earlier authors have reported that the faster crystallization at higher aluminum contents may be due a greater decrease in pH.[51,52] This explanation is not valid in the present case as aluminum isopropoxide does not alter the pH significantly. Perez-Pariente *et al.*[53] reported that the

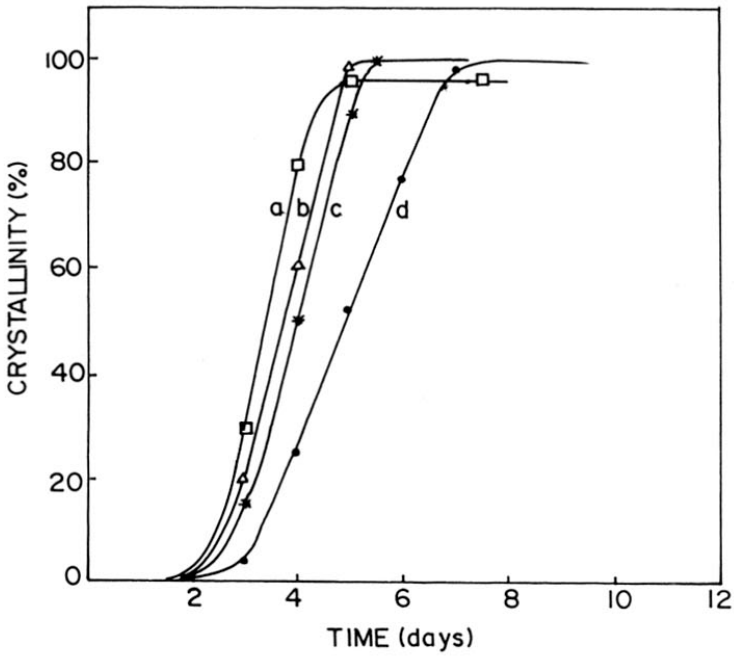

Fig. 3.32 Influence of SiO_2/Al_2O_3 mole ratio on the crystallization. Curves 'a' to 'd' correspond to SiO_2/Al_2O_3 mole ratios, 40, 120, 200 and 400, respectively.
Gel composition : SiO_2 : x Al_2O_3 : 0.0125 VO_2 : 0.47 TEAOH : 22 H_2O.

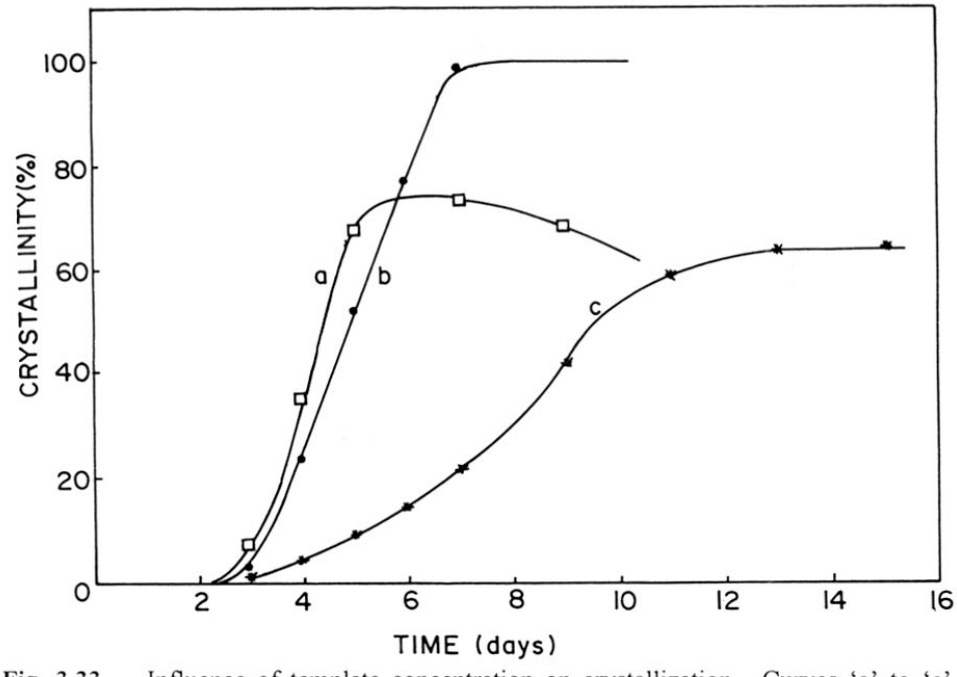

Fig. 3.33 Influence of template concentration on crystallization. Curves 'a' to 'c' correspond to $TEAOH/SiO_2$ mole ratios of 0.60, 0.47 and 0.35, respectively.
Gel composition : SiO_2 : 0.0025 Al_2O_3 : 0.0125 VO_2 : x TEAOH : 22 H_2O.

dissolution of aluminum species from the amorphous solid is rate determining. At high aluminum contents in the gel, this rate appears to be enhanced and the crystallization is faster.

iv) *Effect of template concentration*

In figure 3.33, the influence of $TEAOH/SiO_2$ molar ratio on the crystallization of V-Al-β is depicted. The crystallization becomes faster with increase in the $TEAOH/SiO_2$ ratio. The increase of $TEAOH/SiO_2$ ratio leads to an increase in the alkalinity (pH) of the reaction gel. At low concentrations of the template ($TEAOH/SiO_2 = 0.35$), the crystal growth takes place very slowly and leads to maximum crystallization (65%) after 14 days. At high concentrations of the template ($TEAOH/SiO_2 = 0.64$), the crystal growth is faster and leads to maximum crystallization (75%) on the 6th day. But, after 6 days the crystallinity decreases due to the dissolution of the crystals at high pH. At an optimum concentration of the template ($TEAOH/SiO_2 = 0.47$), the crystallization is complete (100 %) after 7 days. An increase in pH accompanies the crystallization.

v) *Effect of water concentration*

Figure 3.34 shows that H_2O/SiO_2 molar ratio in the range of 15-35 significantly influence the crystallization. A lower H_2O/SiO_2 ratio favours a faster crystallization with shorter induction period. The faster crystallization at lower H_2O/SiO_2 ratio may be due to the high pH of the gel. Maximum crystallization of 90% and 75% respectively are observed for gels with H_2O/SiO_2 ratios of 15 and 95. An optimum concentration of water ($H_2O/SiO_2 = 22$) leads to 100% crystallization after 7 days.

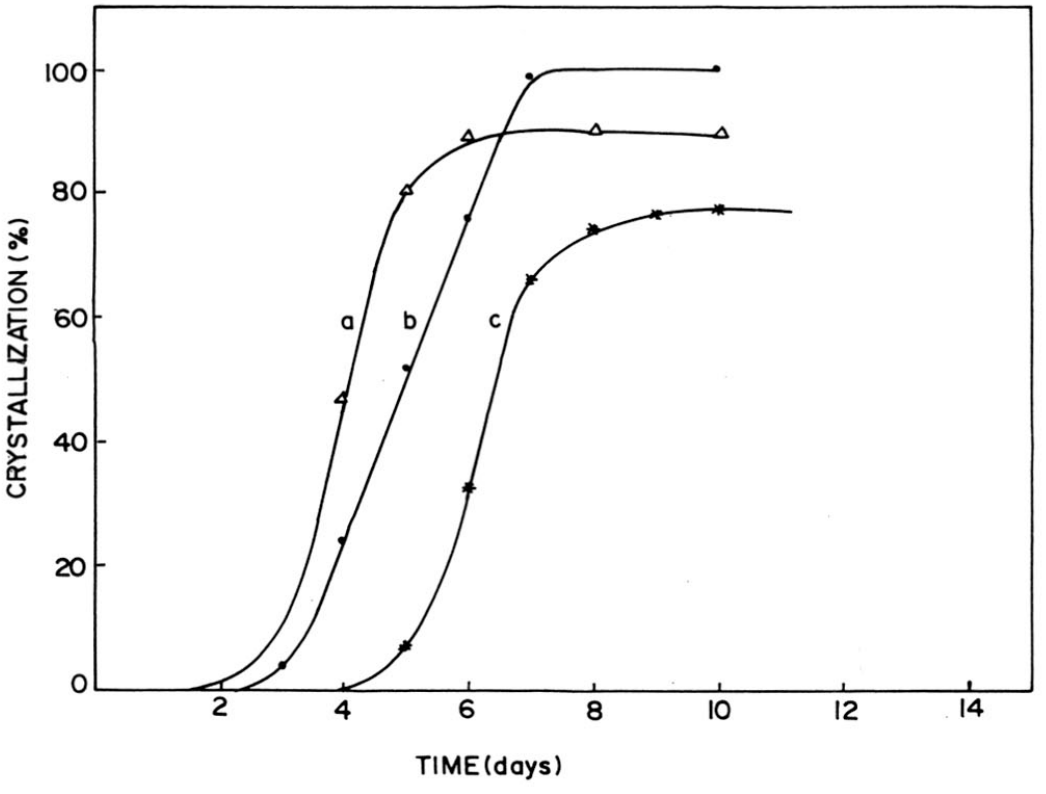

Fig. 3.34 Influence of water concentration on crystallization. Curves 'a' to 'c' correspond to H_2O/SiO_2 mole ratios of 15, 22 and 35, respectively.
Gel composition : SiO_2 : 0.0025 Al_2O_3 : 0.0125 VO_2 : 0.52 TEAOH : x H_2O.

b. Characterization

i) Analytical data

All the samples V-Al-β(a to c) were prepared using $VOSO_4$ possessing V in V^{4+} state. However, when the precursor gels were analyzed, both the V^{4+} and V^{5+} were present in the gels of a and b, whereas only V^{5+} was present in the gel of V-Al-β(c). The V^{5+} is formed by the aerial oxidation of the V^{4+} in alkaline medium (pH > 10).[21] The as-synthesized and calcined samples V-Al-β(a and b) contain both V^{4+} and V^{5+} ions, whereas V-Al-β(c) contains only V^{5+} ions (Table 3.6). On extraction with NH_4OAc (1N) solution, 61% and 44% of the total vanadium are extracted out respectively from V-Al-β (a and b), while a negligible amount of vanadium is extracted out from V-Al-β(c).

ii) XRD studies

All the V-Al-β(a to c) are highly crystalline. The unit cell expansion with respect to vanadium free aluminum β is small and within the experimental error. This may be due to the low concentration of vanadium in the framework of these zeolites (Fig. 3.35).

iii) SEM

SEM pictures of the three samples (Fig. 3.36) reveal spheroidal crystallites (0.1-0.2 μm). Smaller crystals are formed as the nonextractable (1N NH_4OAc solution) vanadium content of the samples increases. This may be due to the creation of the defect sites by framework V.

Table 3.6

Composition of the V-Al-β Samples.

Sam-ple	pH of the gel	Color of the gel	Concentration of vanadium and aluminum ($x10^{-3}$)												
			Gel				As-synthesized				Calcined				Ext*
			Si/ Al	V/ Si+V	V^{4+}/ Si+V	V^{5+}/ Si+V	Si/ Al	V/ Si+V	V^{4+}/ Si+V	V^{5+}/ Si+V	Si/ Al	V/ Si+V	V^{4+}/ Si+V	V^{5+}/ Si+V	V/ Si+V
a	12.6	pale green	200	25.0	17.5	8.5	75	8.3	5.5	2.8	7.5	8.3	1.2	7.1	3.2
b	12.7	pale green	200	16.6	6.1	10.5	78	6.4	3.3	3.1	78	6.4	0.6	5.8	3.6
c	12.8	color-less	200	12.5	-	12.5	80	4.0	-	4.0	80	4.0	-	4.0	4.0

* → Calcined and extracted with 1N NH_4OAc solution

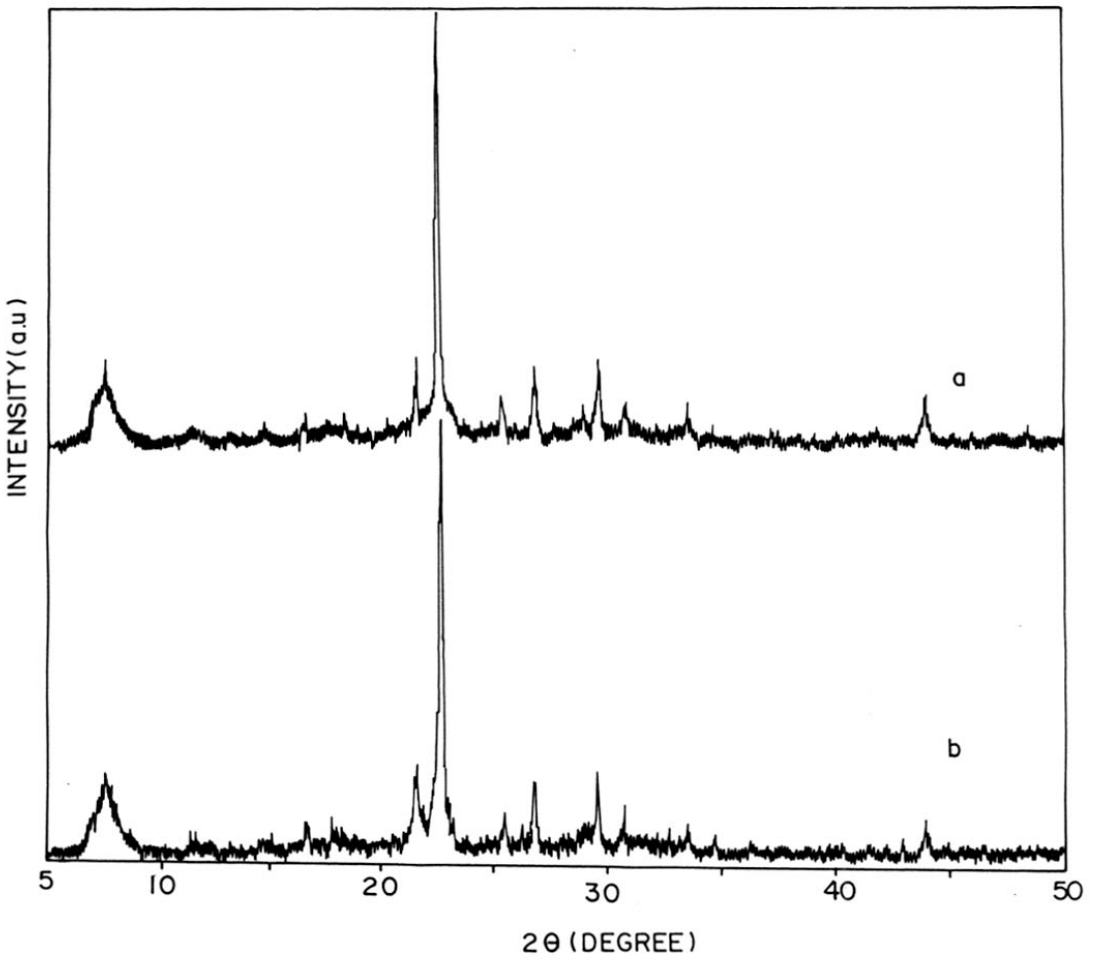

Fig. 3.35 XRD patterns of V-Al-β samples. a : V-Al-β(c); b : Al-β.

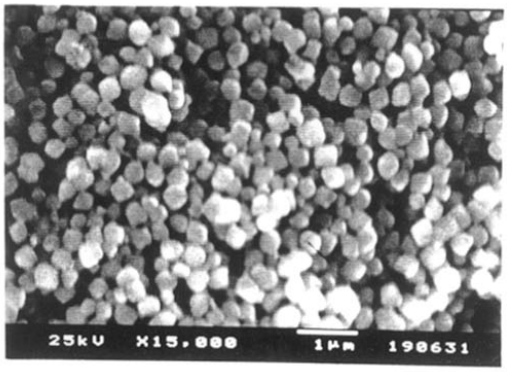

(a)

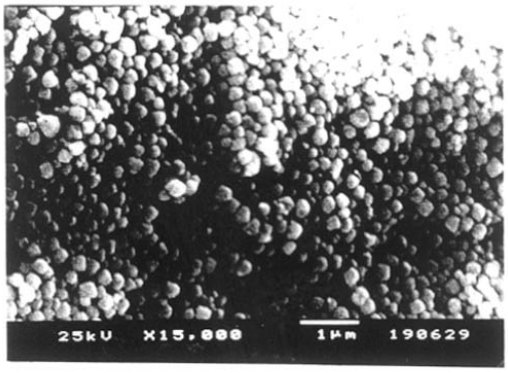

(b)

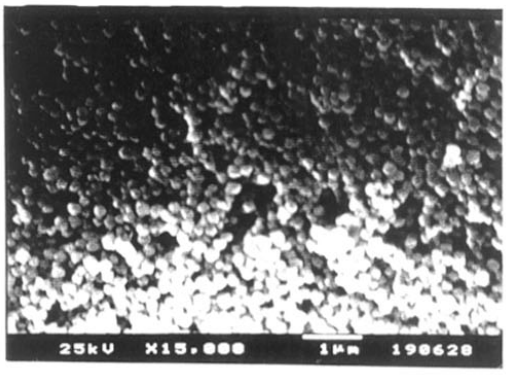

(c)

Fig. 3.36 SEM photographs of V-Al-β samples. a : V-Al-β(a); b : V-Al-β(b); c : V-Al-β(c).

iv) ESR spectroscopic studies

Figure 3.37a presents the ESR spectrum of the precursor gel of sample V-Al-β(c). It reveals an eight line hyperfine spectrum without any anisotropy (g = 1.960 and A = 92.7G) at RT after immediate addition of $VOSO_4$ solution (0h). On ageing the gel at 298K for 3h, no ESR signal was observed (Fig. 3.37b). The ESR parameters of the 0h sample suggest that free VO^{2+} ions are present[28], whereas no V^{4+} species are present in the aged gels.

The as-synthesized V-Al-β(a) and V-Al-β(b) exhibit eight line hyperfine spectra (Fig. 3.38a,b) at RT and 77K, whereas sample V-Al-β(c) does not exhibit any ESR signal (Fig. 3.38c). The ESR parameters (g_{11} = 1.935, $g_{\perp}$ = 1.992, A_{11} = 190.5G, $A_{\perp}$ = 71.4G) correspond typically to a SqPy environment.[31]

Upon calcination, samples V-Al-β(a and b) exhibit a weak and broad ESR signal at RT, whereas the calcined V-Al-β(c) does not exhibit any ESR signal (Fig. 3.39). Upon reduction, samples V-Al-β(a and b) exhibit ESR signals both at RT and 77K but V-Al-β(c) exhibits only at 77K (Fig. 3.40). The ESR parameters (g_{11} = 1.938, $g_{\perp}$ = 1.992, A_{11} = 190.5G, $A_{\perp}$ = 71.4G) were similar for all the samples and correspond typically to SqPy environments.[31]

v) FT-IR spectroscopic studies

The IR spectra of the calcined forms of samples V-Al-β(a to c) are shown in figure 3.41. The IR band at 958 cm^{-1} is attributed to $Si\text{-}O^{\delta-}$ linkages associated with defect sites arising from vanadium incorporation. The high intensity of the IR band at 575 cm^{-1} indicates the high purity of the samples.[54] The ratio of I_{958}/I_{575} increases with the

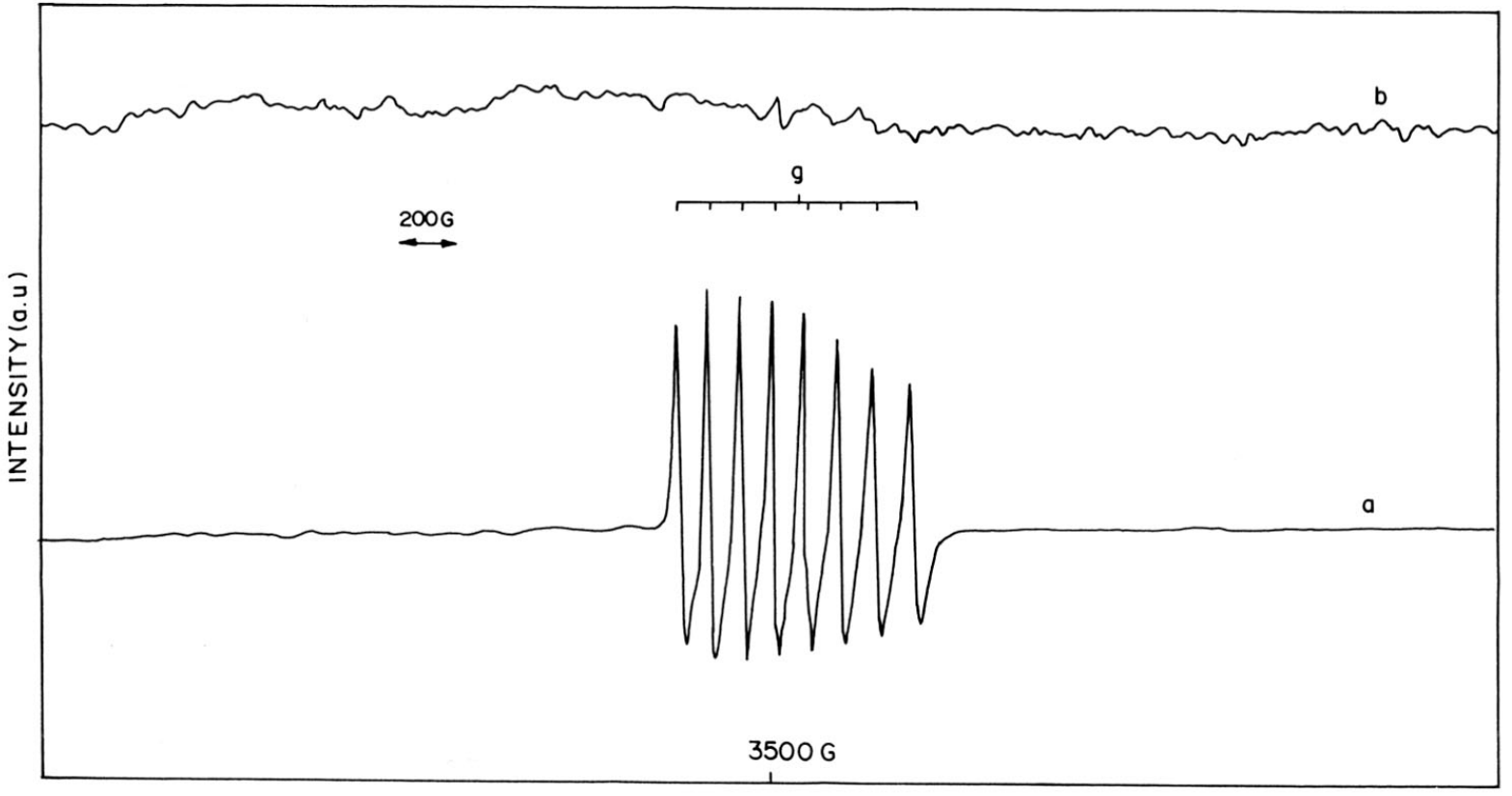

Fig. 3.37 ESR spectra of the synthesis gel of V-Al-β(c) sample. Initial time, 0h (a) and final time, 5h (b).

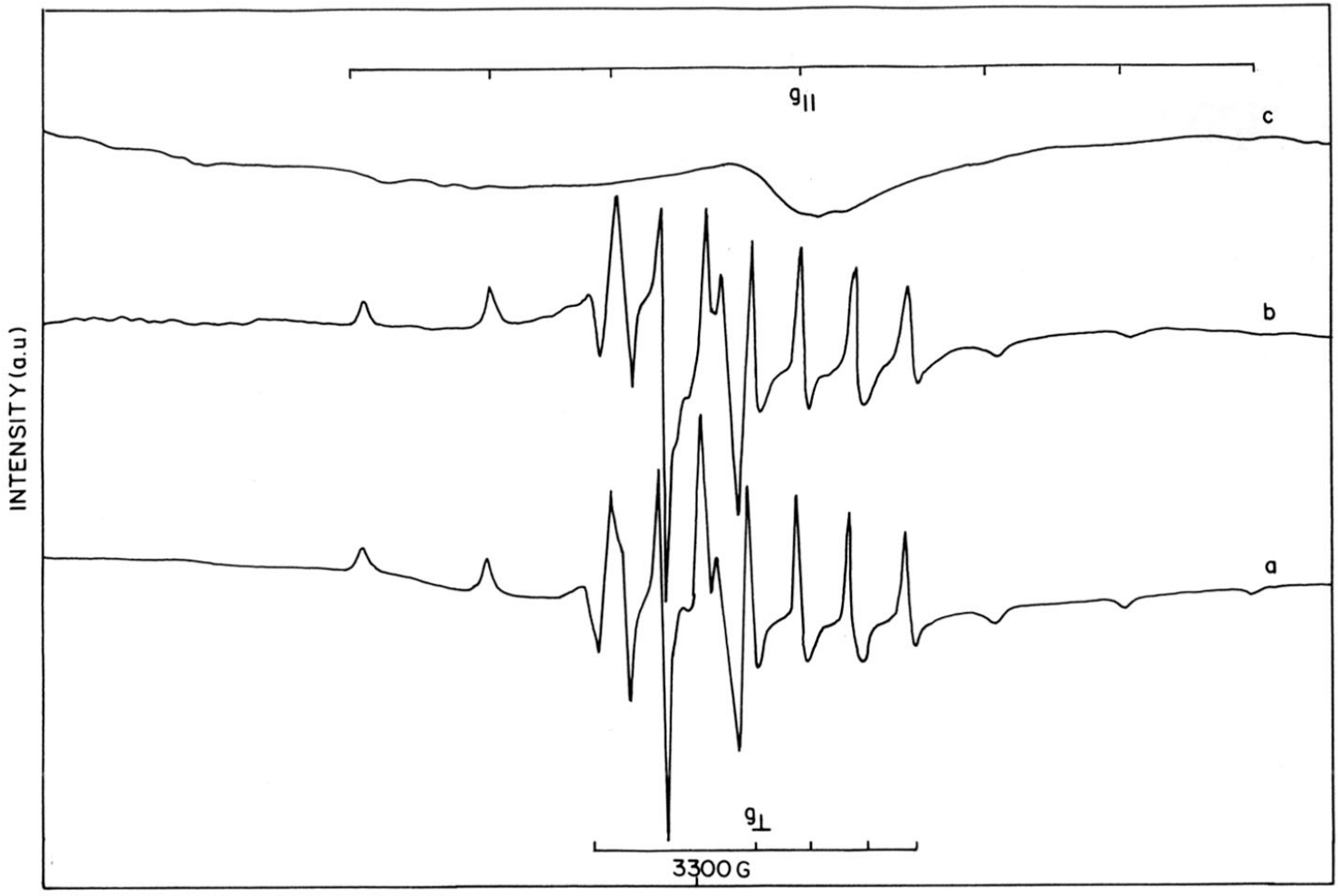

Fig. 3.38 ESR spectra of the as-synthesized V-Al-β samples. a : V-Al-β(a), b : V-Al-β(b), c : V-Al-β(c).

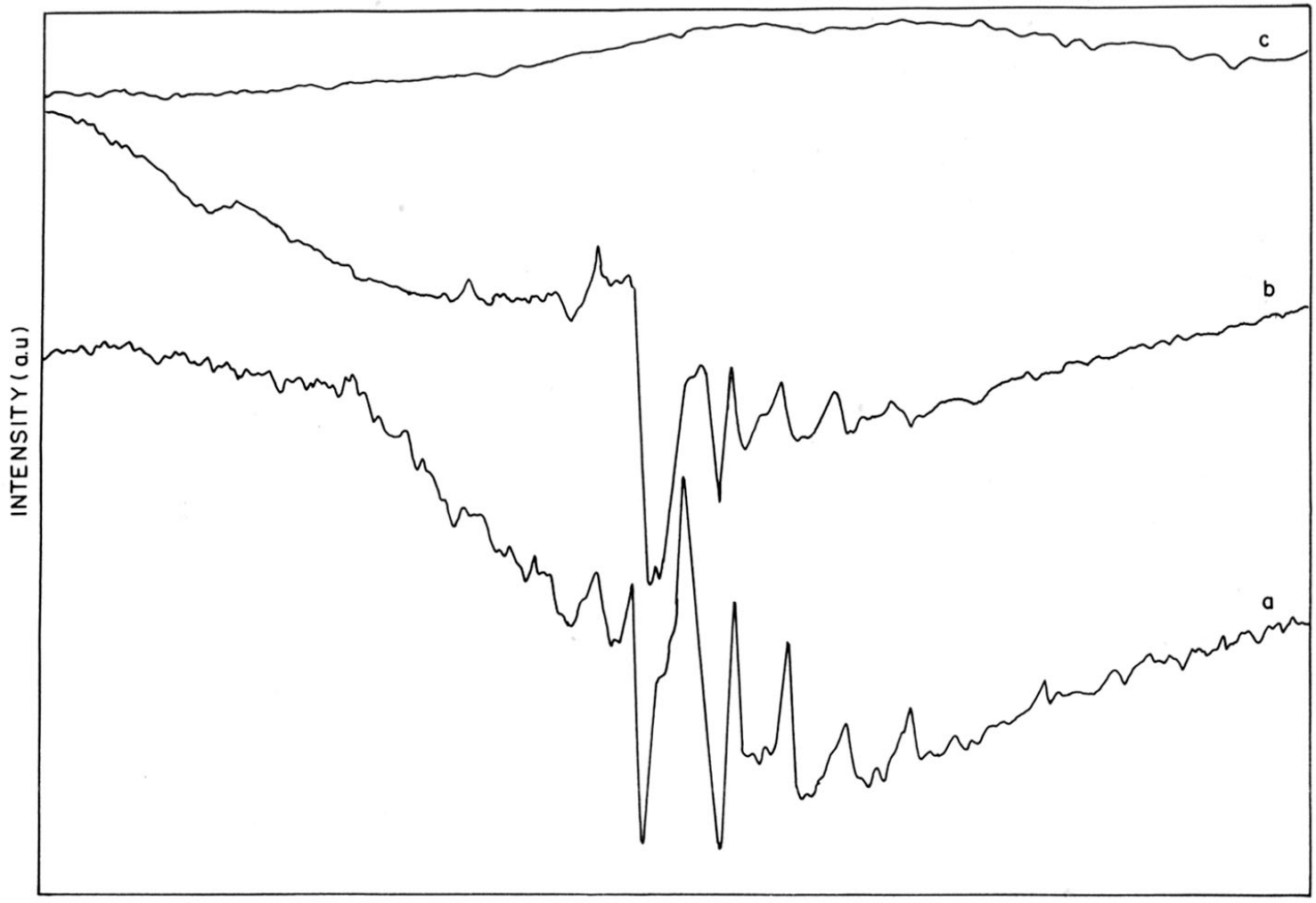

Fig. 3.39 ESR spectra of the calcined V-Al-β samples. a : V-Al-β(a), b : V-Al-β(b), c : V-Al-β(c).

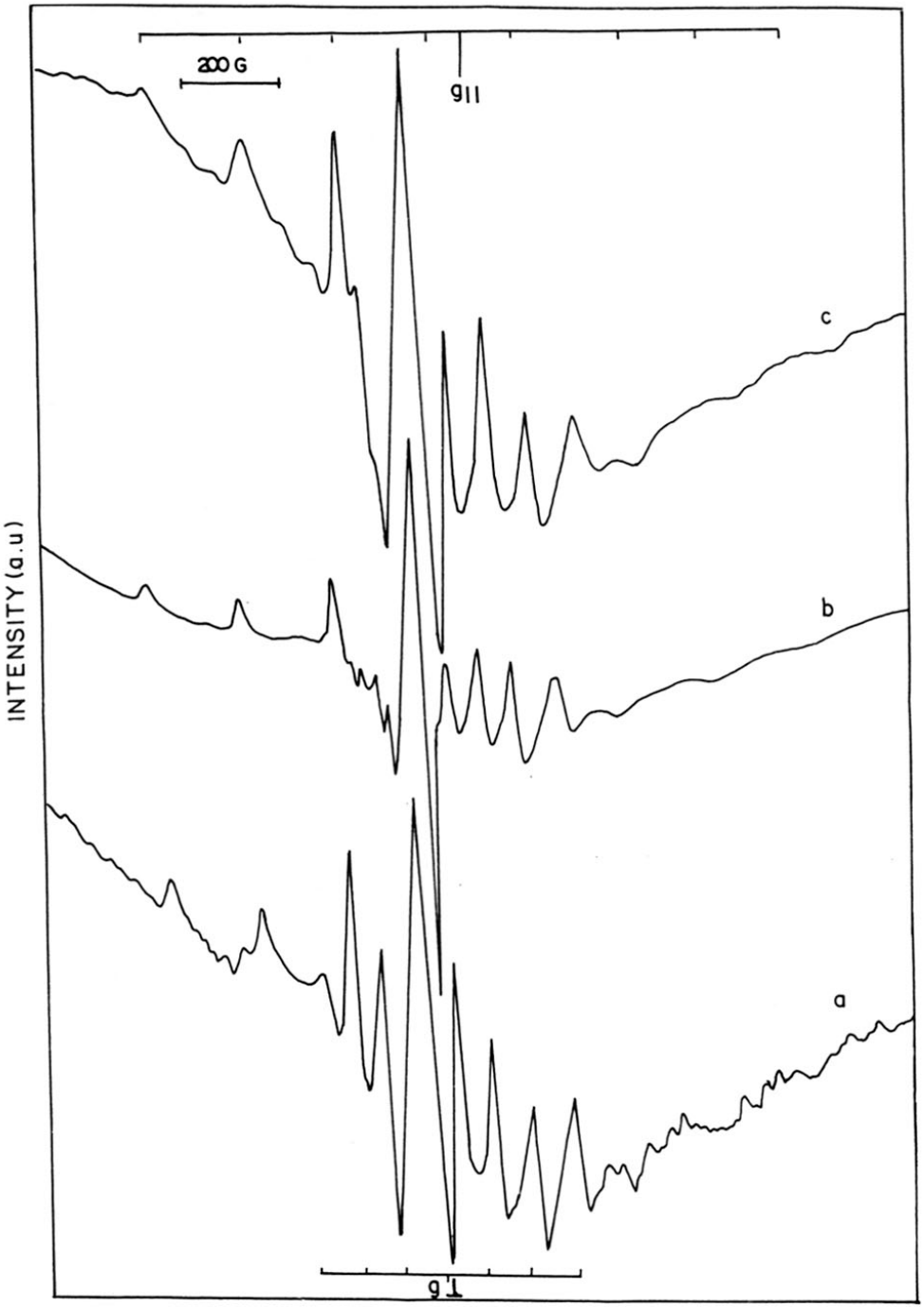

Fig. 3.40 ESR spectra of the reduced V-Al-β samples. a : V-Al-β(a), b : V-Al-β(b), c : V-Al-β(c).

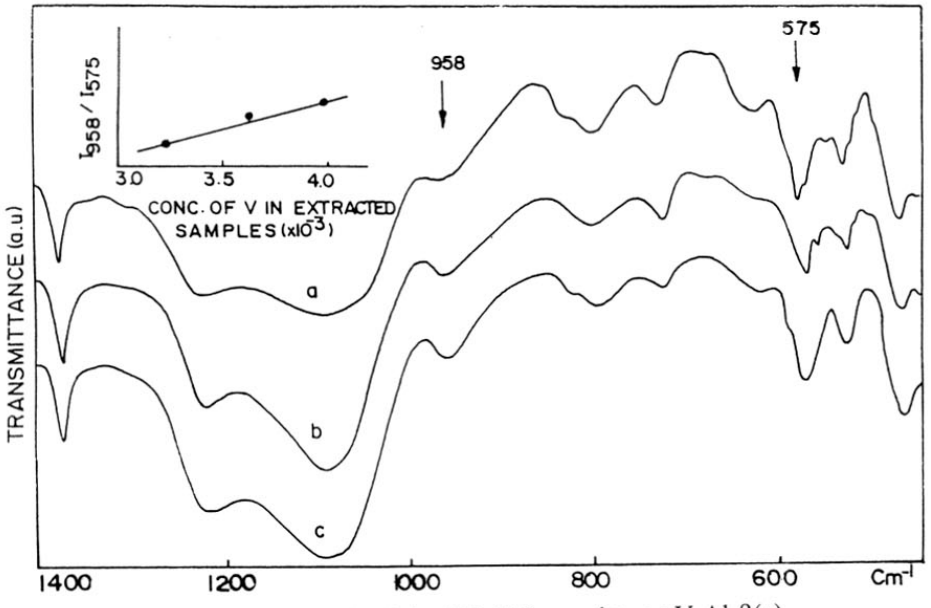

Fig. 3.41 Framework IR spectra of calcined V-Al-β samples. a : V-Al-β(a), b : V-Al-β(b), and c : V-Al-β(c).

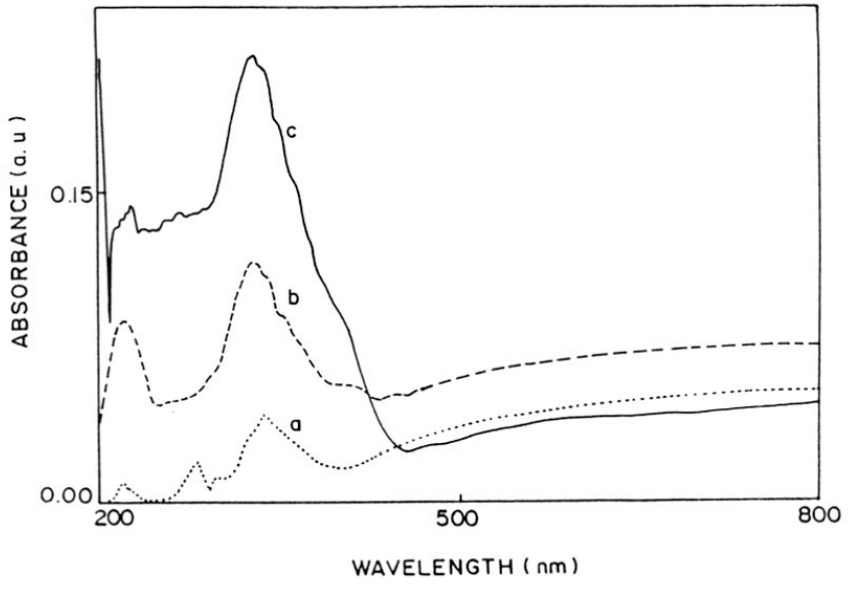

Fig. 3.42 UV-Visible DR spectra of the calcined V-Al-β samples. a : V-Al-β(a), b : V-Al-β(b) and c : V-Al-β(c).

concentration of vanadium present in the extracted samples (Fig. 3.41). This indicate that the non-extractable V-species are present in the framework of zeolite beta.

vi) UV-visible (DR) spectroscopic studies

The UV-Vis DR spectra of V-Al-β(a to c) samples exhibit UV-VIS DR band at 330 nm (Fig. 3.42) suggesting the presence of Td vanadium species (Table 3.2).

vii) NMR spectroscopic studies

The liquid state ^{51}V NMR spectrum of the gel of V-Al-β sample(c) is shown in figure 3.43a. The gel exhibits an intense signal at δ = -533 ppm along with a weak signal at δ = -565 ppm. The signal at -533 ppm corresponds to the HVO_4^{2-} species. This is the major V^{5+} species suggested to be present at pH > 10.[17] The signal at δ = -558 and -565 ppm are probably due to $V_2O_7^{4-}$ and its protonated form, $HV_2O_7^{3-}$, respectively.

The solid state ^{51}V MAS NMR spectrum of the as-synthesized and calcined V-Al-β(c) is shown in figure 3.43a,b. Both the as-synthesized and calcined forms of the sample V-Al-β(c) exhibit NMR spectra with a typical anisotropic pattern (isotropic chemical shift, δ = -620 ppm, scanning at three different spinning speeds) with negligible contribution of the quadrupolar effects of the I = 7/2 ^{51}V nucleus. No change in the NMR spectra is observed upon hydration/dehydration indicating that the spectra are those of stable V-species.

The solid state ^{29}Si MAS NMR spectra of the calcined V-Al-β samples are shown in figure 3.44. All the samples V-Al-β(a to c) exhibit a broad signal at δ = -98 to -102 and δ = -115 ppm corresponding to defect silanol (Si-OH) and Q^4(Si) sites. The broadness of the spectrum is probably due to the presence of framework V-species. The intensity of the signal at δ = -98 to -102 ppm increases with framework vanadium concentration from sample V-Al-β(a to c). This is a very good evidence that framework V-species are present at the defect sites in the lattice of zeolite β.

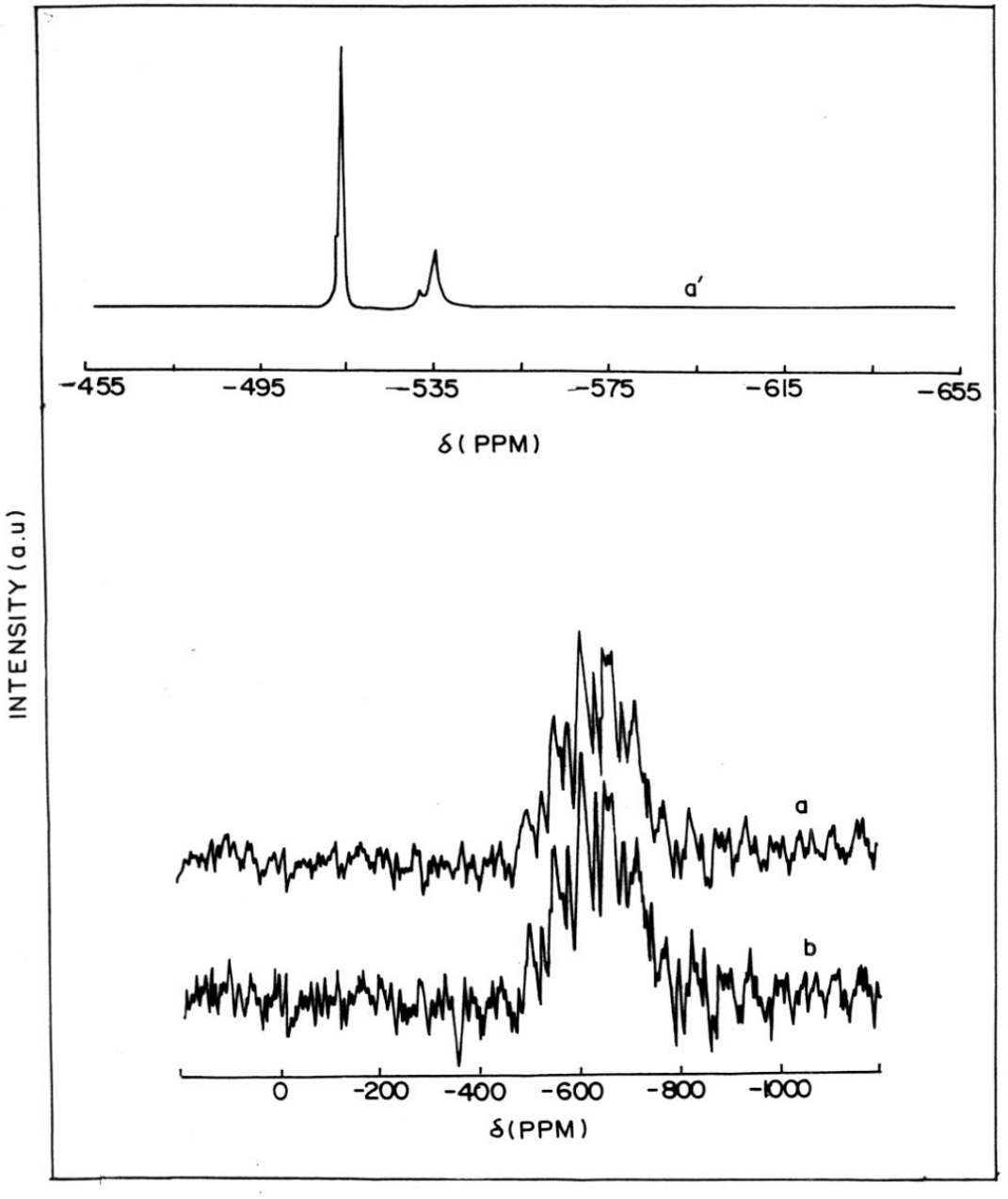

Fig. 3.43 ^{51}V spectra of V-Al-β(c). a' : final gel (liquid state);
a : as-synthesized (solid state MAS); and b : calcined (solid state MAS)

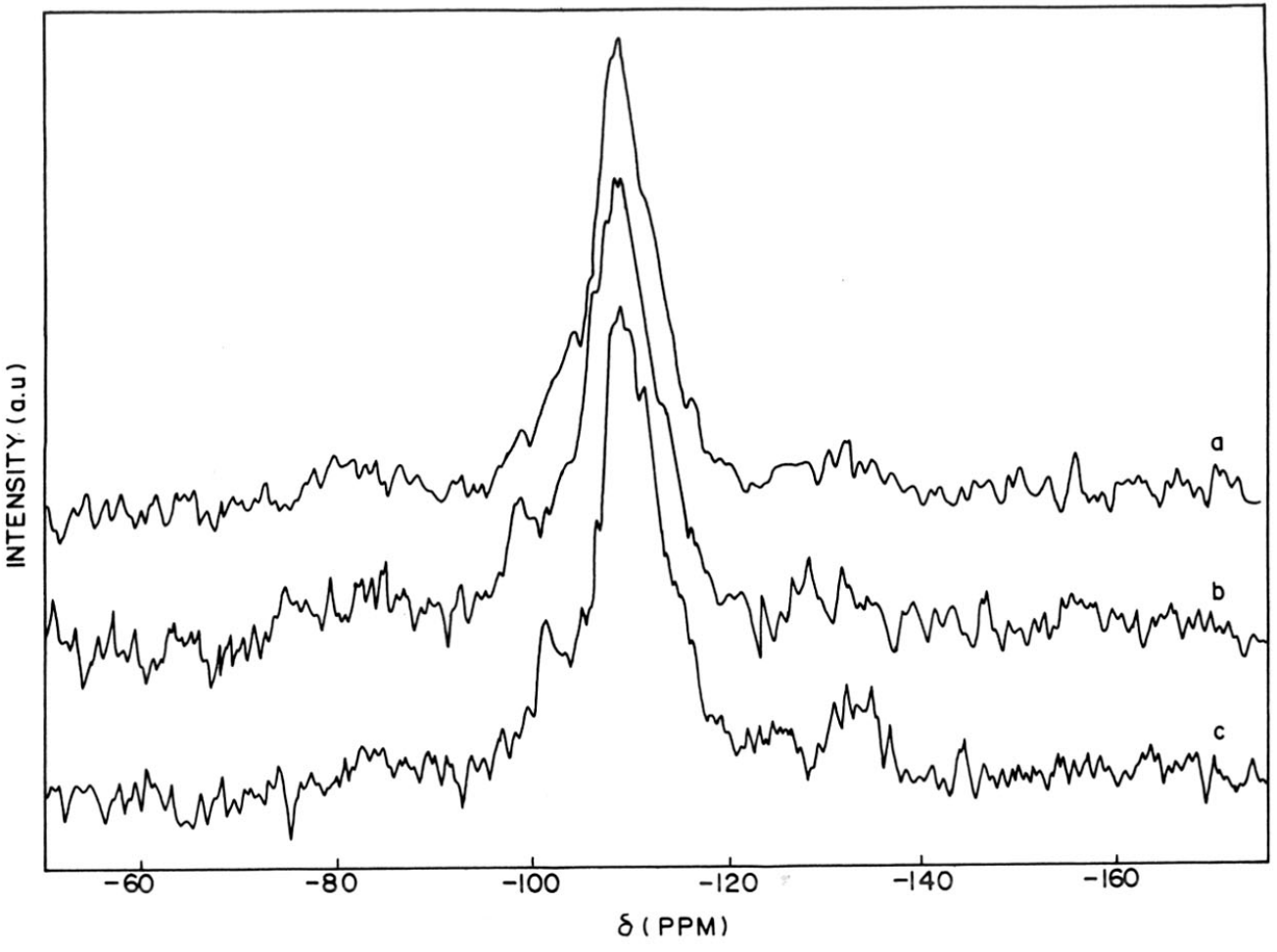

Fig. 3.44 ^{29}Si MAS NMR spectra of the calcined V-Al-β samples. a : V-Al-β(a), b : V-Al-β(b), c : V-Al-β(c).

viii) Thermal analysis

Figure 3.45 shows the TG-DTA profiles for V-Al-β(c). Four distinct steps of weight loss in the TG profile (step I, 311-329K; step II, 474-638K; step III, 640-754K; step IV, 770-987K) are noticed. The first step is slightly endothermic and results from the dehydration of the occluded water and the other three steps are exothermic and are related to the oxidation of the organic material. The samples V-Al-β(a and b) show a similar pattern. The TG-DTA profile of vanadium free Al-β is similar to Al-β but the exotherm of step II starts at a slightly higher temperature (step II, 490-640K).

ix) Surface area and adsorption studies

The surface areas of the V-Al-β samples (Table 3.7) with different Si/V ratios are similar to that of Al-β indicating the absence of pore blockage due to vanadium. The sorption capacities for n-hexane and cyclohexane do not vary with Si/V ratio. However, the sorption capacity for water increases with a decrease in total Si/V ratio due to the hydrophilic nature of the V-species.

Table 3.7

Physicochemical properties of V-Al-*β* samples.

Sample	Surface area	Sorption capacity (wt %)*		
	m^2g^{-1}	n-hexane	cyclohexane	water
a	688	19.5	20.1	25.6
b	692	19.8	20.5	23.5
c	698	19.6	20.8	22.4
Al-β	690	19.2	20.0	21.3

* → at $p/p_0 = 0.5$; temp. = 300K.

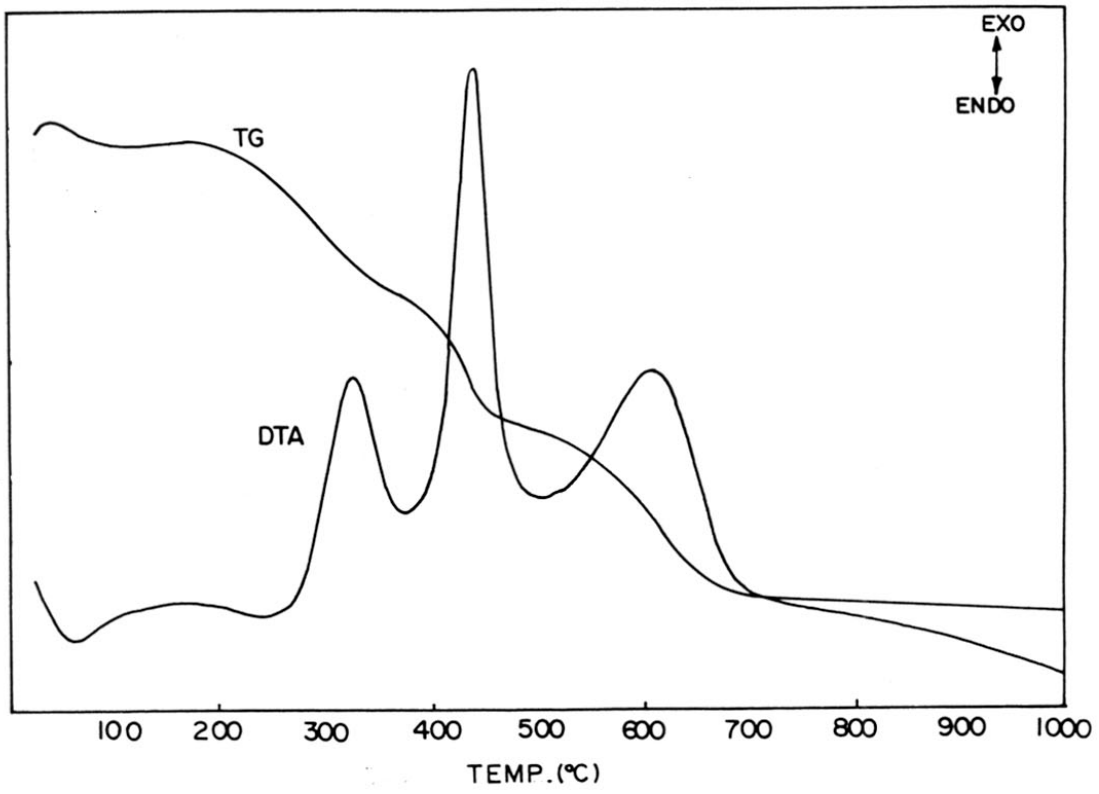

Fig. 3.45 TG - DTA curves of the as-synthesized V-Al-β(c).

3.3. CONCLUSIONS

The synthesis of V-MFI in an acidic medium using fluoride ions gives defect free orthorhombic crystals which transform into a monoclinic symmetry on calcination. Synthesis in an acidic medium is unfavorable for the incorporation of vanadium in the framework of V-MFI. The V-species present in V-MFI synthesized from acidic medium are mostly nonframework polymeric species with Td and Oh environments. Synthesis in an alkaline medium favours the incorporation of vanadium in the framework of MFI molecular sieves. These framework V-species (mostly V^{5+}) are in a distorted Td environment located at the defect sites.

Both V^{4+} and V^{5+} ions are present in the as-synthesized V-MEL. The V^{5+} ions are present in a distorted Td environment, and the V^{4+} ions are in an Oh environment. The V^{5+} ions appear to be present in the framework, while the V^{4+} ions are outside the framework. The framework V-species are formed from the V^{5+} species (HVO_4^{2-}) present in the gel. The V^{4+} species present in the extraframework positions in the as-synthesized material transform into V^{5+} on calcination. These nonframework species are easily extracted by NH_4OAc. The framework V-species are easily reducible, whereas the non-framework V-species are difficult to reduce.

Two types of vanadium species are present in the as-synthesized V-Al-β samples. One is in the distorted Oh environment and the other one is a distorted Td environment. The distorted Td V-species are present in the framework near the defect sites. The distorted Td V-species are formed from the gel, which contains V^{5+} ions.

In general, the incorporation of vanadium in zeolite/molecular sieves occurs preferably in an alkaline medium. The concentration of framework V-species is related to the concentration of monomeric V^{5+} species present in the gel.

3.4 REFERENCES

1. Marosi, L., Staberow, J., Schwarzmann, M., Ger. Pat. 2831631 (1978)
2. Xu, R., and Pang, W., *Stud. Surf. Sci. Catal.*, **24**, 27 (1985)
3. Miyamoto, A., Medhanavyn, D., and Inui, T., *Appl. Catal.*, **28,** 89 (1986); in "proceedings , 9th International Congress on Catalysis, Calgary, 1988" 9M. J. Phillips and M. Ternan, Eds.), Vol.1, p. 437. Chem. Inst. of Canada, Ottawa, Ontario, 1988.
4. a) Kuchrov, A. V., and Slinkin, A. A., *Zeolites*, **6**, 175 (1986).
   b) Kuchrov, A. V., and Slinkin, A. A., *Zeolites,* **7**, 38; 43; 583 (1987)
5. Sass, C. E., Chen, X., Kevan, L., *J. Chem. Soc., Faraday Trans.*, **86**, 189 (1990)
6. ElMalki, ElMekki., Davidson, A., Massiani, P., Barthomeuf, D., Che, M., *Am. Chem. Soc., Div, Pet., Chem.*, **40(1),** 114 (1995)
7. Anderson, J. R., and Whittington, W., *J.Phys.Chem.*, **97,** 1031 (1993)
8. a) Zatorski, L. W., Centi, G., Nieto, J. L., Trifiro, F., Bellusi, G., and Fattore, V., *Stud. Surf. Sci. Catal*, **B 49**, 1243 (1989).
   b) Trifiiro, F., and Jiru. P., *Catal. Today* **3**, 519 (1991).
   c) Rigutto, M. S., and Van Bekkum, H., *Appl. Catal.*, **68**, L1 (1991).
9. Prasad Rao, P. R. H., Ramaswamy, A. V., and Ratnasamy, P., *J. Catal.*, **137,** 225 (1992).
10. Tuel, A., and Ben Tarrit, Y., *Zeolites* **14,** 18 (1994).
11. Chattterjee, M., Bhattacharya, D., Venkatathri, N., and Sivasanker, S., *Catal. Letter.*, **35**, 313 (1995).
12. Kornatowski, J., Wichterlova, B., Rozwadowski, M., and Baur, W. H., *Stud. Surf. Sci. Catal.*, **84,** 117 (1994).
13. Das, N., Eckert, H.; Hu, H., Wachs, I. E., Waizer, J. F., Feher, F., *J. Phys. Chem.*, **97**, 8240 (1993).
14. Rdddy, K.M., Moudrakovski, I., and Sayari, A., *J. Catal.*, **143**, 275 (1993).
15. a) Reddy, K. M., Moudrakovski, I., and Sayari, A., *J. Chem. Soc., Chem. Commun.*, 1491 (1994).
   b) Moudrakovski, I., Sayari, A., Ratcliffe, C. I., Ripmeester, J. A., and Preston, K. F., *J. Phys. Chem.*, **98,** 10895 (1994).

16. Geon-Joong, K., Dong-Sucho., Kwang-Hokim., Wan-Sukko., Jong-Ho, K., and Hiroshi, S., *Catal. Lett.*, **31,** 91 (1995).

17. Sen, T., Chatterjee, M., and Sivasanker, S., *J. Chem. Soc., Chem. Commun.*, **207** (1995).

18. Reddy, K. M., Moudrakovski, I., and Sayari, A., *J. Chem. Soc., Chem.Commun.*, 1049 (1994).

19. Luan. Z., Xu, J., He, H., Klinowski, J., and Kevan, L., *J. Phys. Chem.*,100, 19595 (1996).

20. Morey, M., Davidson, A., Eckert, H., Stucky, G., *Chem. Mater.*, **8,** 486 (1996).

21. Chasteen, N.D., Struct. Bonding. 53, 112 (1983).

22. Sen, T., Rajamohanan, P. R., Ganapathy, S., and Sivasanker, S., *J. Catal.*, **163,** 354 (1996).

23. Sen, T., Ramaswamy, V., S. Ganapathy, Rajamohanan, P. R., and Sivasanker, S., *J. Phys. Chem.*, **100,** 3809 (1996).

24. Hay, D. G., and Jaeger, H., *J. Chem. Soc., Chem. Commun.*, 1433 (1984).

25. Perego, G., Bellusi, G., Corno, C., Taramasso, M., Buonomo, F., and Esposito, A., in "Developments in Zeolite Science and Technology" (Y. Murakami et al., Eds.), p. 129, Elseveir, Amsterdam, 1986.

26. Wu, E. L., Lawton, S. L., Olson, D.H., Rohrmann, A. C., Jr., and Kokotailo, G. T., *J. Phys. Chem.*, **83,** 2777 (1979).

27. Fyfe, C. A., Kokotailo, G. T., Strobl, H., Gies, H., Kennedy, G. J., Pasztor, C. T., and Barlow, G. E., *Stud. Surf. Sci, Catal*, **46**, 827 (1989).

28. a. Ballhausen, C. J., Gray, H. B., *Inorg. Chem.*, 1, **111** (1962).
    b. Rogers, R. N., Pake, G. E., *J. Chem. Phys.*, 33, **1107** (1960).

29. Busca, G., Centi, G., Marchetti, L., and Trifiro, J., *Langmuir*, **2,** 568 (1986).

30. Cavani, F., Centi, G., Feresti, E., Trifiro, F., and Vusca, G., *J. Chem. Soc., Faraday. Trans. 1* **84**, 237 (1988).

31. Davidson, A., and Che, M., *J. Phys. Chem.*, **96**, 9909 (1992).

32. Taramasso, M., Perego, G., and Natari, B., U.S. Patent 4410501 (1983).

33. Reddy, J. S., and Kumar, R., *J. Catal.*, **130,** 440 (1991).

34. Camblor, M. A., Corma, A., and Perez-pariente, J., *J. Chem. Soc., Chem. Commun.*, **557** (1993).

35. Boccuti, M. R., Rao, K. M., Zecchina, A., Leofanti, G., and Petrini, G., in "Structure and Reactivity of Surfaces" (C. A. Morterra, A. Zecchina, and G. Costs, Eds.), *Studies in Surface Science and Catalysis,* 48, **133** (1989).
36. Howarth, O. W., Richards, R. E., *J. Chem. Soc.,* 864 (1965).
37. O'Donnell, S. E., Pope, M. T., *Chem. Soc., Dalton Trans.,* 2290 (1976).
38. Lapina, O.B., Mastikhin, V. M., Shubin, A., Krasilnikov, V. N., and Zamaraev, K. I., *Prog. NMR Spectrosc.,* **24,** 457 (1992).
39. Engelhardt, G., and Michel, D., "High Resolution Solid State NMR of Silicates and Zeolites," Wiley, New York, 1987.
40. Chezeau, J. M., Delmotto, L., Guth, J. L., and Soulard, M., *Zeolites.,* **9,** 78 (1989).
41. Axon, S. A., and Klinowski, J., *Appl. Catal.,* **56,** L9 (1989).
42. Hauka, S., Lakomaa, E. L., and Root, A., *J. Phys. Chem.,* **97,** 5085 (1993).
43. Fejes, P., Marsi, I., Kiricsi, I., Halasz, J.; Hannus, I., Rokenbauer, A., Tasi, Gy., Korez, L., Schobel, Gy., *Stud. Surf. Sci. Catal.,* **69,** 173 (1991).
44. Cavani, F., Centi, G., Foresti, E., Trifiro, F., Busca, G., *J. Chem. Soc., Faraday, Trans., I* **84(1),** 237 (1988).
45. Sharma, V. K., Wokaun, A., Baiker, A., *J. Phys. Chem.,* **90,** 2715 (1986).
46. Cotton, F. A., Wilkinson, G., Advanced Inorganic Chemistry, A Comprehensive Text; Wiley Eastern Limited: New Delhi, p. 825, 1988.
47. Meiboom, S., Gill, D., *Rev. Sci. Instrum.,* **29,** 688 (1958).
48. Hardcastle, F. D., Wachs, I. E., Eckert, H., Jefferson, D. A., *J. Solid State Chem.,* **90,** 194 (1991).
49. Coustumer, L. R. Le., Taouk, B., Meur, M. Le., Payen, E., Guelton, M., Grimblot, J., *J. Phys. Chem.,* **92,** 1230 (1988).
50. Thangaraj, A., and Sivasanker, S., *J. Chem, Soc., Chem. Commun.,* 123 (1992).
51. Jacobs, P. A., Derouane, E. G., and Weitkemp, J., *J. Chem. Soc., Chem. Commun.,* 591 (1982).
52. Mostowicz, R., and Sand, L. B., *Zeolites,* **2,** 143 (1982).
53. Parez-pariente, J., Martens, J. A., and Jacobs, P. A., *Appl. Catal.,* **31,** 35 (1987).
54. Smith, C. A., Ainscough, E. W., and Brodie, A. M., *J. Chem. Soc., Dalton Trans.,* 1121 (1995).

55. a) Hush, N. S., and Hobba, R., *J. Prog. Inorg. Chem.*, **10,** 259 (1968).

b) Selbin, J., *Chem, Rev.*, **65,** 153 (1965).

c) So, H., and Pope, M. T., *Inorg. Chem.*, **11,** 1441 (1972).

d) Iwamoto, M., Furukawa, H., Matsukami, K., Takenaka, T., and Kagawa, S., *J. Am. Chem. Soc.*, **105,** 3719 (1983).

56. a) Ronde, H., and Snijders, J. G., *Chem.Phys. Lett.*, **50,** 282 (1977).

b) Jhung. S. H., Uh. Y. S., and Chon, H., *Appl. Catal.*, **62,** 61 (1990).

57. Centi, G., Perathoner, S., Trifiro, F., Aboukais, A., Aissi, C. F., and Guelton, M., *J. Phys. Chem.*, **96**, 2617 (1992).

CHAPTER IV

CATALYTIC APPLICATIONS

4.1 PART A - LIQUID PHASE OXIDATION

4.1.1 INTRODUCTION

The presence of transition metals in micro and mesoporous molecular sieves has the potential for generating oxidation catalysts with shape selective properties. The titanium containing microporous (TS-1[1], TS-2[2] and Ti-Al-β[3]) and mesoporous (Ti-MCM-41[4]) molecular sieves are effective in the liquid phase oxidation of various organic molecules using hydrogen peroxide or tertiary butyl hydrogen peroxide as the oxidant.[5-12] Recently, vanadium containing microporous (VS-1,[13] VS-2[14], V-ZSM-48[15], V-Al-β[16], VS-12[17]) and mesoporous (V-MCM-41[18]) molecular sieves were reported to be effective in the oxyfunctionalization of alkanes,[19] hydroxylation of aromatics,[20] oxidation of alkyl aromatics,[21] oxidation of aniline,[22] and the oxidation of sulfides[23] with aqueous hydrogen peroxide as the oxidant in the liquid phase. During the reaction, the bulk of the nonframework V-species are easily extracted into the liquid phase by dil. H_2O_2 in the reaction medium. However, the extracted V-species are poor oxidation catalysts.[24] The V-peroxo complexes of bidentate chelating ligands (O-N ≡ picolinato, pyrazine) have been reported to be useful oxidation catalysts in homogeneous media.[25]

This section presents the studies on the liquid phase hydroxylation of phenol and the oxidation of toluene over vanadium containing medium (V-MFI (VS-1) and V-MEL (VS-2) and large pore (V-Al-β) molecular sieves. The effect of addition of a promoter (picolinic acid) to the reaction medium has also been studied systematically.

4.1.2 EXPERIMENTAL

Details of the synthesis of vanadium containing medium (V-MFI and V-MEL) and large pore V-Al-β molecular sieves and their characterization were presented in chapter II and

chapter III. The various samples used in the liquid phase oxidation reactions and their characteristic properties are presented in table 4.1.

Details of the experimental aspects of the catalytic reactions are presented in chapter II. Water and acetonitrile were used as solvents as these have been reported to be suitable solvents for the hydroxylation of phenol[20] and oxidation of toluene[21] using hydrogen peroxide as the oxidant.

4.1.3 RESULTS AND DISCUSSION

a. Hydroxylation of phenol

The direct catalytic hydroxylation of phenol is an industrially important reaction and is catalyzed by strong mineral acids such as $HClO_4$ or by Fenton's reagent.[26] Titanium containing molecular sieves (TS-1[6] and TS-2[7]) are effective in the catalytic hydroxylation of phenol to hydroquinone and catechol. Hydroxylation of phenol over TS-1 has already been commercialized by Enichem, Italy.[2,5,6] The reactions occuring during the hydroxylation of phenol over vanadium containing molecular sieves are shown in Scheme 4.1.

(i) Studies over V-MFI samples

Table 4.2 presents the results of the hydroxylation of phenol over the two V-MFI samples reported and characterized in Chapter III. The activity of sample V-MFI(B) was more (TON = 24; TON = turn over number = number of moles of phenol converted per hour per atom of vanadium in the used catalyst) with a larger hydrogen peroxide selectivity (48.5 %). The conversion of phenol was low over V-MFI(A) (TON = 4.6) with a poor hydrogen peroxide selectivity (17.6 %). Both the extracted samples [V-MFI(A#) and V-MFI(B#)]

Table 4.1

Chemical composition of the samples used in liquid phase oxidation reactions.

Catalyst	Pretreatment	V/Si+V ($x10^{-3}$)	Nature of V-species	Ref
V-MFI(A)	Calcined in air at 823K for 12h	10.2	x_1	24
V-MFI(A*)	After first reaction cycle	0.8	x_2?	24
V-MFI(A#)	Extracted with 1N NH_4OAc solution at 333K for 12h; calcined at 723K for 6h	1.1	x_2	24
V-MFI(B)	Calcined in air at 823K for 12h	5.4	x_1	24
V-MFI(B*)	After first reaction cycle	4.2	x_2?	24
V-MFI(B#)	Extracted with 1N NH_4OAc solution at 333K for 12h; calcined at 723K for 6h	3.9	x_2	24
V-imp-sil-1	Impregnation of V on silicalite-1	10.2	x_1	24
V-MEL(1-He)	Calcined in air at 773K for 10h	10.2	x_3	43
V-MEL(1)	-do-	7.5	$x_2 + x_3$	43
V-MEL(2)	-do-	4.1	x_2	43
V-MEL(3)	-do-	3.5	x_2	43
V-MEL(4)	-do-	2.5	x_2	43
V-imp-sil-2	Impregnation of V on silicalite-2	10.2	x_2	42
V-Al-β(a)	Calcined in air at 773K for 10h	8.3	$x_1 + x_2$	53
V-Al-β(b)	-do-	6.4	$x_1 + x_2$	53
V-Al-β(c)	-do-	4.0	x_2	53
V-imp-Al-β	Impregnation of V on Al-β	8.3	x_1	53
V-imp-Cab-o-sil	Impregnation of V on cab-o-sil	10.2	x_1	24

x_1 → Nonframework, polymeric Td and Oh.

x_2 → Framework, distorted Td.

x_3 → Nonframework, monomeric mobile Td and loosely bound Td.

x_2? → not characterized, presumbably framework ions.

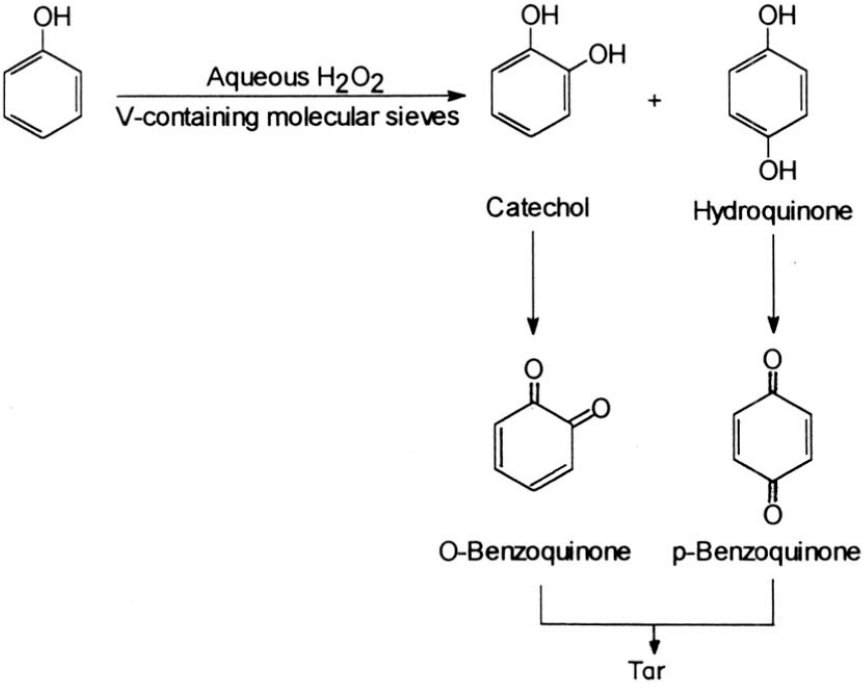

SCHEME 4.1 Hydroxylation of phenol over vanadosilicate molecular sieves.

Table 4.2

Hydroxylation of phenol over V-MFI samples.

Catalyst	TON	H_2O_2 selec. (mol %)	Product distribution (mol %)			Cat/HQ
			Cat	HQ	BQ	
V-MFI(A)	4.6	17.6	68.9	27.6	3.5	2.5
V-MFI(B)	24.0	48.5	53.2	45.0	1.8	1.2
V-MFI(A)#	29.8	8.6	57.5	40.2	2.3	1.4
V-MFI(B)#	30.3	44.1	51.2	47.6	1.2	1.1
V-imp-sil-1	3.3	13.1	70.2	24.2	5.6	2.9
NH_4VO_3	1.5	5.6	78.5	14.6	6.9	5.3

→ extracted with 1N NH_4OAc solution (see Table 4.1)

Table 4.3

Hydroxylation of phenol over V-MEL samples.

Catalyst	TON	H_2O_2 selec. (mol %)	Product distribution (mol %)			Cat/HQ
			Cat	HQ	BQ	
V-MEL(1-He)	3.4	11.8	64.5	27.0	8.5	2.4
V-MEL(1)	9..3	27.5	58.4	34.2	7.4	1.7
V-MEL(2)	28.3	42.9	50.8	46.7	2.5	1.1
V-MEL(3)	29.0	36.8	49.7	48.2	2.1	1.1
V-MEL(4)	26.8	25.4	49.3	49.1	1.6	1.1
V-imp-sil-2	0.5	11.8	70.8	24.7	4.5	2.9

Footnotes for tables 4.2 and 4.3.

TON → Turn over number i.e., number of moles of phenol converted per hour per atom of vanadium present in the used catalyst.

H_2O_2 selectivity = (number of moles of H_2O_2 utilized for the product formation) / (total number of moles of H_2O_2 used during the reaction)

Cat → catechol; HQ → hydroquinone; BQ → benzoquinone;

Reaction conditions : Catalyst : 0.1g; phenol/H_2O_2 (mole) = 2; temp. = 353K; phenol/catalyst (wt) = 10; solvent (water) = 10ml.

exhibited nearly the same activity (TON = 29.8 and 30.3). The increase in TON of the extracted samples indicates that the vanadium centres present in the extracted samples are the catalytically more active ones. V-imp-sil-1 and pure NH_4VO_3 show poor activities (TON = 3.3 and 1.5; Table 4.2) with low hydrogen peroxide selectivities.

It is found that the formation of catechol is more favourable than hydroquinone over all the catalysts. The ratio of catechol to hydroquinone is highest (5.3) in the homogeneous medium in the presence of ammonium metavanadate. The ratio is lowest (1.1-1.2) in the case of V-MFI(B) and V-MFI(B*). The ratio decreases from 2.5 to 1.4 upon ammonium acetate extraction of V-MFI(A). The ratios in the case of V-imp-sil-1 and V-MFI(A) are nearly similar being 2.9 for the former and 2.4 for the latter sample. Overall, it is noticed that samples containing more framework vanadium (V-MFI(B), V-MFI(B*) and V-MFI(A*)) produce more hydroquinone and samples containing more extraframework vanadium produce more catechol. Besides, the V-species present in the framework position is more active that the extraframework vanadium. It is interesting to note that the TON values of V-MFI(A*) and V-MFI(B*) are nearly the same (TON ~ 30) suggesting that the nonextractable V-species present in them possess similar activities and similar structures eventhough the samples were prepared by different procedures. The reasons for the higher activity of the framework V-species could be 1) its monatomic dispersion 2) its unique stereochemistry and 3) activating effect of Si-O linkages. It is noticed that benzoquinone production is more in samples containing extraframework V and in the case of NH_4VO_3.

(ii) Studies over V-MEL samples

Table 4.3 presents the results of the hydroxylation of phenol over V-MEL samples. The TON for the different samples passes through a maximum (Fig. 4.1a). The TON is maximum (29) for V-MEL (3) and is minimum (3.4) for V-MEL(1-He).

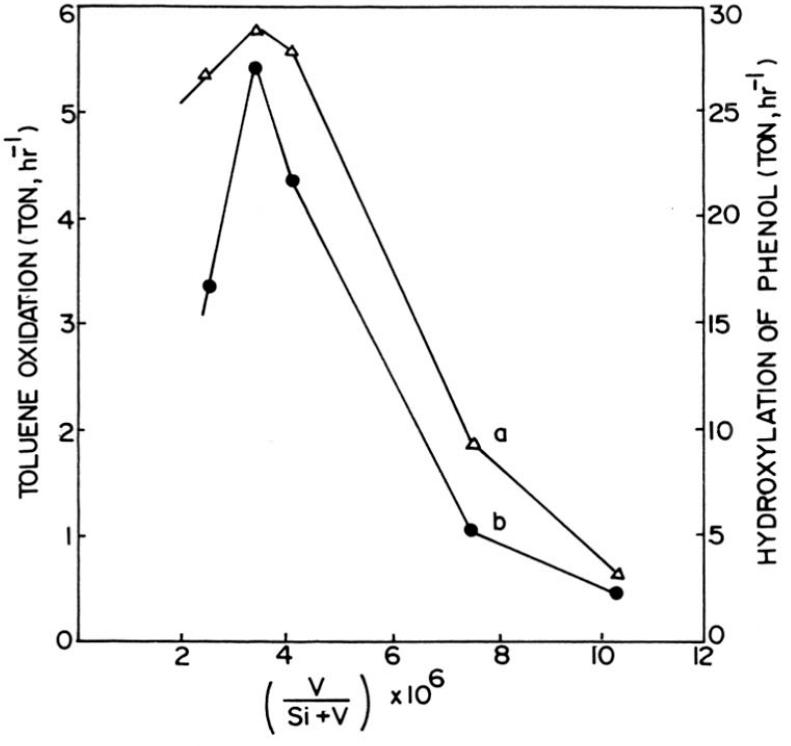

Fig. 4.1 Catalytic activities (TON) as a function of vanadium content of the calcined V-MEL samples. (•) toluene oxidation, (Δ) phenol hydroxylation.

The ratio of catechol to hydroquinone is maximum (2.4) over V-MEL(1-He) and decreases to 1.1 for V-MEL (2, 3 and 4). The V-imp-sil-2 sample shows nearly the same Cat/ HQ ratio as the V-MEL(1-He). This again indicates that the framework V-species (distorted Td) are active for the hydroxylation of phenol with more hydroquinone formation in the case of the MEL system also. Generally, the results are very similar to those obtained over V-MFI.

(iii) Studies over V-Al-β samples

Table 4.4 presents the results of the hydroxylation of phenol over V-Al-β samples. The TON calculated in terms of vanadium present in the calcined samples increases (9.3 to 28.2) from V-Al-β(a) to V-Al-β(c) (Fig. 4.2a) but it is nearly the same (~25) with respect to the vanadium present in the extracted samples. The V-imp-sil-2 sample is less active (TON = 6.8) than the other samples. The ratio of catechol to hydroquinone decreases (1.7 to 1.1) from V-Al-β(a) to V-Al-β(c). The Cat / HQ ratio is higher (2.1) over V-imp-Al-β. The results further confirm the earlier observation that the nonextractable V-species present in the V-Al-β structure are active for the hydroxylation of phenol and produce more hydroquinone.

(iv) Comparative studies over V-MFI, V-MEL and V-Al-β

Table 4.5 compares results of the hydroxylation of phenol over V-MFI(B), V-MEL(3) and V-Al-β(c) in which the V-species are present mostly in the framework in a distorted Td environment (Table 4.1). The TON values are similar for the three samples, being 24, 29 and 28 respectively for V-MFI(B), V-MEL(3) and V-Al-β(c). The ratio of

Table 4.4

Hydroxylation of phenol over V-Al-β samples.

Catalyst	TON	H_2O_2 selec. (mol %)	Product distribution (mol %)			Cat/HQ
			Cat	HQ	BQ	
V-Al-β(a)	9.3 (24.4)	23.1	60.2	36.3	3.5	1.7
V-Al-β(b)	13.8 (24.4)	28.4	35.6	41.4	3.0	1.3
V-Al-β(c)	28.2 (28.2)	32.6	51.0	48.5	0.5	1.1
V-imp-Al-β	6.8	21.8	65.2	30.6	4.2	2.1

The values in the brackets indicate the TON calculated based on the nonextractable V atoms present in the used catalysts.

Table 4.5

Phenol hydroxylation: comparative studies over V-containing different molecular sieves.

Catalyst	TON	H_2O_2 selec. (mol %)	Product distribution (mol %)			Cat/HQ
			Cat	HQ	BQ	
V-MFI(B)	24.0	48.5	53.2	45.0	1.8	1.2
V-MEL(3)	29.0	36.8	49.7	48.2	2.1	1.1
V-Al-β(c)	28.2	32.6	51.0	48.5	0.5	1.1

Footnotes for tables 4.4 and 4.5.

TON → Turn over number i.e., number of moles of phenol converted per hour per atom of vanadium present in the used catalyst

H_2O_2 selectivity = (number of moles of H_2O_2 utilized for the product formation) / (total number of moles of H_2O_2 used during the reaction)

Cat → catechol; HQ → hydroquinone; BQ → benzoquinone;

Reaction conditions : Catalyst : 0.1g; phenol/H_2O_2 (mole) = 2; temp. = 353K; phenol/catalyst (wt) = 10; solvent (water) = 10ml.

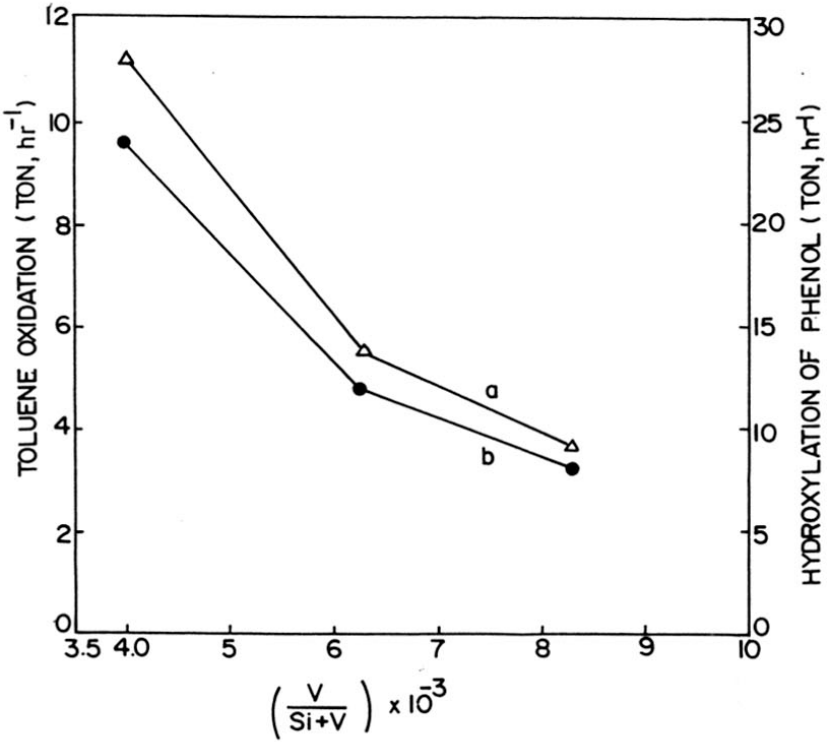

Fig. 4.2 Catalytic activities (TON) as a function of vanadium content of the calcined V-Al-β samples. (•) toluene oxidation, (Δ) phenol hydroxylation.

catechol to hydroquinone is nearly the same (~1.1) over these three molecular sieves. This indicates that the TON and selectivity depend more on the nature of the V-species present in the molecular sieves rather than the pore dimensions or structural aspects of the molecular sieves. Besides, the observation of a constant Cat/HQ ratio over all the three catalysts with different pore sizes and characteristics suggests that the ratio is not determined by product selectivity effects (pore dimensions). It is probably due to steric hindrance at the rigidly fixed active sites (framework V-peroxo species) to o-hydroxylation. The extraframework vanadium species are mostly leached into the reaction medium forming soluble peroxo complexes. Hydroxylation by these complexes in solution is not sterically hindered and more catechol is produced.

b. Oxidation of toluene

Oxidation of toluene to benzaldehyde has been reported on an (acetylacetanato) oxo vanadium catalyst with H_2O_2 in CF_3COOH.[27] Ru (III) complex[28] also catalyzes this reaction. Titanium substituted molecular sieves (TS-1 and TS-2) catalyze the hydroxylation of toluene to cresols and are inactive in the oxidation of the alkyl group.[7,11] Vanadium silicalites are active in both the hydroxylation of the aromatic nucleus and the oxidation of the alkyl substituent. The reactions occurring during the oxidation of phenol over vanadium containing molecular sieves are shown in Scheme 4.2.

(i) Studies over V-MFI samples

Table 4.6 presents the results of the oxidation of toluene over V-MFI samples. In the case of V-MFI(B^*), the TON values of the fresh sample, after NH_4OAc extraction (V-MFI(B^*)) and during the second reaction cycle (V-MFI($B^\#$)) are, respectively 10, 13.5 and

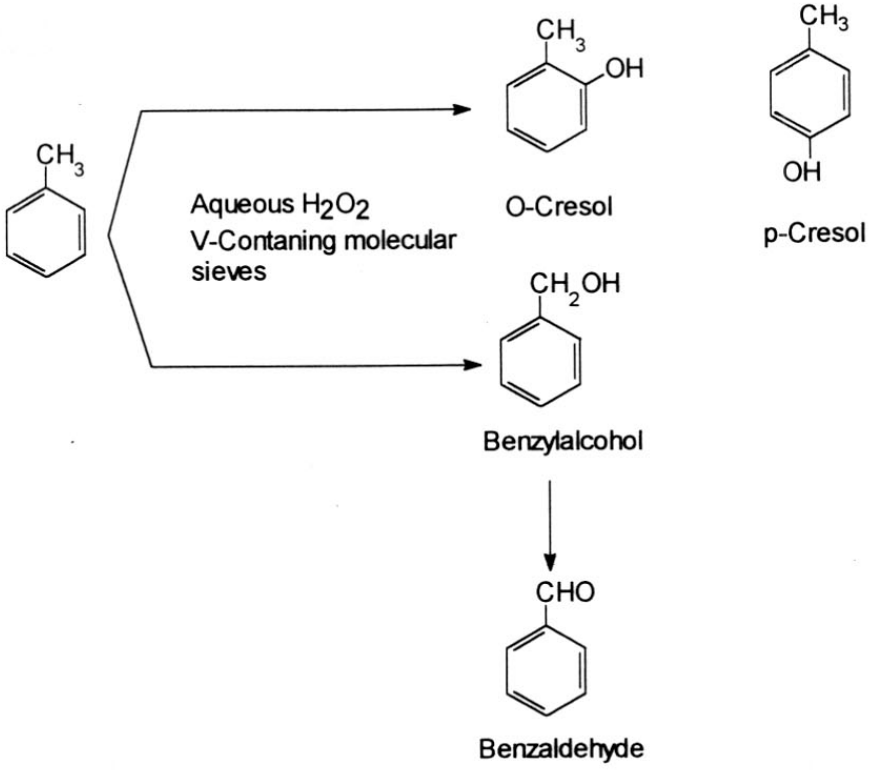

SCHEME 4.2 Oxidation of toluene over vanadosilicate molecular sieves.

Table 4.6

Oxidation of toluene over V-MFI samples.

Catalyst	TON	H_2O_2 selec. (mol %)	Product distribution (mol %)				o/p cresol
			al	ol	cresol		
					ortho	para	
V-MFI(A)	1.2	6.2	52.8	8.2	21.4	17.6	1.21
V-MFI(B)	10.0	26.0	41.5	11.9	23.0	23.6	0.97
V-MFI(B*)	12.8 (9.3)	23.7	40.8	10.9	23.2	25.1	0.92
V-MFI(B#)	13.5	27.6	41.2	11.4	23.5	23.9	0.98
V-imp-sil-1	1.9	6.6	74.3	6.3	10.9	8.4	1.24
NH_4VO_3	1.0	6.4	68.9	4.2	14.4	12.5	1.15

Table 4.7

Oxidation of toluene over V-MEL samples.

Sample	TON	H_2O_2 selec. (mol %)	Product distribution (mol %)				o/p cresol
			al	ol	cresol		
					ortho	para	
V-MEL(1-He)	0.5	3.8	62.8	8.7	15.9	12.6	1.25
V-MEL(2)	1.0	5.5	54.6	6.5	20.7	18.2	1.11
V-MEL(3)	4.4	9.8	49.2	05.7	21.6	23.5	0.90
V-MEL(4)	5.5	10.5	48.7	6.2	21.6	24.5	0.90
V-MEL(5)	3.4	7.4	49.5	4.8	22.1	23.6	090
V-imp-sil-1	0.6	6.2	72.5	7.6	11.2	8.7	1.24

Footnotes for tables 4.6 and 4.7.

al → benzaldehyde; ol → benzyl alcohol;

Reaction conditions : Catalyst : 0.1g; toluene / H_2O_2 = 2; temp. = 353K; toluene / catalyst (wt) = 10; solvent (acetonitrile) = 10ml; reaction time = 12h;

TON → Turn over number i.e, number of moles of toluene converted per hour per atom of vanadium present in the used catalyst.

H_2O_2 selectivity = (number of moles of H_2O_2 utilized for the product formation) / (total number of moles of H_2O_2 used during the reaction)

9.3 based on the original vanadium content. The TON calculated on the basis of the actual vanadium content of the sample in the 2nd cycle is 12.8. The near constancy of the TON values for the two samples (V-MFI(B^*) and V-MEL($B^\#$)) further confirms the earlier observations in the case of phenol hydroxylation that only similar type of V-species (framework) with similar catalytic activities are present in the two samples and both NH_4OAc and H_2O_2 in the reaction medium extract the less active nonframework V-species. The conversion over V-MFI(A), V-imp-sil-1 and NH_4VO_3 were low (TON ~ 1-2) due to poor activity of the non-framework V-species. Studies were not carried out over V-MFI($A^\#$) and V-MFI(A^*) as the absolute conversions were very low due to the low vanadium content and the results were not reliable. In the case of sample V-MFI(A), maximum conversion was achieved within 2h, whereas in the case of sample V-MFI(B), the conversion increased upto 12h (Fig. 4.3). It appears that the vanadium species in V-MFI(A) are rapidly extracted into solution by H_2O_2 (V-peroxo- complexes) leading to maximum toluene conversion within 2h, while in the case of V-MFI(B), the reaction proceeds slowly over the framework V-ions inside the pores of the sample and consequent diffusion limitations. The extracted V-ions (V-MFI(A)) apparently are much less active than the framework V-ions present in the molecular sieve. This is further confirmed by the poor activity of NH_4VO_3.

The shift in the product pattern with duration of run is different for the two catalysts (Fig. 4.3). In the case of sample V-MFI(B), the yield of the side chain oxidation products decreases and the yield of cresols increases with time, whereas, in the case of V-MFI(A), the relative yields of the two types of products remains nearly constant (Fig. 4.3). These observations further confirm that the catalytically active V-species are different in the two cases. The slow build up of the ring-hydroxylation products probably suggests that these are mainly produced over the framework V-species located inside the pores. Further

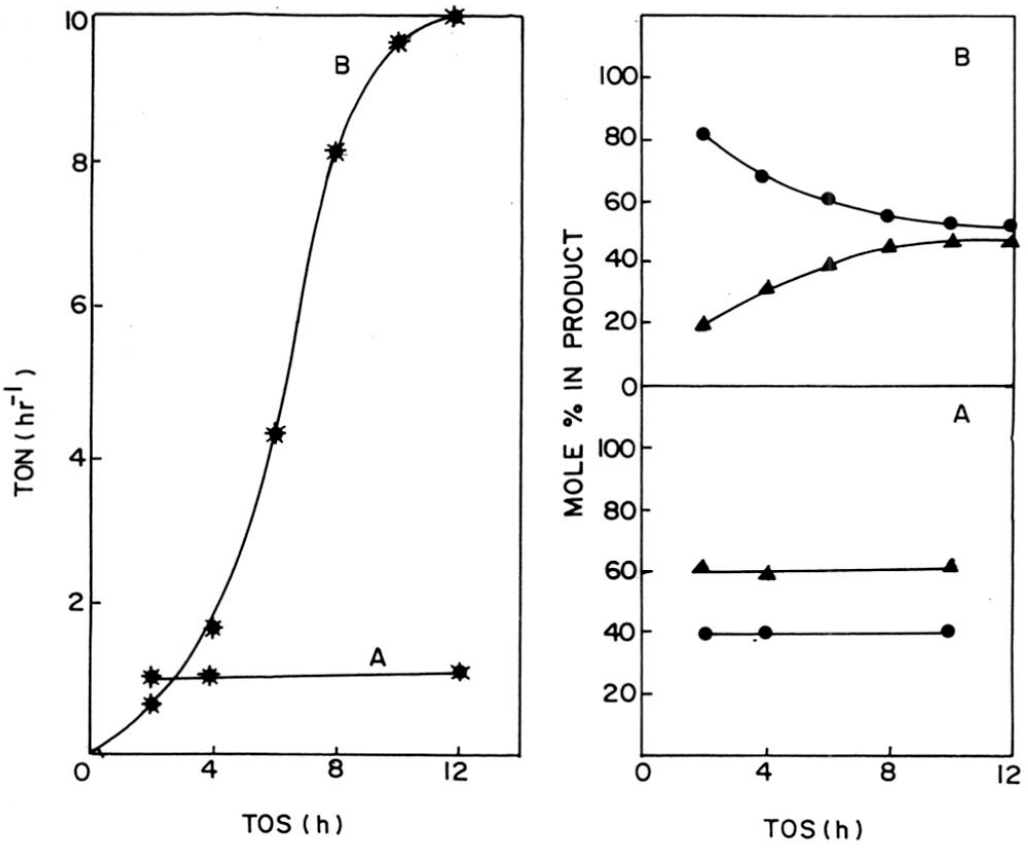

Fig. 4.3 Oxidation of toluene over V-MFI samples : Influence of duration of run on conversion and product distribution. A : V-MFI(A), B : V-MFI(B), (•) side chain oxidation products and (Δ) cresols.

confirmation of the presence of the V-species inside the pore system in sample V-MFI(B) comes form an examination of the o/p ratio of the cresols in the product. Besides kinetic, mechanistic and structural factors,[29] the o/p ratio of the product is also determined by the location of the active species in molecular sieve catalysts, with active centres inside the pore system producing more p-isomer than those outside.[30] The smaller o/p ratio over V-MFI(B) adds evidence to our earlier suggestions that the V-species in sample V-MFI(B) are mostly located inside the pore system attached to the framework in defect sites. The V-species in sample V-MFI(A) are probably located on the surface in an easily extractable form, the catalytic activity of V-MFI(A) is similar to V-imp-sil-1 and pure NH_4VO_3.

(ii) Studies over V-MEL samples

Table 4.7 (page 130) presents the results of the studies on the oxidation of toluene over V-MEL samples. The TON values pass through a maximum. The maximum TON (5.5) was observed in the case of V-MEL(3) and minimum (0.5) for V-MEL(1-He) (Fig. 4.1b). This clearly indicates that the catalytic activity is not related to the total amount of vanadium present in the V-MEL samples (Table 4.1) but it is related to the concentration of active vanadium centers. From figure 4.1, it is found that the order of activity of the V-MEL samples is 3 > 2 > 4 > 1 >1-He. The TON is small (0.6) over V-imp-sil-2.

The yield of benzaldehyde is maximum over V-imp-sil-2 and it decreases from V-MEL(1-He) to V-MEL(3). On the other hand, the yield of cresols increases form V-MEL(1-He) to V-MEL(3). This is due to the increase in the framework V-species from V-MEL(1-He) to V-MEL(3). The ratio of o/p cresol is less than one in the case of samples V-MEL(2, 3 and 4) and more than one in the case of V-MEL(1-He) and V-MEL(1) and

V-imp-sil-2. It has already been noted in the case of V-MFI samples that the o/p cresol ratios are less than 1 when the active centres are mostly in framework positions.

(iii) Studies over V-Al-β samples

Table 4.8 presents the results of the oxidation of toluene over V-Al-β samples. The TON increases from V-Al-β(a) to V-Al-β(c) while the total vanadium content decreases (Fig. 4.2b). The maximum TON is 9.6 over V-Al-β(c) and the minimum value is 3.2 over V-Al-β(a).

The yield of cresols increases from V-Al-β(1-He) to V-Al-β(c) along with an increase in the relative amount of the framework V-species, while the yield of benzaldehyde decreases. The V-imp-Al-β produces only benzaldehyde. The ratio of o/p cresols is nearly the same (~1) over all the samples.

(iv) Comparative studies over V-MFI, V-MEL and V-Al-β

Table 4.9 presents the results of the oxidation of toluene over V-MFI(B), V-MEL(3) and V-Al-β(c) samples. The TON values over the three samples are, respectively, 7.8, 5.5 and 9.6. The yield of cresols was slightly more over V-MFI(B) and V-MEL(3) compared to V-Al-β(c). The reason for the lower production of cresols over V-Al-β(c) containing only framework V-species in not clear. This may be due to the acid sites generated by Al influencing the product selectivities.

c. Effect of promoter (picolinic acid)

The results of the oxidation of toluene and hydroxylation of phenol in the presence and absence of promoter (pyridine α-carboxylic acid; picolinic acid) over different

Table 4.8

Oxidation of toluene over V-Al-β samples.

Sample	TON	H_2O_2 selec. (mol %)	product distribution (mol %)					o/p cresol
			al	ol	cresol		others	
					ortho	para		
V-Al-β(a)	3.2 (8.3)	49.1	70.5	6.2	11.2	11.0	1.0	1.0
V-Al-β(b)	4.9 (8.9)	51.6	66.2	5.8	14.1	13.9	-	1.0
V-Al-β(c)	9.6 (9.6)	64.8	56.0	4.0	21.0	17.5	2.0	1.1
V-imp-Al-β	1.3	10.6	90.0	7.0	-	-	3.0	-

Table 4.9

Toluene oxidation: comparative studies over different V-containing molecular sieves.

Sample	TON	product distribution (mol %)					o/p cresol
		al	ol	cresol		others	
				ortho	para		
V-MFI(A)	10.0	42.5	8.2	25.2	24.1	-	0.9
V-MEL(3)	5.5	48.7	6.2	24.5	21.6	-	0.9
V-Al-β(c)	9.6	56.0	4.0	21.0	17.5	2.0	1.1

Footnotes for tables 4.8 and 4.9.

al → benzaldehyde; ol → benzyl alcohol;

Reaction conditions : Catalyst : 0.1g; toluene / H_2O_2 = 2; temp. = 353K;
toluene / catalyst (wt) = 10; solvent (acetonitrile) = 10ml;
reaction time = 12h;

TON → Turn over number i.e, number of moles of toluene converted per hour per atom of vanadium present in the used catalyst.

H_2O_2 selectivity = (number of moles of H_2O_2 utilized for the product formation) / (total number of moles of H_2O_2 used during the reaction)

catalysts are presented in table 4.10 and 4.11. From table 4.10, it is noticed that V-MFI(B), V-MEL(3), and V-Al-β(c) are good catalysts for the oxidation of toluene even in the absence of the promoter, whereas, V-MFI(A) and V-MEL (1-He) are poor catalysts. The catalysts V-MFI(B), V-MEL(3), and V-Al-β(c) contain mostly the framework V-species which are not extractable by dilute H_2O_2 in the reaction medium, whereas V-MFI(A) and V-MEL(1-He) contain mostly the extractable V-species (table 4.10). In the absence of the promoter, the conversion of toluene is highest (14%) over V-Al-β(c) sample with ~65% selectivity of H_2O_2. The selectivity ratios of the various products, benzaldehyde, o-cresol, p-cresol and m-cresol is roughly 2 : 1 : 1 : 0 over all the vanadium containing molecular sieves. The pure V-picolinato complex and the complex impregnated on silicalite-1 sample exhibit a significant activity (~9% conversion) with a different product selectivity (benzaldehyde : o-cresol : p-cresol : m-cresol = 1: 10: 6: 5 and 1: 4: 2: 2, respectively). Mimoun *et al.*[25] have reported a similar product selectivity over V-picolinato complexes in homogeneous solution phase reactions as that observed for the neat complex (1 : 10 : 6 : 5).

In the presence of the promoter (picolinic acid (mole) : V (atom) = P : V = 1:1), the conversion and the product selectivity increase significantly in the case of V-MFI(A) and V-MEL(1-He), whereas, no change is observed over V-MFI(B), V-MEL(3) and V-Al-β(c) catalysts. These catalysts were quite active even in the absence of the promoter and contain mostly framework V-species. Besides, the amount of vanadium leached out from the samples decreases in the presence of the promoter. The conversion was enhanced nearly 15 fold and the leaching of vanadium into the reaction medium was only about 14% and 18% instead of 82% and 84%, respectively, for V-MFI(A) and V-MEL(1-He). The selectivity to cresols increased on addition of the promoter. In homogeneous medium (V-picolinato complex), the formation of meta cresol was very high (~21%), whereas it was negligible over V-MFI(A)

Table 4.10

Promoter induced catalysis (oxidation of toluene).

Sample	P/V	Conv. (mol %)	H_2O_2 (mol %)	Product distribution (mol %)					%V leached
				al	ol	Cresol			
						ortho	meta	para	
V-MFI(A)	0	1.5	6.8	50.8	4.2	23.4		21.6	82
V-MFI(A)	1	15.2	50.8	12.4	2.5	35.9	3.8	45.4	14
V-MFI(B)	0	7.7	32.9	42.5	8.2	25.2	-	24.1	23
V-MFI(B)	1	7.9	33.3	40.7	8.2	23.0	1.2	25.9	21
V-MEL(1-He)	0	0.9	3.8	62.8	8.7	15.9	-	12.6	84
V-MEL(1-He)	1	13.6	46.8	14.8	4.5	38.2	4.8	37.7	18
V-MEL(3)	0	3.5	10.7	48.7	6.2	24.5	-	21.6	26
V-MEL(3)	1	3.7	16.1	45.2	5.8	27.6	-	21.4	23
V-Al-β(c)	0	14	64.8	56.0	4.0	17.0	-	21.0	8
V-Al-β(c)	1	14.3	65.6	52.8	4.2	18.2	-	21.8	3
V-complex	1	9.5	29.7	4.2	2.7	46.5	21.5	25.1	-
V-com-imp-sil2	1	8.7		10.5	3.2	42.4	19.2	24.7	98

al → benzaldehyde, ol → benzyl alcohol, P → promoter (picolinic acid)

Reaction conditions : Catalyst = 0.3gm, toluene/H_2O_2 = 3, toluene/catalyst (wt)= 10, temperature = 353, solvent (acetonitrile) = 30ml, reaction time = 12h.

Table 4.11

Promoter induced catalysis (hydroxylation of phenol).

Sample	P/V	Conv. (mol %)	H_2O_2 selec. (mol %)	Product distribution (mol %)		
				HQ	BQ	Cat
V-MFI(A)	0	8.5	17.6	27.6	3.5	68.9
V-MFI(A)	1	30.6	61.2	48.7	0.7	50.6
V-MFI(B)	0	23.8	48.5	45.0	1.8	53.2
V-MFI(B)	1	24.7	49.4	43.2	1.2	55.6
V-MEL(1-He)	0	6.4	11.8	27.0	8.5	64.5
V-MEL(1-He)	1	25.8	51.6	45.2	0.5	54.3
V-MEL(3)	0	18.4	49.3	48.2	2.1	49.7
V-MEL(3)	1	19.6	39.2	49.4	1.4	49.2
V-Al-β(c)	0	20.5	32.6	51.0	0.5	48.5
V-Al-β(c)	1	22.1	44.2	50.5	0.3	49.2
V-complex	1	12.5	25.0	49.2	2.3	48.5
V-imp-com-sil-2	1	10.9	21.8	48.7	1.8	49.5

Cat → catechol, HQ → hydroquinone, BQ → benzoquinone,

P → promoter (picolinic acid)

Reaction conditions : Catalyst 0.3 g; phenol/H_2O_2 = 2; phenol/catalyst = 10; solvent (water) = 30 ml; temp. = 353K; reaction time = 12h.

and V-MEL(1-He) in the presence of the promoter. This probably suggests that the formation of cresols takes place inside the zeolite pores in the V-silicalite catalysts, the formation of m-cresol being hindered due to its greater bulk.

The conversion of phenol and $H2O_2$ selectivity are again found to be larger in the presence of the promoter (P : V = 1:1) over V-MFI(A) and V-MEL(1-He) samples (table 4.11). Besides, the % of V leached out into the reaction medium also decreases in the presence of the promoter. The selectivity of catechol to hydroquinone is 1:1 over pure V-picolinato complex and impregnated (V-com-imp-sil-2) samples. A similar product selectivity with a good conversion (30.6 % and 25.8 %) is observed when the reaction is performed over V-MFI(A) and V-MEL(1-He) in the presence of the promoter. The selectivity of catechol to hydroquinone is 2.5 : 1 in the absence of the promoter with a poor conversion of phenol (8.5 % and 6.4 %). The presence of the promoter in the reaction medium does not have any influence over V-MFI (B), V-MFI(3) and V-Al-β(c).

The reasons for the enhancement of catalytic activities of V-MFI(A) and V-MEL(1-He) are examined based on the following experiments :

i) Decomposition of H_2O_2 over V-extracted MEL(A) in the presence and absence of promoter.

The decomposition of H_2O_2 in the presence of the promoter (picolinic acid) was carried out by the following procedure : The catalyst (0.3 g; V-MEL(1-He)) was mixed with 20ml water in a round bottom flask (100 ml) at RT. The flask was placed on a magnetic stirrer for constant stirring. Then 10 mg of picolinic acid (V : P = 1:1) was added to the mixture followed by 1.8 ml of analyzed H_2O_2 (30 wt%). 0.5 ml aliquots were taken after every 1h duration and titrated against a standard (0.1N) ceric sulfate solution. The sulfate solution was initially standardized by titrating with standard Mohr's salt, the Mohr's salt

solution having been standardized by titrating against standard $K_2Cr_2O_7$ solution. The same experiment was performed in the absence of picolinic acid. The solid materials were carefully filtered out after the H_2O_2 decomposition study. The materials were dried at RT in a desiccator. *The materials were named as X and Y and correspond to the solid in the presence and absence of picolinic acid.*

Figure 4.4 shows the decomposition of H_2O_2 over the V-MEL(1-He) in the presence and absence of the promoter. The concentration of H_2O_2 rapidly changes from 0.78 mol lit^{-1} to 0.28 mol lit^{-1} within 3 h and less than 0.05 mol lit^{-1} within 8h (Fig. 4.4a) in the presence of the promoter. In the absence of the promoter, the concentration of H_2O_2 is nearly constant upto 6h. After 6h, there is a slow decomposition of H_2O_2 (Fig. 4.4b). The possible reasons may be (1) the V-species leached into the solution form stable V-peroxo complexes in the absence of promoter (picolinic acid), (2) in the presence of picolinic acid, V-peroxo-picolinato complexes are produced which act as catalysts for the decomposition of H_2O_2.

ii) IR spectroscopic studies

The material X (V-MEL(1-He) from H_2O_2 experiment in the presence of picolinic acid) exhibits an IR band at 1384 cm^{-1} due to the symmetric stretching vibration of C=O indicating that picolinato ligands are present in the solid matrix (Fig. 4.5a).[31] The material Y (V-MEL(1-He) from H_2O_2 experiment in the absence of picolinic acid) exhibits no such band (Fig. 4.5b).

iii) ESR spectroscopic studies

The material X exhibits an ESR spectrum with eight hyperfine lines (Fig. 4.6a), whereas material Y is ESR inactive (Fig. 4.6b). The ESR parameters (g_{11} = 1.935, $g_\perp$ = 1.991, A_{11} = 191.2G, $A_\perp$ = 70.6G) correspond to V^{4+} in a SqPy environment.[32] The samples

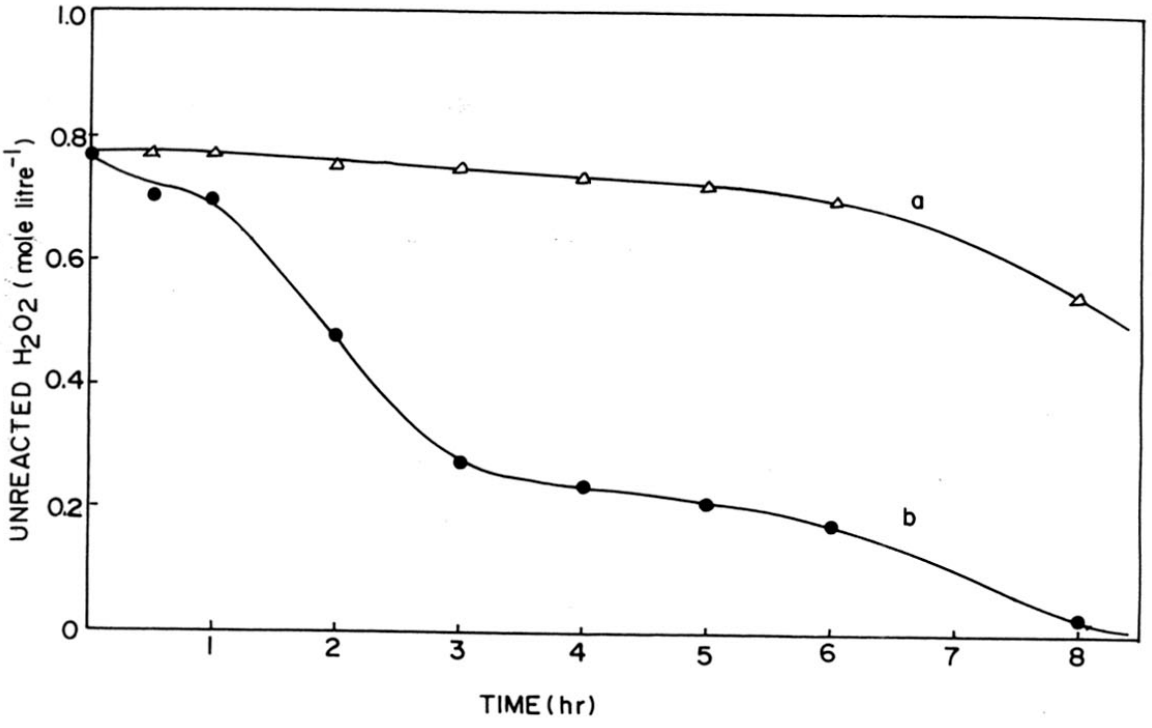

Fig. 4.4 Study of the decomposition of H_2O_2 in the presence of V-MEL(1-He). a : in the absence of picolinic acid, b : in the presence of picolinic acid.

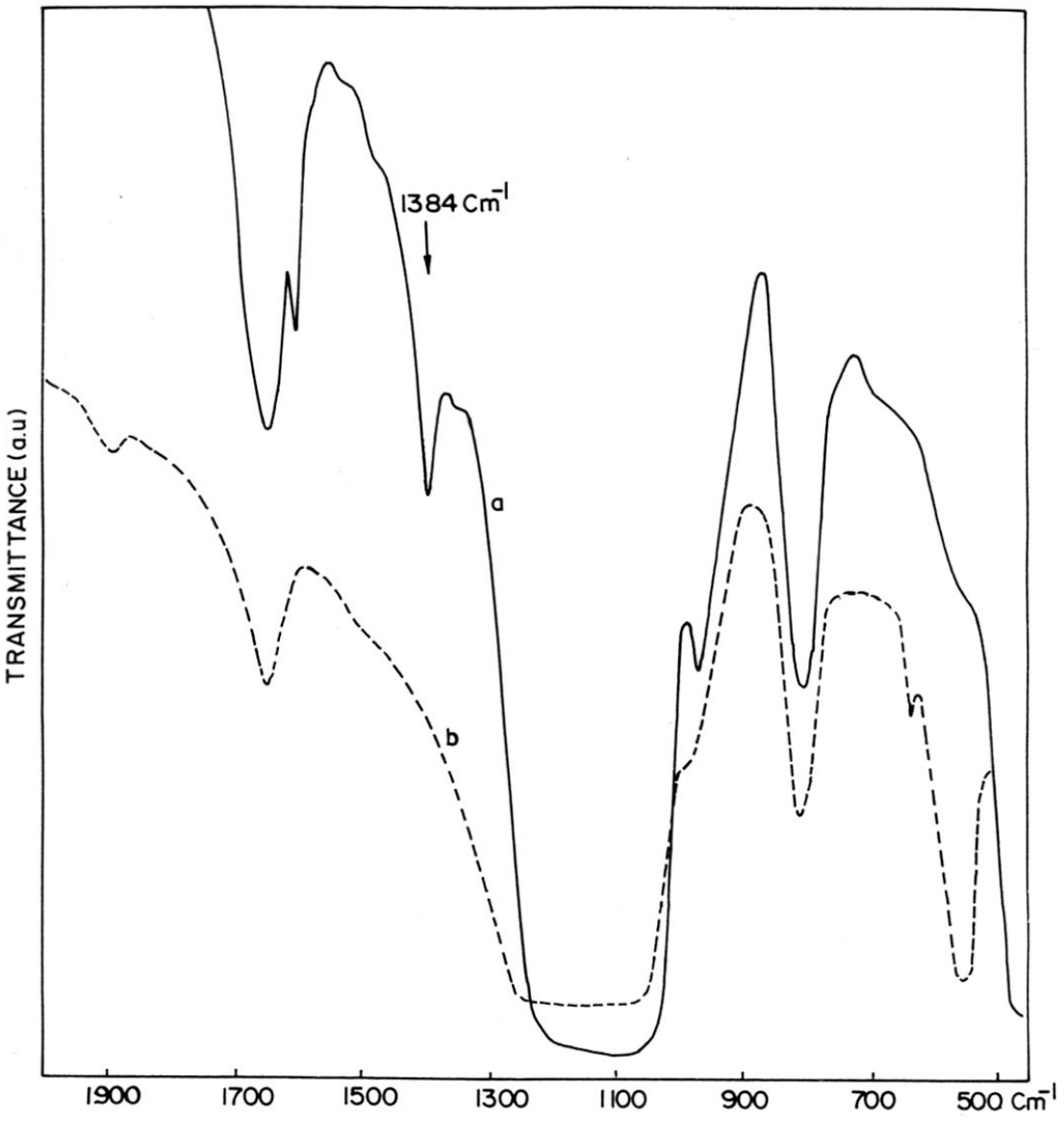

Fig. 4.5 FT-IR spectra of different forms of V-MEL(1-He). a : material X, b : material Y.

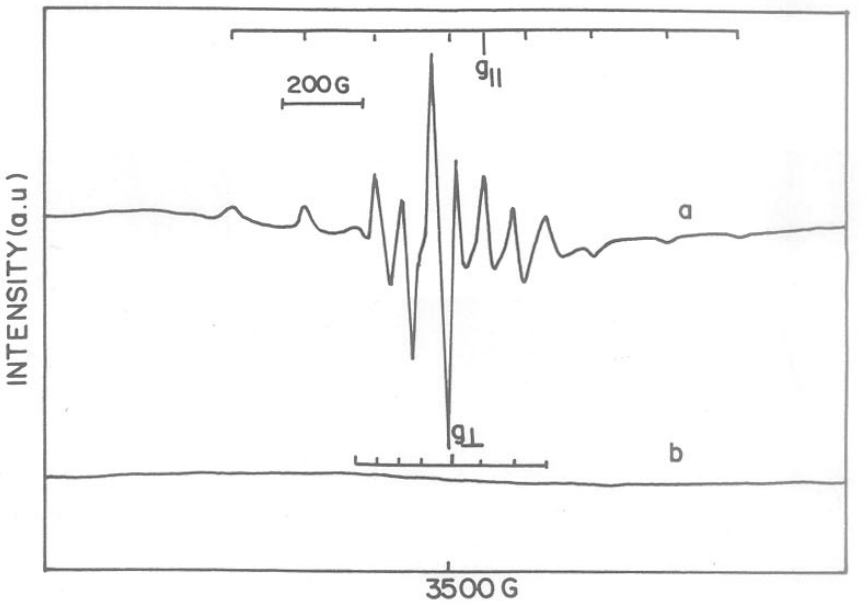

Fig. 4.6 ESR spectra of different forms of V-MEL(1-He). a : material X; b : material Y.

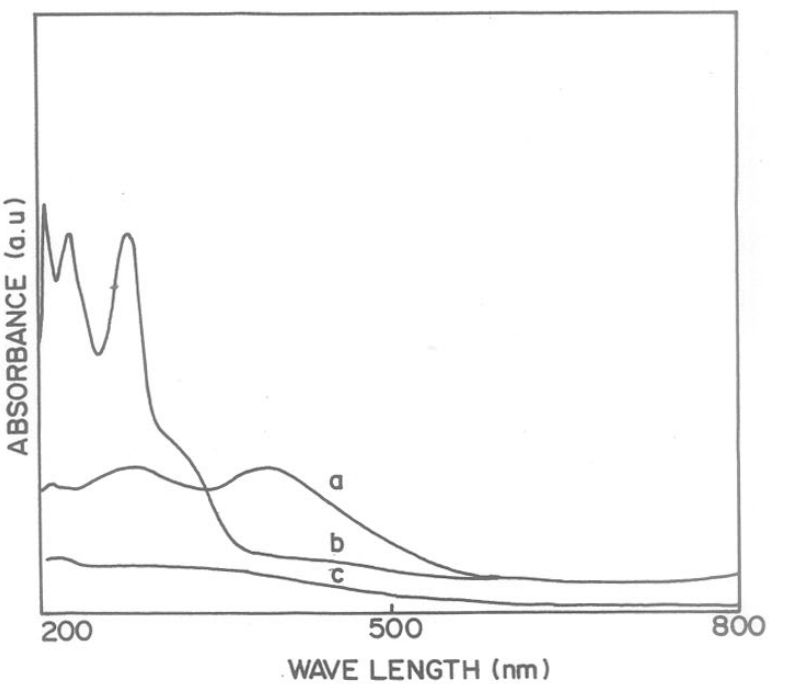

Fig. 4.7 UV-visible DR spectra of different forms of V-MEL(1-He). a : calcined V-MEL(1-He), b : material X, c : materialY.

V-MFI(A) and V-MEL(1-He) exhibit a strong ESR signal with eight hyperfine lines after the oxidation of toluene in the presence of the promoter, whereas no signal is observed in the absence of the promoter. The easy reducibility of the nonframework V-species in the presence of the promoter is an indication of the good catalytic activities. The V-picolinato complex and its impregnated form in silicalite-2 sample exhibit no ESR signal indicating the absence of V^{4+} species.

iv) UV-visible diffuse reflectance (DR) spectroscopic studies

The UV-Vis DR spectra of V-MEL(1-He) after the H_2O_2 experiment (material X and Y) are shown in figure 4.7. The pure V-MEL(1-He) shows two DR bands at 285 and 384 nm due to the presence of Td and Oh vanadium species. The bands disappear after treatment with dilute H_2O_2 (material Y; Fig. 4.7b) due to the extraction of vanadium species into the solution from the solid matrix. The sample X exhibits two strong DR bands at 220 and 270 nm, along with a shoulder at 320 nm (Fig. 4.7c). The DR bands at 220 and 270 nm are due to the charge transfer transition of $V^{4+}\rightarrow$ picolinato ligand (ESR evidence). Smith *et al.*[33] reported a similar DR band due to the charge transfer transition of $V^{4+}\rightarrow$ tyrosine in human lectoferrin. The band at 320 nm corresponds to V^{5+} in a Td or SqPy environment. The material Y exhibits no UV-Vis DR band (Fig. 4.7a) indicating the absence of V-species. This clearly indicates that the V-species are easily extracted from V-MEL(1-He) on treatment with H_2O_2 in the absence of promoter. From the H_2O_2 decomposition and spectroscopic studies, it is concluded that the vanadium species which are present in the V-MFI(A) and V-MEL(1-He) form stable insoluble vanadyl peroxo picolinato complex attached to the zeolite matrix. The probable structures of these complexes are shown in the Scheme 4.3.

The solid insoluble complex I reported by Mimoun *et al.*[25] is formed initially which later transforms into complex II in the presence of H_2O_2. The transformation of I to II

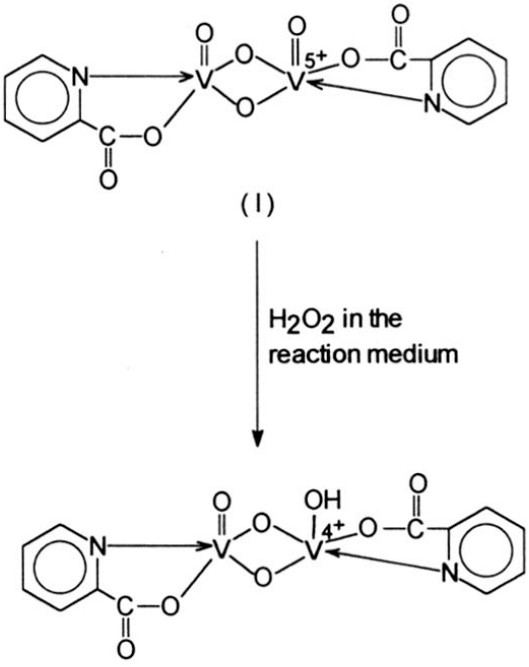

SCHEME 4.3 Plausible structure of differnt forms of V-MEL(1-He). I : Material X, II : Material Y.

may be responsible for the catalytic activity. The stability of the nonframework V-species may be due to the proper fitting of complex II inside the channel of V-MEL(1-He) and V-MFI(A).

4.1.4 CONCLUSIONS

Framework V-species are active in the hydroxylation of phenol and the oxidation of toluene. Non-framework V-species are easily extracted by dilute H_2O_2 into the reaction medium and are poor oxidation catalysts. The framework V-species are relatively more active in ring hydroxylation than primary carbon oxidation. The stability and activity of non-framework V-species is enhanced in the presence of a promoter (picolinic acid).

4.2 PART B - VAPOUR PHASE OXIDATION OF ETHANOL

4.2.1 INTRODUCTION

Selective oxidation of ethanol to value added chemicals has deserved recently an increasing technological interest in connection with the utilization of biomass as a chemical source.[34] Although, silver based catalysts are commercially used, a number of metal oxides have been tested for this reaction in order to find a substitute for this commercial catalyst.[35] Among the oxides screened, molybdenum and vanadium based catalysts are the promising candidates for the above reaction.[36] Oyama and co-workers[37] have studied the oxidation of ethanol over silica-supported vanadium oxide catalysts. No remarkable change in the activity was observed with vanadium loading and particle size of the catalyst indicating that the reaction is structure insensitive. Quaranta *et al.*[38] have extended the earlier study by supporting V_2O_5 on a TiO_2-coated SiO_2 support. A good improvement in both activity and selectivity (to acetaldehyde) was observed for the V-Ti-Si catalyst when compared to both V-Si and V-Ti catalysts. The enhanced activity was attributed to the interactive nature of the TiO_2 support and good molecular dispersion. Very recently, selective dehydrogenation of ethanol was carried out over V_2O_5 supported on α-Al_2O_3.[39] An improved selectivity for acetaldehyde was observed, accounted on the basis of greater heat dissipation and catalyst bed isothermicity. Wan *et al.*[40] have studied the oxidation of ethanol over the transition metal incorporated microporous aluminophosphate molecular sieve $AlPO_4$-5. VAPO-5 exhibited more acidic behavior yielding mainly diethyl ether and ethylene with small amount of acetaldehyde. Bellusi *et al.*[41] have studied the oxidation of methanol over vanadium containing MFI silicalites. V-silicalites showed a higher activity than V_2O_5 supported on silica with similar selectivity for formaldehyde and the difference in the activity was

explained based on the different sorption strengths. Recently, we have reported the oxidation of ethanol over vanadium containing MEL silicalites.[42]

This part presents the vapour phase oxidation of ethanol over vanadium containing medium (V-MFI, V-MEL) and large pore (V-Al-β) molecular sieves.

4.2.2 EXPERIMENTAL

Details of the synthesis of various samples and their characterization were presented in chapter II and III. The various samples used in the vapour phase oxidation of ethanol and their characteristic properties are presented in table 4.12.

Details of the experimental part of catalytic reactions have been presented in chapter II.

4.2.3 RESULTS AND DISCUSSION

A. Studies over V-MEL samples

(i) Effect of temperature

Table 4.13 presents the results of the oxidation of ethanol over various V-MEL catalysts at different temperatures. The conversion of ethanol increases with temperature over different catalysts (Fig. 4.8). Comparison of the catalysts with different Si/V atomic ratios indicates that an increase in the concentration of incorporated vanadium in the zeolite lattice increases the catalytic activity (Table 4.13). Although the impregnated catalyst contains nearly four times the concentration of vanadium present in V-MEL(2)-Ex; a lower activity is observed indicating the higher intrinsic activity of incorporated vanadium. During reaction, on all the catalysts, acetaldehyde, diethylether and ethylene were observed as the major products and acetone, acetic acid, ethylacetate and CO_x were observed as the minor products. A comparison of the activity of V-MEL(1) and its post modified forms indicates

Table 4.12

Chemical composition of the samples used in the vapour phase oxidation of ethanol.

Catalyst	Pretreatment	V/Si+V ($x\ 10^{-3}$)	Nature of V-species	Ref.
V-MEL(1)	Calcined at 773K for 10h.	7.46	x_2+x_3	43
V-MEL(1)-Ex	NH_4OAc extraction at 333K for 12h.	0.7	x_2	43
V-MEL(1)-Ex-Na	NH_4OAc extraction at 333K for 12h; Exchange with 1(N) $NaNO_3$ solution at 333K for 12h.	0.7	x_2	43
V-MEL(2)	Calcined at 773K for 10h.	4.1	x_2	43
V-MEL(2)-Ex	NH_4OAc extraction at 333K for 12h.	2.4	x_2	43
V-imp-sil-2	Impregnation of V_2O_5 on silicalite-2	9.8	x_1	43
V-MFI(B)-Ex	Calcined and NH_4OAc extraction at 333K for 12h	3.9	x_2	24
V-Al-β(c)-Ex	Calcined at 773K for 10h and NH_4OAc extraction at 333K for 12h	4.0	x_2	53

$x_1 \rightarrow$ Polymeric O_h

$x_2 \rightarrow$ Framework distorted T_d

$x_3 \rightarrow$ Monomeric mobile nonframework T_d and Framework distorted T_d

Table 4.13

Oxidation of ethanol over various V-MEL catalysts at space velocity $2.6h^{-1}$.

Catalyst	Temp. (K)	Conv. (mol %)	Product distribution (mol %)			
			C_2H_4	CH_3CHO	$(C_2H_5)_2O$	Others[a]
V-MEL(1)	523	2.9	21	73	3	2
	548	8.8	18	82	-	-
	573	28.1	16	77	7	-
	598	54.2	30	67	3	-
	623	82.1	33	60	7	-
V-MEL(1)-Ex	523	3.1	10	35	55	-
	548	7.3	14	37	49	-
	573	18.1	29	31	40	-
	598	35.3	52	29	19	-
	623	54.7	52	34	14	-
V-MEL(1)-EX-Na	523	5.1	16	80	4	-
	548	11.1	14	77	9	-
	573	32.6	20	73	6	3
	598	52.6	21	61	7	11
	623	67.4	39	61	-	-
V-MEL(2)-Ex	523	13.3	4	49	49	-
	548	36.3	7	43	50	1
	573	69.4	21	43	35	12
	598	100	50	33	5	3
	623	100	74	18	5	-
V-imp-sil-2	523	3.8	8	92	-	-
	548	15.6	11	88	1	-
	573	27.8	21	76	3	-
	598	68.4	21	77	2	-
	623	92.4	28	69	3	-

a → Mostly acetone, acetic acid, ethyl acetate and methanol.

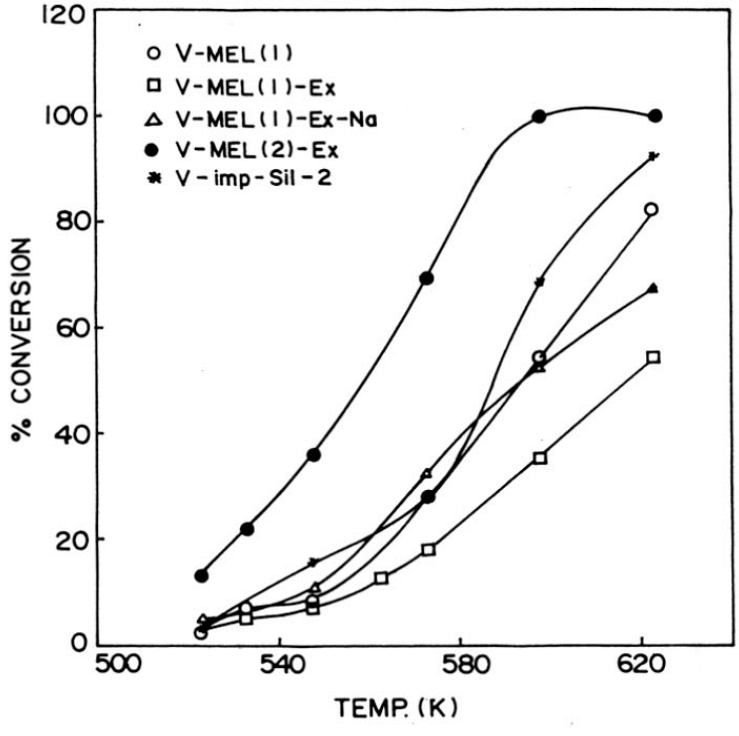

Fig. 4.8 Variation of conversion with temperature over various V-MEL catalysts.

that V-MEL(1) and V-MEL(1)-Ex-Na samples possess similar activities while V-MEL(1)-Ex possesses lower activity.

Figure 4.9 (a to d) shows the plots of selectivity to the major products at constant conversion levels (10% and 50%). V-MEL(1) and V-MEL(1)-Ex-Na samples exhibit similar selectivity pattern and favour the dehydrogenation reaction (acetaldehyde formation), whereas the sample V-MEL(1)-Ex favours the primary dehydration product, namely diethyl ether (Fig. 4.9a,b). Furthermore, the selectivity to acetaldehyde decreases with an increase in reaction temperature for the former samples, while it is not affected much over the latter sample (Table 4.13). At higher temperatures, however, the selectivity for the secondary dehydrogenation product, ethylene, is enhanced with a loss in the selectivity of acetaldehyde and diethylether. The catalytic activity of V-MEL(1)-Ex-Na sample is similar to that of the calcined sample. The objective of the exchange of V-MEL(1)-Ex with Na^+ ion was to remove the weakly Bronsted acidic sites associated with the defect centres created on V-incorporation[43] thereby increasing the selectivity towards acetaldehyde. In fact, a three fold increase in the selectivity was observed especially at low conversions, upon exchange (Fig.4.9; Table 4.13). Figure 4.9 (c and d) presents the plot of selectivity of the major products for the catalysts with different Si /V atomic ratios at constant conversion. Among the samples, the impregnated catalyst shows a maximum selectivity for acetaldehyde and a minimum selectivity for diethyl ether at both lower and higher conversions. The V-MEL(1)-Ex and V-MEL(2)-Ex possess a higher selectivity for diethyl ether at the lower conversion, while ethylene and acetaldehyde are the major products at the higher conversion level. At higher temperatures, the secondary dehydration reaction leading to ethylene is favored over all the catalysts. However, the selectivity to acetaldehyde is not affected much

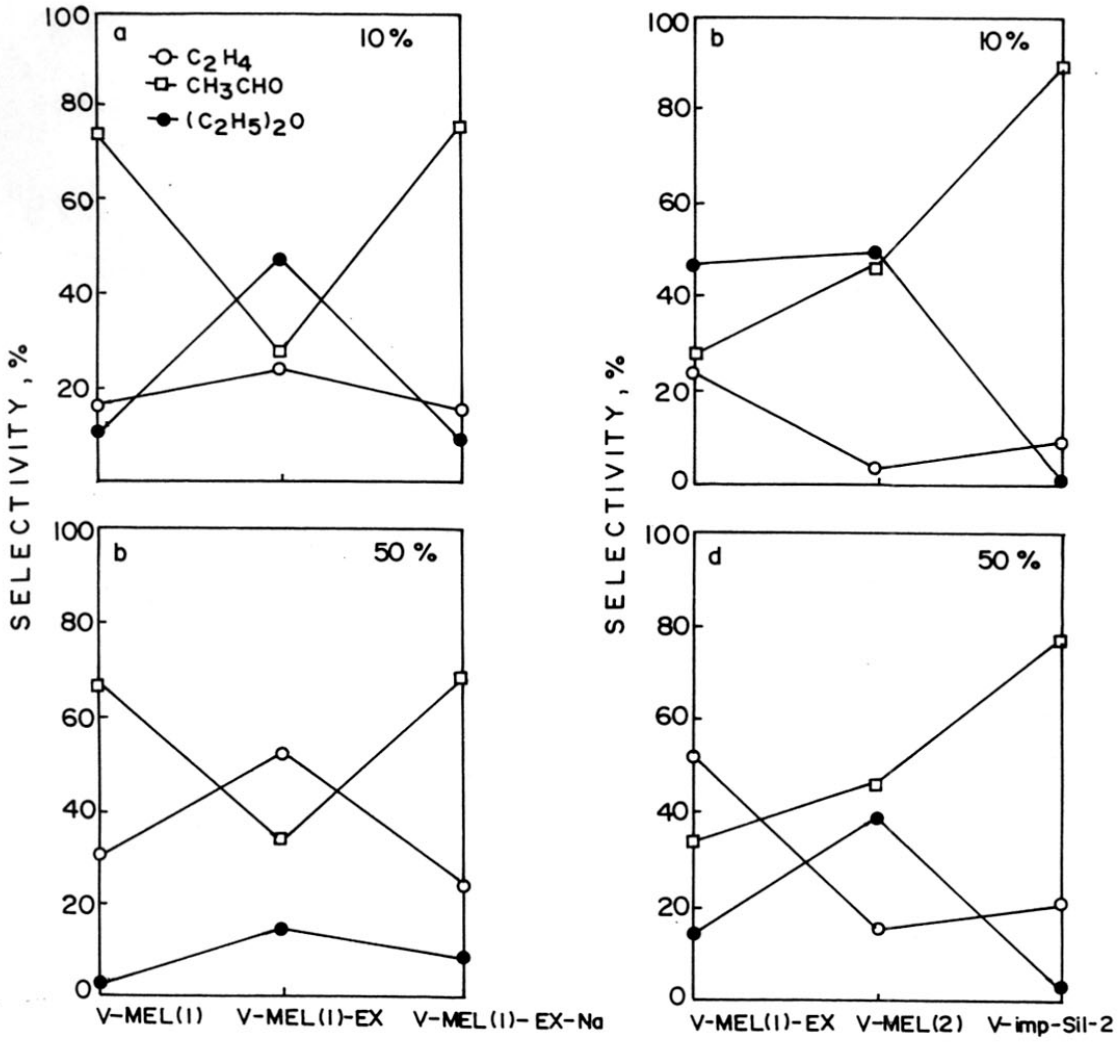

Fig. 4.9 Variation of selectivity of major products at constant conversions (10 % and 50 %) over various V-MEL catalysts.

at both conversion levels (10 and 50%) indicating that the sites responsible for aldehyde formation are not perturbed by an increase in the temperature (Table 4.13).

(ii) Kinetics of the reaction

In order to understand the kinetics of the reaction over these samples, it is essential to know the order dependence of ethanol on the rate of formation of the major products (C_2H_4, CH_3CHO and $(C_2H_5)_2O$). Figure 4.10 shows the logarithmic plot of partial pressure of ethanol with turn over rate. Turn over rates were calculated based on the total V-ions present in the samples (Table 4.14).

The partial pressure effect of ethanol for acetaldehyde formation over V-MEL(1) at 523K shows (Fig. 4.10) a rate dependence corresponding to first order rate expression. The E_{app} values were calculated based on Arrhenius equation

$$\ln (x / 1-x) = \ln A - E_{app} / RT \quad \ldots\ldots\ldots\ldots\ldots\ldots\ldots\ldots\ldots\ldots\ldots\ldots\ldots\ldots\ldots\ldots (1)$$

where x is the total conversion at temperature T, E_{app} is the apparent activation energy and A is the preexponential factor. The apparent activation energy appearing in the equation (1), however, is composed of two terms

$$E_{app} = E + \Delta H$$

where E is the activation energy of the rate determining step and ΔH is the heat of adsorption of alcohol. Since the adsorption of alcohol in the active catalyst surface is exothermic, ΔH is a negative quantity which results in a smaller activation energy. This explains why the observed activation energies are substantially lower than the C-H bond dissociation energy of $CH_3CH(H)$-OH of 398 kJ / mol. The E_{app} for the formation of aldehyde were calculated based on the same equation [$\ln(x_1/1-x) = \ln A - E_{app}/RT$], where x_1 is the fractional yield of aldehyde (Table 4.14). The E_{app} (aldehyde) values of samples containing framework

Table 4.14

Kinetic parameters for the oxidation of ethanol over various catalysts.

Catalyst	Temp. (K)	lnk [a]	E_{app} (kJ / mol)	k_{tor} (x 10^{-3}) (s^{-1})[b]
V-MEL(1)	523	-3.511	122.5[c]	3.7
	533	-2.587	(116.4)[d]	8.9
	548	-2.338		11.2
	563	-1.301		27.2
	573	-0.939		35.7
V-MEL(1)-Ex	523	-3.442	94.1	42.3
	533	-2.883	(133.5)	72.3
	548	-2.541		99.6
	563	-1.913		174.6
	573	-1.509		247.0
V-MEL(1)-Ex-Na	523	-2.923	109.0	69.6
	548	-2.080	(115.2)	151.4
	573	-0.726		444.8
V-MEL(2)-Ex	523	-1.875	135.3	52.7
	533	-1.254	(132.5)	88.1
	548	-0.562		144.0
	563	0.385		236.0
	573			275.3
V-imp-sil-2	523	-3.231	113.8	3.7
	548	-1.685	(109.4)	15.1
	573	-0.954		26.9

a → calculated employing first order rate expression.

b → turnover rate calculated as number of molecules of ethanol converted per vanadium atom per second.

c → E_{app} calculated based on the conversion of ethanol.

d → E_{app} calculated based on the acetaldehyde formation.

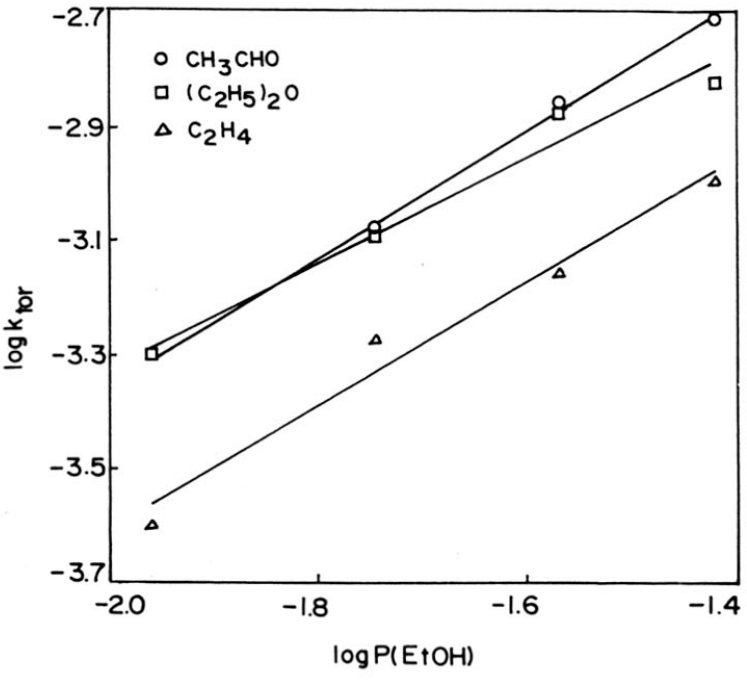

Fig. 4.10 Effect of partial pressure of ethanol on the reaction rate for various V-MEL catalysts.

V-species (V-MEL(1)-Ex and V-MEL(2)-Ex) are similar (~130 kJ mol^{-1}), while the values for the other samples (V-MEL(1) and V-imp-sil-2) containing extraframework V-species are also similar though of a lower magnitude (110 - 120 kJ mol^{-1}, Table 4.14). This suggests that the formation of acetaldehyde is less favourable over samples containing only framework V-species. Though the similarity of E_{app} (aldehyde) values for V-MEL(1)-Ex and V-MEL(2)-Ex are understandable, the reasons for the differences in the E_{app} (conversion) are not clear. The E_{app} (conversion) values are similar for the other samples containing mainly non-framework V-species (Table 4.14).

iii) Effect of space velocity

Table 4.13 and 4.15 presents the conversion of ethanol at various reaction temperatures over two different space velocities (2.6 h^{-1} and 1.3 h^{-1}). It is clear that the conversion increases, irrespective of the contact time, with increase in reaction temperature. The conversion of ethanol increases with decreasing space velocity (increase in contact time) at a fixed reaction temperature.

The selectivity towards acetaldehyde decreases with increasing temperature for V-MEL(1) especially at the higher space velocity. However, at the lower space velocity, no significant change in the selectivity is observed. The selectivity pattern, however, is not significantly affected with contact time for V-MEL(1)-Ex and V-MEL(1)-Ex-Na samples indicating the intrinsic stability of the incorporated vanadium in the zeolite lattice. However, for V-MEL(1)-Ex-Na at the higher contact time, a drop in the selectivity of CH_3CHO was observed with increase in reaction temperature. This could be due to the subsequent reaction of the aldehyde leading to the formation of ethyl acetate (Table 4.15). The formation of diethyl ether is very high at the higher contact time over V-MEL(1)-Ex and V-MEL(2)-Ex

Table 4.15

Oxidation of ethanol over various V-MEL catalysts at space velocity of $1.3h^{-1}$.

Catalyst	Temp. (K)	Conv. (mol %)	Product distribution (mol %)			
			C_2H_4	CH_3CHO	$(C_2H_5)_2O$	others[a]
V-MEL(1)	523	25.4	27.3	72.7	-	-
	548	67.6	35.8	55.2	8.9	-
	573	100	36.9	57.3	5.7	-
	598	100	32.6	61.6	5.8	-
	623	100	37.5	62.5	0.0	-
V-MEL(1)-Ex	523	8.3	9.7	25.3	65.0	-
	548	11.1	10.8	32.4	56.8	-
	573	31.7	26.5	30.0	43.5	--
	598	60.7	50.7	31.2	18.2	-
	623	75.7	65.1	29.6	5.3	-
V-MEL(1)-Ex-Na	523	5.0	10.0	78.0	12.0	-
	548	12.1	12.4	74.4	12.4	-
	573	42.5	10.6	71.3	5.2	13.1
	598	72.5	18.3	69.9	-	11.7
	623	82.9	37.2	62.8	-	-
V-MEL(2)-Ex	523	73.6	15.2	40.7	36.0	8.1
	548	100	45.2	24.9	8.6	21.3
	573	100	69.2	8.6	-	22.2
	598	100	77.5	2.9	-	19.6
	623	100	100	-	-	-
V-Imp-sil-2	523	62.6	15.8	84.2	-	-
	548	100	32.0	60.5	4.3	3.1
	573	100	43.2	51.1	5.7	-
	598	100	48.7	47.4	3.8	-
	623	100	99.7	-	0.3	-

a → Mostly acetone, acetic acid, ethyl acetate and methanol

samples. In all cases, at higher temperatures, the selectivity towards ethylene is favoured over all the catalysts irrespective of the contact time.

b. Comparative studies over V-MFI, V-MEL and V-Al-β samples

Table 4.16 presents the comparative studies of oxidation of ethanol over three different catalysts. The maximum conversion is observed over V-Al-β(c)-Ex at both low and high space velocities, whereas, V-MFI(B)-Ex exhibits a poorer conversion both at high and low space velocities. V-MEL(2)-Ex possess an intermediate activity. Conversion increases with temperature over all the catalysts both at high and low space velocities. All the three catalysts exhibit higher conversions at lower space velocities (increase in contact time) at a fixed reaction temperature.

The selectivity towards diethyl ether increases in the order V-Al-β(c) > V-MFI(B)-Ex > V-MEL(2)-Ex. It is well established that all the three catalysts contain framework V-species. The amount of diethylether produced is directly related to the amount of framework V-species in the samples. At high temperature, ethylene is the major product over all the catalysts both at high and low space velocities.

c. Probable mechanism

The selective oxidation of ethanol over supported metal oxide surfaces has been studied extensively.[44-46] The important steps involved in the reaction are 1) adsorption and activation of ethanol on the active metal site and 2) decomposition of the ethoxide species (rate determining step) to form different products. However, the selective formation of any specific product is essentially controlled by the nature of the active sites present on the surface (M=O, M-O-M and M-O-M′ where M is the active metal ion and M′ is the support).[47]

Table 4.16

Comparative studies of oxidation of ethanol over various catalysts.

Catalyst	Space velocity (h^{-1})	Temp. (K)	Conv. (mol %)	Product distribution (mol %)			
				C_2H_4	CH_3CHO	Et_2O	others[a]
V-MEL(2) -Ex	2.6	523	13.3	4.0	49.0	49.0	-
		548	36.3	7.0	43.0	50.0	-
		573	69.4	21.0	43.0	35.0	1.0
		598	100	50.0	33.0	5.0	1.2
do	1.3	523	73.6	15.2	40.7	36.0	5.4
		548	100	45.2	24.9	8.6	5.0
		573	100	69.2	8.6	-	5.6
		598	100	77.5	2.9	-	5.3
V-MFI(B)-Ex	2.6	523	1.6	4.9	22.0	73.1	-
		548	4.0	5.0	23.5	70.2	-
		573	12.8	6.1	23.0	70.5	0.4
		598	12.7	20.2	25.4	53.8	0.5
-do-	1.3	523	22.6	4.1	6.2	87.5	2.2
		548	25.4	8.5	5.8	83.0	2.8
		573	32.5	21.6	4.3	70.7	3.4
		598	38.8	46.3	4.7	43.4	5.6
V-Al-β(c)-Ex	2.6	523	56.4	6.9	2.5	89.4	1.2
		548	72.3	26.7	4.4	67.5	1.4
		573	77.6	56.6	8.6	33.5	1.3
		598	93.7	82.6	14.6	1.7	1.1
-do-	1.3	523	79.2	30.9	30.9	35.5	2.7
		548	93.7	63.0	33.6	1.9	1.5
		573	100	72.3	27.7	-	-
		598	100	74.5	25.5	-	-

a → Mostly acetone, acetic acid, ethyl acetate and methanol.

Trifiro *et al.*[48] reported that the V=O is the active site whose labilization (reducibility) plays a crucial role in controlling the selectivity of the oxidation products. According to them, the activity of the catalyst is directly connected with the metal oxygen double bond which opens with the addition of H atom from the alcohol, which in turn, leaves a free valence on the metal used for bonding with the dehydrogenated molecule (oxyreductive mechanism). A similar perception was realized on MoO_3 based catalysts for ethanol oxidation in which it was suggested that Mo=O sites were responsible for acetaldehyde formation.[49] The involvement of acidity apart form redox property in controlling the selectivity of the products has been observed in various catalytic transformations, over vanadium containing compounds.[50,51] In general, the selectivity pattern appears to be considerably influenced by the acidity of the catalyst (around the active site). Ai *et al.*[52] has observed a linear correlation during the oxidation of methanol over V_2O_5 based catalysts between formaldehyde formation and the acidity of the catalyst suggesting that the oxidation activity is largely governed by the activation of the methanol on the acidic sites rather than on the oxidation function. Based on these observations, a mechanism can be proposed for the formation of products resulting from the decomposition of ethanol (Scheme 4.4).

4.2.4 CONCLUSIONS

The intrinsic activity of vanadium present in the framework is higher than the in nonframework ions. The V-Al-β(c)-Ex sample is the most active catalyst. The framework V-species are active for the formation of ether and nonframework V-species are active for the formation of the aldehyde. The oxidation of ethanol over vanadium containing molecular sieves is a first order reaction.

Site - I

Ether formation

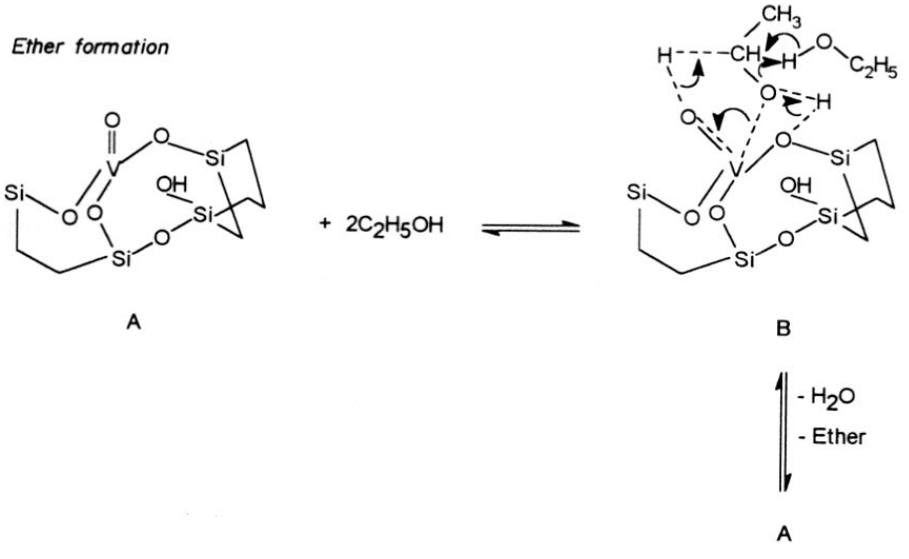

Ethylene formation

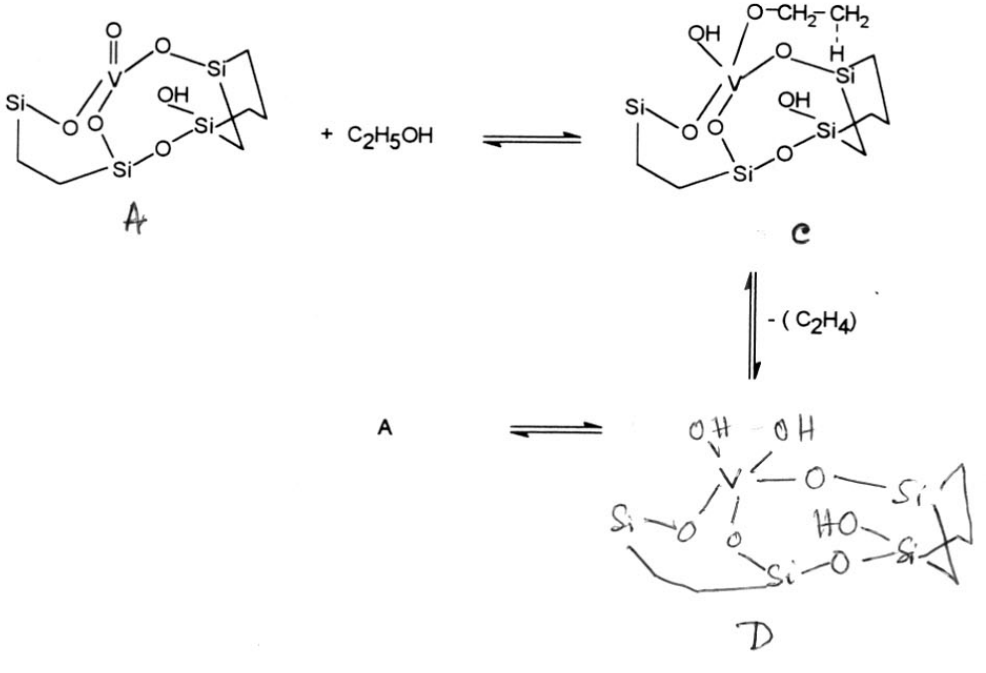

Site - II

Acetaldehyde formation

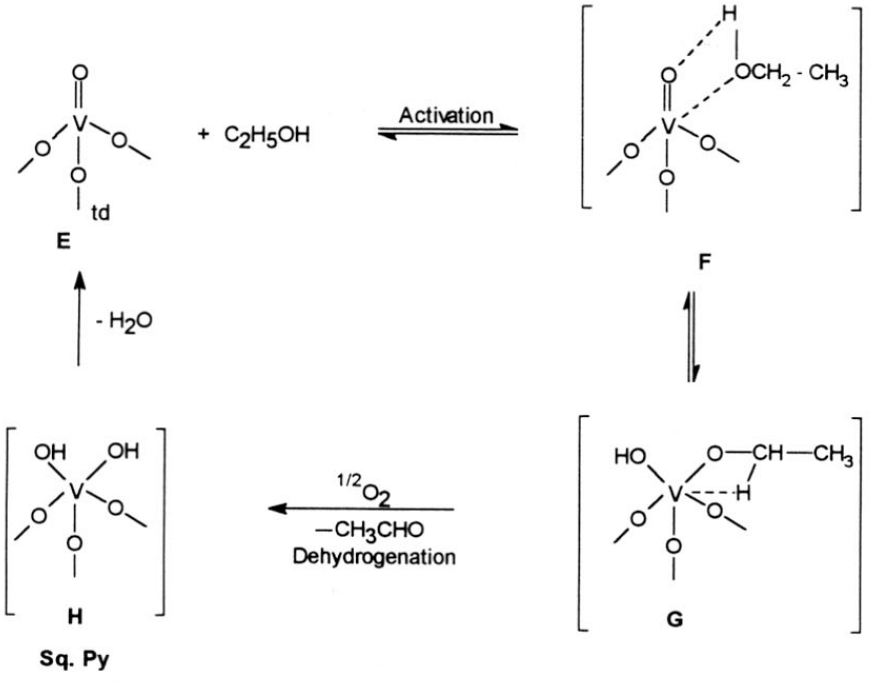

Ethylene formation

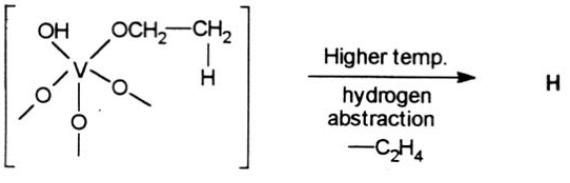

SCHEME 4.4 Plausible mechanism for the formation of products during the transformation of ethanol.

4.3 REFERENCES

1. Taramasso, M., Perego, G., and Notari, B., U.S. Pat. 4410501 (1983).
2. Esposito, A., Taramasso, M., Neri, C., and Bonomo, F., U.S Pat. 2116974
3. Camblor, M. A., Corma, A., and Perez-pariente, J., *Zeolites,* **13,** 82 (1993).
4. Tanev, P. T., Chibne, M., and Pinnavaia, T. J., *Nature,* **368**, 321 (1994).
5. Romono, U., Esposito, A., Maspero, F., Neri, C and Clerici, M. G., *Chem. Ind., (Milan)* **72,** 610 (1990).
6. Notari, B., *Stud. Surf. Sci. Catal.,* **37**, 413 (1987).
7. Thangaraj, A., Kumar, R., and Ratnasamy, P., *Appl. Catal.,* **57**, L1 (1990); *J. Catal.,* **131**, 394 (1991).
8. Tatsumi, T., Nakamura, M., Nefishi, S., and Tominaga, H., *J. Chem.Soc., Chem. Commoum.,* **476** (1990).
9. a) Hubrechts, D. R. C., Bruycker, L. D., and Jacobs, P. A., *Nature,* **345**, 240 (1990).
   b) Reddy, J. S., Sivasanker, S., and Ratnasamy, P., *J. Mol. Catal.,* **70**, 335 (1991).
10. Thangaraj, A., Sivasanker, S., and Ratnasamy, P., *J. Catal.,* **131,** 394 (1991).
11. Reddy, F. S., Sivasanker, S., and Ratnasamy, P., *J. Mol. Catal.,* **69**,383 (1991).
12. Tatsumi, T., Nakamure, M., Yuasa, K., and Tominaga, H., *Chem. Lett.* **297** (1990).
13. a) Miyamoto, A., Medhanavyn, D., and Inui, T., *Appl. Catal.,* **28,** 89 (1986); in "proceedings , 9th International Congress on Catalysis, Calgary, 1988" (M. J. Phillips and M. Ternan, Eds.), Vol.1, p. 437. Chem. Inst. of Canada, Ottawa, Ontario, 1988.
   b) Zatorski, L. W., Centi, G., Nieto, J. L., Trifiro, F., Bellusi, G., and Fattore, V., *Stud. Surf. Sci. Catal,* **B 49**, 1243 (1989).
   c) Trifiiro, F., and Jiru. P., *Catal. Today* **3**, 519 (1991).
   d) Rigutto, M. S., and Van Bekkum, H., *Appl. Catal.,* **68**, L1 (1991).
14. Prasad Rao, P. R. H., Ramaswamy, A. V., and Ratnasamy, P., *J. Catal.,* **137,** 225 (1992).
15. Tuel, A., and Ben Tarrit, Y., *Zeolites* **14,** 18 (1994).
16. Sen, T., Chatterjee, M., and Sivasanker, S., *J. Chem. Soc., Chem. Commun.,* **207** (1995).
17. Reddy, K. M., Moudrakovski, I., and Sayari, A., *J. Chem. Soc., Chem. Commun.,* 1491 (1994).

18. Reddy, K. M., Moudrakovski, I., and Sayari, A.., *J. Chem. Soc., Chem.Commun.*, 1049 (1994).

19. a) Prasad Rao, P. R. H., Ramaswamy, A. V., *J. Chem. Soc., Chem. Commun.*, 1245 (1992).

    b) Prasad Rao, P. R. H., Ramaswamy, A. V., and Ratnasamy, P., *J. Catal.*, **141(2),** 604 (1993).

20. Prasad Rao, P. R. H., Ramaswamy, A. V., and Ratnasamy, P., *Appl. Catal., A* **93(2),** 123 (1993).

21. Prasad Rao, P. R. H., Belhekar, A. A., Hedge, S. G., Ramaswamy, A. V., and Ratnasamy, P., *J. Catal.*, **141(2),** 595 (1993).

22. Ph. D Thesis submitted to "The University of Poona," India by P. Raja Hariprasad Rao, Nov'92.

23. Ramaswamy, A. V., and Sivasanker, S., *Microporous Mater.*, **2(5),** 451 (1994).

24. Sen, T., Rajamohanan, P. R., Ganapathy, S., and Sivasanker, S., *J. Catal.*, **163**, 354 (1996).

25. Mimoun, H., Saussine, L., Daire, E., Postel, M., Fischer, J., and Weiss, R., *J. Am. Chem. Soc.*, **105,** 3101 (1983).

26. a) Bourdin, F., Costantini, M., Jouffret, M. and Lartigan, G., Ger. Pat., DE 2064497 (1971).

    b) Maggioni, P., US Pat. 3914323 (1972).

27. Moiseeva, I. I., *Kinet. Katal.*, **29**, 970 (168).

28. Barak, G., and Sasson, Y., *J. Chem.Soc., Chem. Commun.*, 637 (1968).

29. Ingold, C. K., "Structure and Mechanism in Organic Chemistry," 2nd Ed. Bell and Hyman, London, 1967.

30. Tuel. A., Moussa-Khouzami, S., Ben Taarit, Y., and Naccache, C., *J. Mol. Catal.*, **68**, 45 (1991).

31. Weiss, R., *J. Am. Chem. Soc.*, **105**, 3101 (1983).

32. Rigutto, M. S., and Van Bekkum, H., *Appl. Catal.*, **68,** L1 (1991).

33. Smith, C. A., Ainscough, E. W., and Brodie, A. M., *J. Chem. Soc., Dalton. Trans.* 1121 (1995).

34. Palsson, B. O., Fathi-Afshar, S., Rudd, D. F., and Lightfoot, E. N., *Science*, **231**, 513 (1981).

35. Lgosdon, J.E., in "Kirk-Othmer Encyclopedia of Chemical Technology", Fourth Edition, Vol.9, p.812, John Wiley and Sons Inc., U.S.A. 1994.

36. Kung, H.H., "Transition metal oxides-surface Chemistry and Catalysis". *Stud. Surf. Sci. Catal.*, **45**,200 (1989)..

37. Oyama, S.T., Lewis, K.B., Carr, A.M., and Somarjai, G.A., in "Proc.9th Int. Congr. Catal.", Calgary (M.J.Phillips and M. Ternan, Eds), Vol.3, p.1489. 1988.

38. Quaranta, N.E., Corberan, V.C., and Fierro, J.L.G., *Stud. Surf. Sci. Catal.*, **72**, 147. (1992)..

39. Quaranta, N. E., Martino, R., Gambaro, L., and Thomas, H., *Stud. Surf. Sci. Catal.*, **82**, 811 (1994)..

40. Wan, B-Z., Huang, K., Yang, T.C., and Tai, C-Y., *J. Chin. Insti. Chem Engg.* **22**, 17 (1975).

41. Bellusi, G., and Rigutto, M.S., in "Advance Zeolite Science and Applications", Stud. Surf. Sci. Catal., Vol.85, p.179. elsevier, Amsterdam.1994.

42. Kannan, S., Sen, T., and Sivasanker, S., *J. Catal.*, (in press)

43. Sen, T., Ramaswamy, V., Ganapathy, S., Rajamohanan, P. R., and Sivasanker, S., *J. Phys. Chem.*, **100**, 3809 (1996).

44. Takezawa, N., Hanamaki, C., and Kobayashi, H., *J. Catal.* **38**, 101 (1975).

45. Wang, L., Eguchi, K., Arai, H., Seiyama, T., *Chem. Lett.* 1173 (1986).

46. Zhang, W., Desikan, A. And Oyama, S.T., *J.Phys. Chem.* **99**, 14468 (1995).

47. Deo, G., and Wachs, I.E., *J. Catal.* **129**, 307 (1991)

48. Trifiro, F., and Pasquon, I., *J. Catal.* **12**, 412 (1968).

49. Nakagawa, Y., Ono, T., Miyata, H., and Kubokawa, J., *J.Chem.Soc., Faraday Trans.* **175**, 2929 (1983).

50. Iwasawa, Y., Nakano, Y., and Ogasawara, S., *J. Chem.Soc., Faraday Trans. I.* **74**, 2986 (1978).

51. Tatibouet, T.M., Germain, J.E., and Volta, J.C., *J. Catal.* **82**, 240 (1983).

52. Ai, M., *J. Catal.* **54**, 426 (1978).

53. Sen, T., El Mekki.El. Malki and Sivasanker, S., Microporous Materials (in preparation).

CHAPTER V

SUMMARY AND CONCLUSIONS

Isomorphous substitution of metal ions in the silica framework of molecular sieves produces metallosilicates with interesting catalytic properties. The substitution of Fe^{3+} or Ga^{3+} influences the Bronsted acidity, whereas transition metal ions such as Ti^{4+}, $V^{4+/5+}$, Zr^{4+} and Cr^{5+} in the zeolite lattices are effective oxidation catalysts. Though the synthesis of a number of vanadosilicate molecular sieves, their physicochemical characterization and catalytic properties have been reported, no detailed reports are available on how and in which form the V-species enter the lattice during hydrothermal synthesis and the reasons for the differences in the reactivities of the different V-species. This thesis describes in detail (a) the methodologies for the synthesis of a novel large pore (V-Al-β) and two medium pore (V-MFI and V-MEL) and vanadium containing molecular sieves, (b) the identification of the different V-species in the gel and crystalline phases by physicochemical techniques and (c) the catalytic oxidation properties of these materials.

The chemistry of vanadium in aqueous solutions at different pH is well established. The nature of the V-species present in the solution depends on its pH. The synthesis therefore of vanadium containing molecular sieves at different pH is interesting from the angle of vanadium incorporation in the lattice of molecular sieves. Generally, though the synthesis of zeolites is carried out at high pH (>10), the synthesis of MFI (ZSM-5) at low pH in the presence of fluoride ions is also reported. The synthesis of V-MFI was carried out at two different pH (acidic, 6.8; alkaline, 11.0) using $VOSO_4$ (VO^{2+}) as the vanadium source, tetrapropyl ammonium ion as the template and tetraethyl orthosilicate (for alkaline synthesis) or fumed silica (for acidic synthesis) as the silica source. The V^{4+} and V^{5+} contents were estimated by standard titrimetric procedures (Chapter II).

Studies on V-MFI

Physicochemical characterization of the crystalline V-MFI samples was carried out using analytical methods, XRD, spectroscopic methods (SEM, ESR, IR, UV-VIS,, NMR), thermal analysis methods (TG/DTA) and adsorption techniques (Chapter III).

Analytical data indicate that the pick up of V^{4+} and V^{5+} by the crystalline phase is related to the concentration of the respective V-ions in the gel phase. However, while 84% of the V^{4+} ions in the acidic gel were picked up by the crystalline material, only 50% of the V^{5+} ions were picked up from the alkaline gel. More V-ions were extracted out by NH_4OAc solution (after calcination) from the sample synthesized from the acidic gel than from the alkaline gel.

XRD data indicate that the samples are highly crystalline. There was a phase transformation during the calcination of the V-MFI (A; acidic) and not in the case of V-MFI (B; basic) suggesting that incorporation of vanadium has not occurred in the case V-MFI(A). Besides, no change in unit cell parameters was observed for V-MFI(A) while an expansion was observed in the case of V-MFI(B). The expansion of the unit cell volume is due to presence of V-species in the framework of V-MFI(B).

SEM showed the formation of apparently defect-free large crystals (6-8 μm) when synthesized from the acidic medium. Alkaline synthesis lead to submicrometer particles (0.1-0.2 μm).

ESR experiments have indicated that V^{4+} species are present as freely mobile VO^{2+} ions in the gel of V-MFI(A) and in a distorted Oh environment in the gel of V-MFI(B). In the as-synthesized V-MFI(A), V^{4+} ions are in an agglomerated (polymeric) state, whereas in V-MFI(B), they are well dispersed in an Oh environment. The polymeric V^{5+} species

(in V-MFI(A)) are more difficult to oxidize or reduce, whereas the framework V^{5+} species (in V-MFI(B)) undergo redox transformations easily.

The IR band at 969 cm^{-1} attributed to Si-O^- linkages is related to the presence of framework V^{5+} species in defect sites.

UV-visible spectra suggest that distorted Td-V^{5+} species are present in the as-synthesized and calcined forms of the V-MFI(B), while both the Td and Oh V-species are present in the calcined V-MFI(A).

NMR experiments indicate that monomeric HVO_4^{2-}, polymeric $V_2O_7^{4-}$, and the protonated species ($HV_2O_7^{3-}$) are present in the alkaline gel. Distorted Td-V^{5+} species are present in V-MFI(B). ^{29}Si MAS NMR indicate the absence of defect sites in V-MFI(A), whereas defect sites are present in V-MFI(B). The broadening of the ^{29}Si spectrum of V-MFI(B) indicates that V is distributed in the [SiO_2] lattice. The ^1H MAS NMR experiment indicates the presence of V-OH linkages from nonframework vanadium in the calcined V-MFI(A).

TG-DTA studies reveal that the V-ions are in intimate contact with the template molecules only in the sample synthesized from the alkaline medium.

Surface area and sorption studies indicate the materials are microporous in nature without any occluded materials in the channels.

Studies on V-MEL

The influence of synthesis parameters (atmosphere and V-concentration) at alkaline pH in the case of V-MEL (VS-2) has been studied systematically. Tetraethyl orthosilicate, and $VOSO_4$ (VO^{2+}) were used as ingredients and tetrabutyl ammonium hydroxide was used as the templating agent. The ratio of V^{5+}/V^{4+} increases on decreasing the concentration

ofvanadium in the gel. The ratio is minimum in the case of the gel prepared in an inert atmosphere.

The pick up of V^{4+} by the solid is linearly related to the V^{4+} concentration in the gel suggesting pickup at the surface. The V^{5+} content in the solid goes through a maximum with an increase in the V^{5+} content of the gel; at higher V^{5+} concentrations, oligomeric solids (V^{5+}) are probably formed, preventing the pickup of V^{5+} by the zeolite material.

XRD data confirm unit cell expansion with vanadium incorporation. The expansion is related to nonextractable vanadium in the samples, providing direct evidence that these ions are present in the lattice.

SEM pictures reveal that the V-MEL crystallites are wheat grain shaped; the crystallites are small (2 μm) in the case of V-MEL(D) and larger (5 μm) in the case of V-MEL(A) which is similar to pure silicalite-2. The crystallite size decreases with increasing vanadium incorporation in the framework.

V^{4+} ions appear to be present as discrete ions in both the gels and as-synthesized samples, as ESR estimations match analytical values. The calcined (dehydrated) samples exhibit a signal attributable to $O_2^{\cdot-}$ radical ions; no hyperfine lines due to V^{4+} ions are detected. On reduction in H_2 (573 K; 6 h), only the V^{5+} rich V-MEL (2, 3 and 4) exhibits ESR lines characteristic of V^{4+}. The calcined V-MEL(1-He) and V-MEL(1), do not exhibit ESR spectra on reduction and presumably possess mostly extralattice V^{5+} species originating form the extralattice V^{4+} species.

The intensity of the band at 967 cm^{-1} attributed to $Si\text{-}O^{-}$ linkages is related to the nonextractable V^{5+} species in the calcined sample.

UV-visible studies indicate that distorted Td-V^{5+} species are present in the as-synthesized samples. Two types of V^{5+} species are present in the calcined samples, one type being extracted by NH_4OAc.

Liquid state ^{51}V NMR studies indicate that both monomeric HVO_4^{2-} and oligomeric $V_2O_7^{4-}$ are present in the gels. Two types of nonframework V^{5+} species and one framework V^{5+} species are detected by solid state ^{51}V MAS NMR. The extractable V^{5+} species are found to be sensitive to hydration/dehydration and are probably outside the framework. Nutation NMR experiments indicate that one of the nonfamework V-species is mobile in the zeolite channels, and the other one is loosely bound. ^{29}Si NMR data indicate that interaction between Si^{4+} and V-ions occurs in the gel during crystallization.

Thermal analysis indicate interaction between the template with V-species in the framework.

Surface areas and sorption studies indicate that all the samples are microporous in nature without any occluded species in the channels.

Probable structures of V-species present in the gels and crystalline samples have been proposed based on the above physicochemical data.

Studies on V-Al-β

Novel vanadium containing molecular sieves of the large pore BEA structure have been prepared using tetraethyl orthosilicate, $VOSO_4$ and $Al_2(SO_4)_3$ as ingredients and tetraethyl ammonium hydroxide as the templating agent. The effect of various synthesis parameters such as temperature, concentration of the organic additive, Si/V ratios, SiO_2/Al_2O_3 ratio and water content on the crystallization kinetics is presented in chapter III. An increase of Si/V ratio in the reaction mixture enhances the rate of crystallization. $TEAOH/SiO_2$ molar

ratio of 0.52 is found to be optimum for the synthesis of V-Al-beta. An increase in the pH of the mother liquor with crystallization is observed.

Both $V^4$and V^{5+} are present in the synthesis gel of high vanadium content, whereas only V^{5+} is present in the synthesis gel of low vanadium content. The nature of V^{4+} and V^{5+} species has been identified by ESR and NMR spectroscopic methods.

Physicochemical characterization of V-Al-β have been carried out by using numerous techniques. Only V^{5+} species are present in the as-synthesized samples prepared at low vanadium concentration, whereas V^{4+} and V^{5+} species are present in the samples prepared at high vanadium content. XRD studies indicate the samples to be highly crystalline. SEM pictures reveal the crystallites to be spheroidal (0.1 - 0.2 μm). ESR experiments indicate the absence of V^{4+} in the gel, as-synthesized and calcined samples of V-Al-β synthesized at low vanadium concentration; V^{4+} is present in a distorted Oh environment in the as-synthesized and calcined samples synthesized from gels containing high concentrations of vanadium. Upon reduction of the calcined samples in H_2, all the samples exhibit eight line hyperfine spectra corresponding to V^{4+} in a SqPy environment. All the V-Al-β samples exhibit an IR band at 958 cm^{-1}; its intensity increases linearly with increasing framework vanadium content in the samples. The UV-visible spectrum suggests the presence of vanadium in a distorted Td environment in the calcined V-Al-β samples. NMR spectroscopic studies indicate the presence of HVO_4^{2-} species in the gel. ^{51}V MAS NMR spectra indicate the presence of distorted Td-V^{5+} species in the calcined V-Al-β samples and these V-species are stable upon hydration/dehydration. ^{29}Si MAS NMR studies indicate that the intensity of the defect silanol groups increases with increasing framework V-species in the BEA structure.

In conclusion, the synthesis of V-MFI (VS-1) in an alkaline medium favours the incorporation of vanadium in the lattice of MFI molecular sieves. The incorporation of

vanadium in the MEL lattice is related to the concentration of HVO_4^{2-} species present in the gel. High pH synthesis of zeolite β favours greater incorporation of V in the lattice of BEA. The V resides in the defect centres in all the molecular sieves.

V-MFI, V-MEL and V-Al-β are found to have interesting catalytic properties in liquid and vapour phase oxidation reactions. The framework V-species in the different vanadosilicate molecular sieves (e.g., V-MFI(B), V-MEL(3) and V-Al-β(c)) catalyze the hydroxylation of phenol to catechol and hydroquinone. The nonframework V-species which are present in V-MFI(A) and V-MEL(1-He) are easily extracted by dilute H_2O_2 in the reaction medium and are poor oxidation catalysts.

In the oxidation of toluene, the vanadium containing catalysts (V-MFI(B), V-MEL(3) and V-Al-β(c)) are active in both the hydroxylation of the aromatic nucleus as well as the oxidation of the side chain alkyl group. The yield of cresols increases and the yield of benzaldehyde decreases with time over sample V-MFI(B), whereas in the case of V-MFI(A), the relative yield of the two types of products remains nearly constant with time. The slow build up of ring hydroxylation product in the case of V-MFI(B) is due to the presence of framework V-species. A smaller o/p (cresol) ratio is observed over samples containing framework V-species (e.g., V-MFI(B), V-MEL(3) and V-Al-β(c)).

The activity and stability of non-framework V-species is improved in the presence of a promoter (picolinic acid). The catalytic activity of the vanadium containing molecular sieves is due to the redox character of the V-centres. The promoter enhances the reducibility of the V-species (ESR evidence) probably due to the formation of a V-peroxo-picolinato complex.

The vapour phase oxidation of ethanol was carried out over V-MEL, V-MFI and V-Al-β catalysts. The effects of temperature and space velocity on conversion and selectivity

have been studied. The kinetics of the reaction over V-MEL catalysts have been investigated. The conversion increased with increasing temperature and contact time over all the catalysts.

The kinetics of the reaction (at 5% conversion) indicate a nearly first order dependence of the rate of formation of the major products (ethylene, acetaldehyde and diethyl ether). The apparent activation energies (E_{app}) for the formation of acetaldehyde have been calculated. The E_{app} is larger (~ 130 kJ mol^{-1}) for the sample containing framework V-species (V-MEL(2)) than for V-MEL(1-He) (~110 kJ mol^{-1}).

The selectivity towards diethyl ether increases in the order V-Al-β > V-MFI(B) > V-MEL(2). The samples containing extralattice vanadium (V-impregnated samples and V-MEL(1-He)) favour acetaldehyde formation. At high temperatures, ethylene is the major product over all the catalysts both at high and low space velocities. The framework V-species are active in the production of ether, and the nonframework V-species are active for the formation of the aldehyde. Mechanisms for the formation of the major products over these catalysts are proposed.

List of Publications :

1. **T.Sen**, M. Chatterjee and S. Sivasanker, "Novel large pore vanadium alumino- and boro-silicates with BEA structure", *J. Chem. Soc., Chem. Commun.*, 207 (1995).

2. **T. Sen**, V. Ramaswamy, P.R. Rajamohanan, S. Ganapathy and S. Sivasanker, "Incorporation of vanadium in Zeolite lattices: Studies of the MEL system", *J. Phys. Chem.*, 3809, *100* (1996).

3. R. Ravisanker, **T.Sen**, V. Ramaswamy, H.S. Soni, S. Ganapathy and S. Sivasanker, "Synthesis, Characterization and Catalytic properties of Zeolites PSH-3 / MCM-22", *Stud. Surf. Sci. Catal.* 331, *84a* (1994).

4. R. Ravisanker, **T. Sen**, S. Sivasanker, and S. Ganapathy, "Multinuclear MAS NMR studies of the zeolite MCM-22", *J. Chem. Soc., Faraday Trans.*, 3549, *19* (1995).

5. **T. Sen** , P.R. Rajamohanan, S. Ganapathy and S. Sivasanker, "The Nature of Vanadium in Vanado-Silicate (MFI) Molecular Sieves: Influence of Synthesis Methods", *J. Catal.*, 354, *163* (1996).

6. S. Kannan, **T. Sen** and S. Sivasanker, "Catalytic Transformation of Ethanol over Microporous Vanadium silicate Molecular Sieves with MEL structure (VS-2)", *J. Catal* (in press).

7. S. Ganapathy, T.K.Das, R.Vetrivel, S. Roy, **T.Sen** and S. Sivasanker "Anisotropic chemical shielding, T-site ordering and acidity in ETS-10 molecular sieves studies through MAS NMR and Molecular Modeling", *J. Am. Chem. Soc.* (communicated).

8. **T. Sen**, M. Chatterjee and S. Sivasanker, "Synthesis, Characterization and Catalytic properties of V-Al-beta molecular sieves", *Microporous Materials* (in preperation).

9. **T.Sen** and S.Sivasanker, "Enhancement of catalytic oxidation activities over vanadium containing molecular sieves using a promoter", J. Chem. Soc., Chem. Commun., (in preperation).

10. S. Kannan, **T. Sen** and S. Sivasanker, "Selective oxydehydrogenation of ethanol over V-containing medium (MFI and MEL) and large pore (V-Al-beta) molecular sieves," *Appl. Catal.*, (in preperation).

11. **T. Sen** and S. Sivasanker, "Comparative studies of synthesis, characterization and catalytic properties of VS-2 (V-MEL) using tetrabutyl ammonium and phosphonium ions as the template", *Indian Journal of Chemistry* (in preperation)

12. **T. Sen**, M. Chatterjee and S. Sivasanker, "Synthesis, Characterization and Catalytic properties of V-MTW (V-ZSM-12) molecular sieves using methyl triethyl ammonium bromide (MTEABr) as template", *Indian Journal of Chemistry* (in preperation)

13. S. Dzwigaj, M. J. Peltre, P. Massiani, A. Davidson, M. Che, T. Sen, S. Sivasanker, "Incorporation of V-species in a dealuminated β-zeolite using an aqueous solution of ammonium metavanadate" J. C. S. Chem. Commun (1997, Proof